Development of Microfluidic Chips for High Performance Electrophoresis Separations in Biochemical Applications

by

Seyed Mostafa Shameli

A thesis
presented to the University of Waterloo
in fulfillment of the
thesis requirement for the degree of
Doctor of Philosophy
in
Mechanical Engineering

Waterloo, Ontario, Canada, 2013

AUTHOR'S DECLARATION

I hereby declare that I am the sole author of this thesis. This is a true copy of the thesis, including any required final revisions, as accepted by my examiners.

I understand that my thesis may be made electronically available to the public.

Abstract

Electrophoresis separation corresponds to the motion and separation of dispersed particles under the influence of a constant electric field. In molecular biology, electrophoresis separation plays a major role in identifying, quantifying and studying different biological samples such as proteins, peptides, RNA acids, and DNA. In electrophoresis separation, different characteristics of particles, such as charge to mass ratio, size, and pI, can be used to separate and isolate those particles. For very complex samples, two or more characteristics can be combined to form a multi-dimensional electrophoresis separation system, significantly improving separation efficiency. Much effort has been devoted in recent years to performing electrophoresis separations in microfluidic format. Employing microfluidic technology for this purpose provides several benefits, such as improved transport control, reduced sample volumes, simplicity of operation, portability, greater accessibility, and reduced cost. The aim of this study is to develop microfluidic systems for high-performance separation of biochemical samples using electrophoresis methods.

The first part of the thesis concerns the development of a fully integrated microfluidic chip for isoelectric focusing separation of proteins with whole-channel imaging detection. All the challenges posed in fabricating and integrating the chip were addressed. The chip was tested by performing protein and pI marker separations, and the separation results obtained from the chip were compared with those obtained from commercial cartridges. Side-by-side comparison of the results validated the developed chip and fabrication techniques.

The research also focuses on improving the peak capacity and separation resolution of two counter-flow gradient electrofocusing methods: Temperature Gradient Focusing (TGF) and Micellar Affinity Gradient Focusing (MAGF). In these techniques, a temperature gradient across a microchannel or capillary is used to separate analytes. With an appropriate buffer, the temperature gradient creates a gradient in the electrophoretic velocity (TGF) or affinity (MAGF) of analytes and, if combined with a bulk counter-flow, ionic species concentrate at unique points where their total velocity is zero, and separate from each other. A bilinear temperature gradient is used along the separation channel to improve both peak capacity and separation resolution simultaneously. The temperature profile along the channel consists of a very sharp gradient used to pre-concentrate the sample, followed by a shallow gradient that increases separation resolution. A simple numerical model was applied to predict the improvement in resolution when using a

bilinear gradient. A hybrid PDMS/glass chip integrated with planar micro-heaters for generating bilinear temperature gradients was fabricated using conventional sputtering and soft lithography techniques. A specialized design was developed for the heaters to achieve the desired bilinear profiles using both analytical and numerical modeling. To confirm the temperature profile along the channel, a two-color thermometry technique was also developed for measuring the temperature inside the chip. Separation performance was characterized by separating several different dyes, amino acids and peptides. Experiments showed a dramatic improvement in peak capacity and resolution of both techniques over the standard linear temperature gradients.

Next, an analytical model was developed to investigate the effect of bilinear gradients in counter-flow gradient electrofocusing methods. The model provides a general equation for calculating the resolution for different gradients, diffusion coefficients and bulk flow scan rates. The results indicate that a bilinear gradient provides up to 100% improvement in separation resolution over the linear case. Additionally, for some scanning rates, an optimum bilinear gradient can be found that maximizes separation resolution. Numerical modeling was also developed to validate some of the results.

The final part of the thesis describes the development of a two-dimensional separation system for protein separation, combining temperature gradient focusing (TGF) and sodium dodecyl sulfate (SDS) polyacrylamide gel electrophoresis (PAGE) in a PDMS/glass microfluidic chip. An experimental study was performed on separating a mixture of proteins using two characteristics: charge to mass ratio, and size. Experimental results showed a dramatic improvement in peak capacity over each of the one-dimensional separation techniques.

Acknowledgements

I would like to express my deep appreciation for the guidance and support of my supervisor, Professor Carolyn Ren, who believed in my abilities, gave me the chance to work in her research group, and fully supported me in becoming a capable researcher. Her financial support, her expertise and passion for research, and her constant help and advice are truly appreciated. I also appreciate the help, guidance and support of my co-supervisor, Professor Zhen Liu, during my PhD research at University of Waterloo.

I would like to thank my previous colleagues, Dr. Caglar Elbuken and Dr. Tom Glawdel, for their guidance, help and insightful discussions during my research. Without their help, I would not have achieved the level of success I have achieved today. The help and support of my lab work mates Zeyad Almutairi and Cody Chen are also greatly appreciated.

I also appreciate the great help and input of several emeritus members of our group who made my research smooth and enjoyable: Dr. Lin Gui, Dr. Said Boybay, Dr. Junjie Ou, and Dr. Tiemin Huang.

Finally, I would like to thank my family and friends for their gracious help and support; they made my life more enjoyable and encouraged me to continue forward at difficult times in my research.

Table of Contents

List of Figures

List of Tables

Chapter 1

Introduction

1.1 Background of Microfluidics

Devices for the analysis of biological samples and the generation of chemicals have gained significant importance in the field of biology [1, 2]. The conventional systems used to accomplish this analysis and generation usually have limited accessibility because of the complexity of the equipment, which often requires specialists to perform time-consuming operations, and high cost. There is therefore strong motivation to develop new methods for sample analysis and to improve the processing rate of current analysis techniques [2]. The use of microfluidic systems for bio-analysis and point-of-care testing has been studied extensively in recent decades. A microfluidic chip consists of a set of microchannels etched or molded into a material such as glass, silicon, or polydimethylsiloxane (PDMS). The microchannels forming the microfluidic chip are interconnected in order to achieve a desired function, such as mixing, pumping, separating and detecting, redirecting, and allowing chemical reactions in a cell [3, 4]. Integrating one or more microfluidic elements with miniaturized sensors, analysis tools, and automated control units is referred to as a lab-on-a-chip (LOC) device or micro total analysis system (μTAS) [5, 6]. Lab-on-a-chip systems offer several advantages including reduced reagent consumption, lower fabrication costs, shorter analysis time, improved sensitivity, and portability. More importantly, scaling down brings the dimension of the device in line with the samples to be analyzed, allowing for a level of control over the sample that is unattainable with macroscale systems [5, 6]. The history of microfluidic systems has its roots in the development of ink-jet printers and transistors made in blocks of semiconductors in the 1950s, followed by the development of silicon microchannel devices for gas chromatography in the late 1970s, and then by the appearance of the first chip-based electrophoresis separation devices in the1990s [7, 8, 9, 10]. Microfluidic systems have been applied in a number of applications including drug discovery, clinical diagnostics, genetics research, chemical synthesis, cellular analysis, and bio-weapons detection [11, 12, 13, 14].

Figure 1.1 shows several LOC devices that are commercially available in the marketplace for biomedical research and analysis. An LOC device consists of several integrated components such as pumps, mixers,

1

valves, separators, and detectors that are connected by microchannels on the order of 10-500 μm. The first LOC devices were fabricated in glass or silicon using established microfabrication techniques borrowed from the microelectronics industry. However, the high cost and limited access to fabrication facilities restricted the research to a few selected groups.

Figure 1.1 Several examples of commercial LOC products: (a) Agilent Technologies protein kit for protein concentration and proteomic analysis **[15]** (b) RainDance Technologies RDT 1000 chip for high performance production of microdroplets for polymerase chain reaction (PCR) **[16]** (c) Fluidigm cartridge with integrated membrane valves for performing multiplexed proteomic and genomic studies **[17]** (d) Abbott point of care i-STAT PT/INR cartridge for monitoring anticoagulation therapy **[18]**

The exponential growth of LOC research over the past decade began with the introduction of a novel fabrication process known as soft lithography [19, 20, 21, 22]. Soft lithography is a micromolding technique in which a soft polymeric mold such as a polydimethylsiloxane (PDMS) is cast from an original hard master with raised relief structures representing the fluidic network. To complete the chip, the mold is peeled and trimmed, fluidic access holes are punched, and the mold is bonded to another

substrate. The widespread adoption of soft lithography can be attributed largely to the excellent properties of PDMS for LOC applications. PDMS is optically transparent down to 280 nm, is biocompatible and largely inert, a wide temperature range, and is easily modified by several well established surface treatments [23, 24, 25, 26, 27]. PDMS devices are inexpensive; they typically cost between $5 and $30 per mold to build under non-clean room conditions and are therefore disposable – a valuable attribute for biomedical applications. Other materials such as ceramics, glass, metal and plastics are also widely used for fabricating LOC devices depending on the intended application [2].

1.2 Motivation for the study

Proteomics analysis combines various technologies to identify and study proteins. Identifying proteins from cells is the ultimate solution to the understanding of diseases and, thus, to drug discovery [28, 29, 30]. Electrophoresis separation followed by detection methods are the most important parts of proteomics analysis. In recent years, much effort has been devoted to performing proteomics analysis with Lab-on-a-chip devices [30]. The most important advantages of the chips or capillary systems over the conventional systems are the extremely small sample requirement, shorter analysis time, lower fabrication costs, improved sensitivity, portability, and high throughput [31]. Although successful operation of these devices has been reported, some related concerns need to be addressed. First, the motivation to develop microfluidic chips with simpler designs and higher efficiency is still of great importance in proteomics analysis [32, 33]. Second, most of the mechanisms currently used for miniaturized multi-dimensional separations are not continuous and cannot provide repeatable separation results between runs [34]. Third, some of the microfluidic chip designs and mechanisms currently used for proteomics analysis are not optimized, and higher efficiencies can still be achieved by performing improvements to the function and accuracy of their mechanisms, detection sensitivity, and control. There are also opportunities to improve the reliability and robustness of the chips [35, 36, 37]. In general, preliminary evaluation of the design components can be performed by using numerical models and simulations that predict separation performance and the concentration field of the samples. These simulations provide guidelines for the operating conditions required to achieve a better separation. Subsequently, the selected chip designs, based on the numerical analyses, can be investigated experimentally. It is essential to perform experiments in the iterative design process because many factors that influence microfluidic chip

operation are difficult to represent in numerical simulations. The aim of this study is to improve the design and mechanism of some of the currently used separation techniques as well as develop new separation mechanisms for high-performance proteomics analysis. In this case, the design, mechanism, and performance of three currently used separation methods have been improved to achieve a higher separation resolution and better efficiency. A new, continuous, two-dimensional separation mechanism has also been introduced for high performance proteomics analysis. Analytical and experimental studies have been performed to justify the improvements made during this research.

1.3 Thesis Outline

In Chapter 2, an overview of electrophoresis separation in microfluidic chips is provided, discussing the use of these separation techniques in molecular biology as well as the benefits of miniaturizing current chemical and biological systems. The review outlines the fundamentals of electrophoresis separation and the various mechanisms used to concentrate, separate, and detect different biochemical samples through microfluidic networks. The review also highlights some of the pros and cons of different kinds of miniaturized separation systems.

In Chapter 3, the experimental setup and procedures used throughout this thesis are summarized. This includes techniques, materials, and equipment that are used for fabricating the microfluidic chips and performing the separation experiments. Soft lithography and sputtering techniques are explained as two frequently used fabrication methods in this study. The preparation of different samples and buffers for performing the separation experiments has also been addressed.

Chapter 4 focuses on the development of a fully integrated microfluidic chip (PDMS/modified PDMS membrane/SU-8/quartz) for isoelectric focusing separation of proteins with whole-channel imaging detection. The motivation for this work is the need to develop low-cost and fully automated chips that have similar performances to currently used commercial products that are much more expensive and difficult to fabricate. All the challenges posed in fabricating and integrating the chip are addressed. The chip was tested by performing protein and pI marker separations, and the separation results obtained for the chip are compared with those obtained for commercial cartridges. Side-by-side comparison of the results validates the developed chip and fabrication techniques.

Chapter 5 focuses on improving the peak capacity and separation resolution of two counter-flow gradient electrofocusing methods: Temperature Gradient Focusing (TGF) and Micellar Affinity Gradient Focusing (MAGF). In these techniques, a temperature gradient across a microchannel or capillary is used to separate analytes. With an appropriate buffer, the temperature gradient creates a gradient in the electrophoretic velocity (TGF) or affinity (MAGF) of analytes and, if combined with a bulk counter-flow, ionic species concentrate at unique points where their total velocity sums to zero and, therefore, separate from each other. In this chapter, the use of a bilinear temperature gradient along the separation channel is investigated to improve both peak capacity and separation resolution simultaneously. The temperature profile along the channel consists of a very sharp gradient used to pre-concentrate the sample followed by a shallow gradient that increases separation resolution. A simple numerical model is used to validate the resolution improvement when using a bilinear gradient. Then a hybrid PDMS/glass chip integrated with planar micro heaters for generating bilinear temperature gradients is fabricated using conventional sputtering and soft lithography techniques. A specialized design is developed for the heaters to achieve the desired bilinear temperature profiles using both analytical and numerical modeling. To measure the actual temperature profile along the channel, a two-color thermometry technique is developed for measuring the temperature inside the chip. Separation performance is then characterized for each of the techniques by separating several different dyes, amino acids and peptides. Experimental results show a dramatic improvement in the peak capacity and resolution of both techniques over the standard linear temperature gradient methods.

In chapter 6, an analytical model is developed to investigate the effect of bilinear gradients in counter-flow gradient electrofocusing methods. The model solves the convection-diffusion equation and equation of motion of the focused peaks along the separation channel and provides a general equation to calculate the resolution for different gradients, diffusion coefficients, and bulk flow scan rates. The results indicate that any bilinear gradient provides up to 100% improvement in separation resolution compared with the linear case. Additionally, for some scanning rates, an optimum bilinear gradient can be found that maximizes separation resolution. Numerical modeling is also developed to validate some of the results.

In Chapter 7, a two-dimensional separation system is introduced and developed for high-performance protein separation by combining temperature gradient focusing (TGF) and sodium dodecyl sulfate (SDS) polyacrylamide gel electrophoresis (PAGE) on a PDMS/glass microfluidic chip. The proposed method has several advantages over the previously reported techniques, such as continuity, simple design and

fabrication, and the use of single point detection for detecting the focused peaks. An experimental study using two different characteristics, charge to mass ratio and size, is performed to separate a mixture of proteins. Experimental results show a dramatic improvement in the peak capacity compared with the results obtained from each of the separation dimensions.

In Chapter 8, a summary of this work is presented and recommendations are outlined for studies to further improve the separation performance and repeatability of microfluidic devices for electrophoresis separation analysis. The knowledge gained in this thesis will improve our understanding of electrophoresis separation and advance the development of LOC devices for separation analysis. The information obtained during this research will be of interest to researchers in fluid mechanics, analytical chemistry, and bioengineering.

Chapter 2
Literature Review

2.1 Introduction to Electrophoresis Separation in Microfluidic Systems

Electrophoresis, also called cataphoresis and anaphoresis, is the migration of charged particles or molecules through a solution under the influence of an applied electric field. Because molecules in an electric field move with a speed dependent on their charge, shape, and size, electrophoresis has been extensively developed for separating substances and analyzing molecular structures [32]. It is used for the analysis and purification of very large molecules such as proteins and nucleic acids, as well as simpler charged molecules including charged sugars, amino acids, peptides, nucleotides, DNA, and simple ions [38, 39]. Highly sensitive detection methods have been developed to monitor and analyze electrophoresis separation. Traditional electrophoresis of macromolecules is normally carried out by applying a thin layer of sample to a solution stabilized by a porous matrix. Under the influence of an applied voltage, different species or molecules in the sample move through the matrix at different velocities. At the end of the separation, different species are detected as bands at different positions in the matrix. A matrix is usually required because the electric current passing through the electrophoresis solution generates heat, which causes diffusion and convective mixing of bands in the absence of a stabilizing medium. The matrix can be composed of various materials, including paper, cellulose acetate, or gels made of polyacrylamide, agarose, or starch [31, 32]. In acrylamide and agarose gels, the matrix also acts as a size-selective sieve in the separation [31].

Using microfluidic systems for electrophoresis separations, one can achieve several advantages over the conventional separation techniques, such as faster separation, higher efficiency, minimum sample requirement, lower cost, portability, and better detection accuracy. Additionally, due to the high surface to volume ratio of the microchannels, diffusion caused by heat, gravity, and hydrodynamic flow inside the channels can be significantly reduced because of high frictional drag opposing fluid motion in narrow channels. Faster heat dissipation from the system also allows the use of high voltages [2, 31, 32]. Microfluidic-based electrophoresis was developed in 1979 in thin-film Teflon tubes and has been widely used in different formats [2]. Until now, electrophoresis has remained the primary principle of separation

in microfluidic chips, and most of the papers published on separation in microfluidic format are electrophoresis-based [31, 32].

Separation by electrophoresis depends on differences in the migration velocity of ions or solutes through a given medium in an electric field. The electrophoretic velocity of an analyte can be defined as

$$u_{ep} = \upsilon_{ep} E \qquad\qquad (2.1)$$

where υ_{ep} is the electrophoretic mobility of the analyte and E is the applied electric field strength [40]. The electrophoretic mobility is inversely proportional to frictional forces in the buffer and directly proportional to the ionic charge of the analyte. The forces of friction against an analyte depend on the analyte size and the viscosity of the buffer (η). Analytes with different frictional forces or different charges separate from one another when they move through a buffer. At a given pH, the electrophoretic mobility of an analyte is

$$\upsilon_{ep} = \frac{q}{6\pi\eta R} \qquad\qquad (2.2)$$

where q is the total net charge of the analyte and R is the Stokes radius of the analyte [40]. Based on equation (2.2) a difference in charge to size ratio of analytes causes a difference in electrophoretic mobility: small, highly charged analytes have greater mobility than large, weakly charged analytes. The net force acting on an analyte is the balance of two forces: the electrical force acting in favor of motion, and the frictional force acting against the motion. For most electrophoresis methods, these two forces remain steady during the separation. Therefore, electrophoretic mobility is a constant for a given analyte under a given set of conditions [40].

There are many different types of electrophoresis, all having distinct applications. Electrophoresis separation can be migration-based on which analyte movements with different velocities causes the separation or focusing-based on which different analytes focus and separate at their different zero velocity points along the separation column [41]. In another classification, electrophoresis can be one-dimensional (i.e., one direction of separation), or two-dimensional when two techniques are combined. One-dimensional electrophoresis is used for most routine protein and nucleic acid separations. Two-

dimensional separation is used when high resolving power is required for separating complex mixtures [34].

2.2 Biochemical Applications

Electrophoresis has a wide variety of applications in molecular biology, genetics, biochemistry, and microbiology. One of the most common uses of electrophoresis is to analyze different genes and proteins. The study of proteins by various technologies is called proteomics [42], and it contributes to the analysis of the structure and function of biological systems. Healthy and diseased cells can be identified by differences in the electrophoretic separation patterns of their proteins. For example, the protein content of a cancerous cell is often different from that of a healthy cell. Certain proteins in the cancerous cell may not be present in the healthy cell, making these unique proteins good targets for anti-cancer drugs. The realization of this goal is difficult since both purification and identification of proteins in any organism can be hindered by a multitude of biological and environmental factors [28, 29].

Proteins are linear polymers built of amino acids. There are twenty different amino acids. These amino acids form bonds with each other through a reaction of their respective carboxyl and amino groups, with the resulting bond termed a peptide bond. Proteins can spontaneously fold up into three-dimensional structures, with the lowest energy determined by the sequence of amino acids in the protein polymer [43, 44]. By breaking the bonds that hold together the three-dimensional format of a protein, one can denature the protein into its original linear amino acid sequence. This can be done in different ways such as adding special chemicals to the protein or by heating the proteins to around 95 °C to break their bonds. Denaturing proteins is a useful tool to separate proteins according to their molecular size alone [34]. The isoelectric point, pI is the pH at which a particular molecule or surface carries no net electrical charge. The net charge on the molecule is affected by the pH of its surrounding environment and can become more positively or negatively charged through the gain or loss of protons (H^+). Amino acids that make up proteins may be either positive, negative, neutral, or polar, which together give a protein its overall charge. At a pH below their pI, proteins carry a net positive charge; at a pH above, they carry a net negative charge [45]. Proteins can thus be separated according to their isoelectric point (overall charge) inside a pH gradient [35].

2.3 Migration-Based Electrophoresis Separation Techniques

In a typical migration-based separation method, different analytes are separated as they migrate with different velocities through a separation channel or column. It is therefore possible in principle to achieve arbitrarily high resolution in these methods by making the separation column or capillary arbitrarily long [46]. In this section, different migration-based electrophoresis separation methods are addressed.

2.3.1 Capillary Zone Electrophoresis (CZE)

Capillary zone electrophoresis (CZE), also known as free solution capillary electrophoresis, is probably the most studied separation mode in microfluidic format. CZE separates ionic species based on charge and frictional coefficient in a capillary filled with background electrolyte (BGE). BGEs usually have a very high or low pH and influence the overall migration behavior of analytes in different ways such as modifying the magnitude of the electroosmotic flow, affecting the electrophoretic mobility of analytes, and inducing charge on neutral particles. The sample is injected into the capillary, and when a voltage is applied, the solutes migrate through the capillary as zones. Solutes are separated as they move through the capillary due to their electrophoretic mobilities, and are arranged on the basis of their charge-to-mass ratios. Separation of both large and small molecules can be accomplished by CZE. Even small molecules, where the charge-to-mass ratio differences may not be great, may still be separable. Two main injection techniques, electrokinetic and hydrodynamic, are used in CZE, both resulting in a discrete sample plug loaded at the capillary inlet. Under an applied electric field, analytes migrate due to their inherent electrophoretic mobility and electroosmotic flow (EOF). In the absence of BGE additives, neutral molecules remain unresolved and are simply swept away by EOF [47, 48]. Figure 2.1 shows a representation of the elution order in CZE.
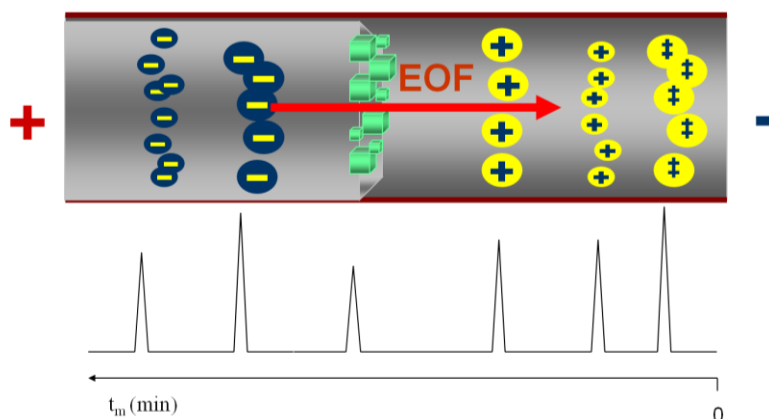
Figure 2.1 Elution order in CZE; Cations elute in order of their charge to size ratios, with small highly charged cations eluting first. Neutral molecules, which move through the capillary under the influence of only the electroosmotic flow and are not separated from each other, elute after the cations. Anions elute in reverse order to their charge to size ratios, with small, highly charged anions eluting last **[49]**.

It was recognized in early studies that capillary electrophoresis could be transferred directly from capillary to microchannel format, because of similar surface properties. In 1994, Jacobson et al. [50] reported the separation of fluorescein and rhodamine B in 11.1 mm long glass microchannels. Since then, hundreds of protein and peptide separations by CZE on different microfluidic chips have been published, featuring different detection schemes such as laser induced fluorescence (LIF), ultraviolent (UV), and mass spectroscopy (MS).

Belder's group achieved a well-resolved CZE separation of proteins within a few minutes using a phosphate buffer at pH 3 on a fused-silica chip. The authors employed fused-silica chips coated with PVA to separate egg-white chicken proteins such as lysozyme, conalbumin and ovalbumin in less than 2 minutes. They used deep UV absorbance detection for the high-sensitive detecting of proteins inside the chip. They achieved good separation efficiency [51].

Lacher et al. [52] compared CZE separation performances of PDMS and Pyrex microfluidic chips. In all cases, Pyrex proved to be superior to PDMS in terms of performance. Moreover, separation in PDMS microfluidic chips proved to be highly sensitive to the separation buffer composition. Separation efficiency was almost lost when detergent was added to the separation buffer. The authors suggested that these phenomena are related to surface reactivity of PDMS microchannels, although they offered no clear explanation.

11

Fu et al. [53] proposed to replace the two high voltage electrodes at the ends of the CZE separation microchannel by an array of microelectrodes evenly spaced within the microchannel, and to apply a traveling field during the separation. Their numerical simulations showed that this design allows the use of voltages that are orders of magnitude lower than those conventionally used in CE, while maintaining the same separation efficiency.

Hauser et al. proposed a novel approach for CZE separation of proteins and peptides on a PMMA microfluidic chip with a contactless conductivity measurement which was found to be suitable for direct detection [54, 55]. They separated a group of proteins in less than 1 min using an acetate buffer. The sensitivity was found to depend on the size of the proteins. This method is favored because of its instrumental simplicity.

Hodges et al. [56, 57] developed a novel approach for protein separation, termed ion-interaction CZE (II-CZE). Molecular properties to control this separation were charge and hydrophobicity; the corresponding separation mechanisms were the CZE mechanism and a novel hydrophobicity based mechanism referred to as ion-interaction (II). Their approach achieved excellent resolution with high peak capacity for separation of different proteins.

One of the major challenges of using CZE in microfluidic chips is that CZE requires long analysis channels for high-resolution separations of similar analytes. Long separation channels require either larger microfluidic chips (defeating the purpose of the technique) or channel turns, which reduce the separation efficiency [58].

2.3.2 Micellar Electrokinetic Chromatography (MEKC)

The development of Micellar Electrokinetic Chromatography (MEKC) on chip was a major advancement in capillary electrophoresis since it provided a method for separating electrically neutral compounds. Using MEKC, even extremely hydrophobic compounds have been separated [59, 60]. In addition to separating electrically neutral compounds, MEKC has been used to separate ionized compounds [61, 62, 63], as well as large proteins and peptides [64]. This mode of capillary electrophoresis is based on the partitioning of analytes between micelles and the run buffer. Detergents, also called surfactants, are

molecules that have a hydrophilic, water soluble moiety on one end of the molecule and a hydrophobic, water insoluble moiety on the other. Sodium dodecyl sulfate, SDS, is an example of a widely used anionic detergent. When a detergent is presented in a solution at a concentration higher than its critical micelle concentration, CMC, it forms micelles, which are aggregations of individual detergent molecules. Micelles are generally spherical. The hydrophilic groups of the detergent molecules are on the outside of the micelle, toward the aqueous buffer, while the hydrophobic molecules are in the center of the micelle, away from the aqueous buffer. This is shown in Figure 2.2, which represents an SDS micelle.
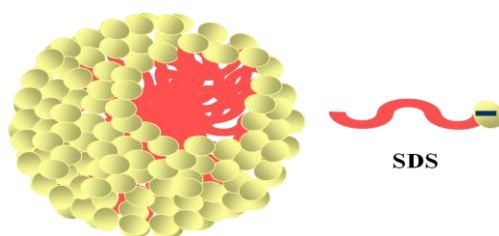
Figure 2.2 Schematic of a SDS micelle; SDS has a negative charge and when forms a micelle, its hydrophilic head appears on the outside of the micelle, toward the aqueous buffer. While it's hydrophobic tail appears in the center of the micelle, away from the aqueous buffer **[49]**.

When a water-insoluble hydrophobic compound is added to an aqueous solution that contains micelles, it partitions into the hydrophobic portions of the micelles. On the other hand, if a water soluble hydrophilic compound is added to the solution, it does not partition into the micelles. A compound of intermediate water solubility will partition between the aqueous solution and the micelles, depending on the hydrophobicity of the compound. MEKC has two phases, aqueous and micellar, both of which move. During MEKC, the electrophoretic migration of the micelles is set to be in the opposite direction of the bulk flow of solvent. As a result, the overall micellar migration velocity is reduced compared with that of the bulk flow. When an analyte is associated within a micelle, its overall migration velocity is reduced; and when an analyte resides in the bulk phase, its migration velocity is that of the bulk flow. Therefore, analytes that have greater affinity for the micelles have slower migration velocities than analytes that spend most of their time in the bulk flow. With SDS micelles, the general migration order is anions, neutrals, and cations. Anions spend more of their time in the bulk phase due to electrostatic repulsions from the micelle. The greater the anionic charge, the more rapid the elution. Neutral molecules are

separated exclusively based on hydrophobicity. Cations elute last due to strong electrostatic attraction. Figure 2.3 illustrates the principle of MEKC.
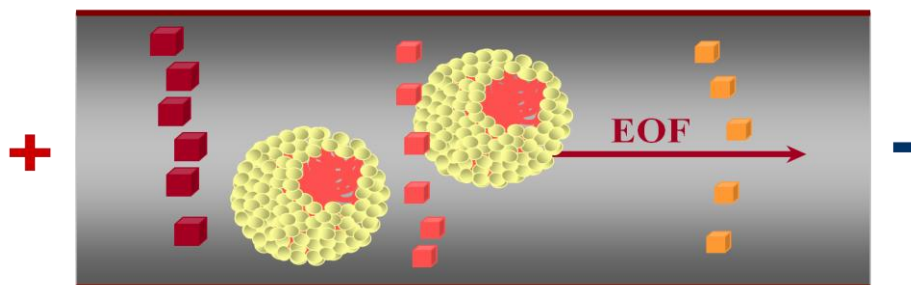
Figure 2.3 Elution order in MEKC. While EOF moves the buffer toward the cathode, negatively charged micelles move slower since they are absorbed through the anode. Samples are separated based on their hydrophobicity. Hydrophilic molecules spend all of their time in the buffer since they do not partition into the micelles and carried out through the capillary at the rate of the electroosmotic flow and are the first to elute. Very hydrophobic molecules that are totally solubilized by the micelles spend all of their time in the micelles and so are carried through the capillary at the same rate as the micelles and are the last to elute **[49]**.

MEKC has seldom been used in the last few years for protein analysis on chips, probably because of the binding of charged surfactants to proteins, which often results in a low efficiency separation [60]. Chip MEKC has however been widely used for small molecules such as amino acid separation. Ramsey et al. developed a 25-cm spiral separation channel on a glass microfluidic chip for high-efficiency separation of 19 fluorescently labeled amino acids using the MEKC separation technique [65]. Separation was accomplished in 165 s using sodium tetraborate-SDS buffer with 20% methanol, 770 V/cm electric field, and within 11.87 cm separation distance (Figure 2.4).

Kutter et al. [66] implemented MEKC on a glass microfluidic chip with a straight separation channel: SDS buffer system was used in the presence of organic modifier and applied for the separation of five fluorescent dyes. In a more refined approach, authors implemented a gradient generator: Two reservoirs were filled with aqueous buffer and organic solvent, respectively, and electroosmotic flow was used to pump the two solutions into the separation channel at different rates. Different gradient shapes were generated and tested. Surprisingly, whereas separation efficiencies were the same throughout the whole electropherogram between runs, plate numbers increased drastically with elution time in gradient runs.

Culbertson et al. [65] used a 50 mM SDS buffer with organic modifiers to separate amino acids in the case where free-zone electrophoresis was inefficient. MEKC reached 280 000 plates in 165 s on glass microfluidic chips.
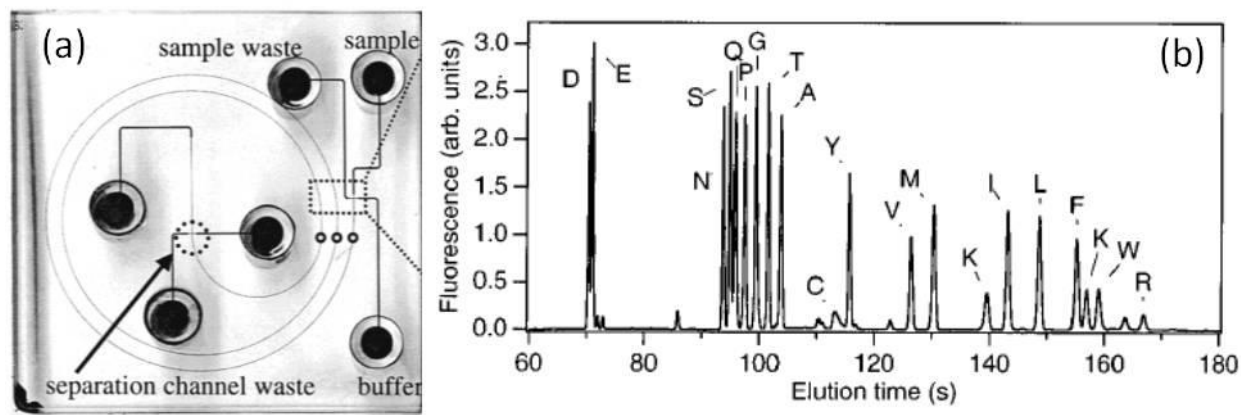
Figure 2.4 (a) Microfluidic chip scheme developed by Ramsey group for MEKC separation of Amino acids (b) Chip MEKC separation of 19 amino acids **[65]**.

2.3.3 Capillary Gel Electrophoresis

Capillary Gel Electrophoresis (CGE) is a miniaturized version of traditional slab gel electrophoresis that separates large biomolecules such as proteins and DNA fragments on the basis of size. Since capillaries dissipate heat better than slab gels, higher electric fields can be used and faster separations can be achieved in chip based format. In CGE, a technique first used by Cohen and Karger (63), the capillary is filled with a gel. There are pores within these gels, and as charged solutes migrate through a gel-filled capillary, they are separated by a molecular sieving mechanism on the basis of their sizes. Small molecules are able to pass through the pores and elute first, whereas large molecules are retarded by the gel and elute later. This is represented in Figure 2.5. Usually the capillary wall is treated to eliminate the electroosmotic flow so that the gel will not be extruded from the capillary. Solutes move through the capillary due to electrophoresis and are separated by the sieving mechanism of the gel.
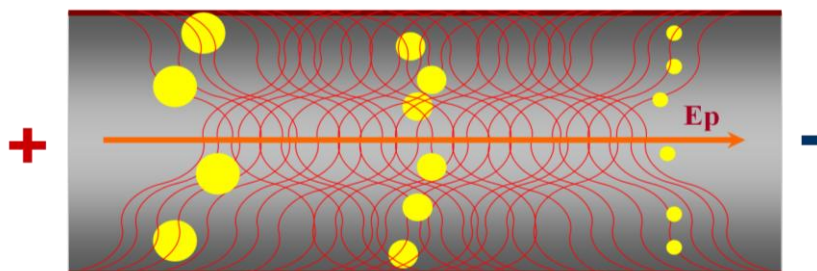
Figure 2.5 Elution order in CGE. Samples are separated by a molecular sieving mechanism on the basis of their sizes. Small molecules are able to pass through the pores and elute first, whereas larger molecules are retarded by the gel and elute later **[49]**.

There are two fundamental classes of gels for use in CGE. The physical gel obtains its porous structure by entanglement of polymers and is quite rugged to changes in the environment. Hydroxy-propyl-methyl-cellulose and similar polymers can be used to form physical gels. Chemical gels use covalent attachments to form the porous structure. These gels are less rugged, and it is difficult to change the running buffers once the gels are formed. Cross-linked polyacrylamide is usually used as the gel-forming agent in these gels. CGE can be performed on chip by introducing physical gels inside the channel or by polymerizing in situ chemical gels to yield a sieving medium [67]. Glass chips bear the strong advantage of being transparent, allowing possible in situ polymerization of the monomers (e.g., polyacrylamide gel) by direct irradiation of the channel with a UV lamp [67]. In the analysis of proteins, surfactants such as SDS are frequently added to denature proteins and to enable the separation of proteins according to their molecular sizes.

Tabuchi et al. [68] investigated the effect of protein denaturation on intensity, migration, and reproducibility, and proposed that denaturing is unnecessary for size separation analysis by microfluidic chip electrophoresis. The fact that chip CGE required only a small amount of proteins probably helped to remove the need for the denaturing procedure. By omitting the protein denaturing process, the researchers achieved protein analysis in a shorter total time and also dramatically improved the sensitivity by an order of 10−100 without compromising size determination. They also applied their method to the analysis of a real biological protein mixture from Jurkat cells during heat shock, and confirmed that the expressed proteins can be readily analyzed by the new method.

Foote et al. [69] used the CGE mode to separate a group of proteins. They concentrated the proteins on micro fabricated devices prior to separation process, using a porous silica membrane between adjacent microchannels that allowed the passage of buffer ions but excluded larger migrating molecules. They tested two basic microfluidic chip designs that allowed sample concentration either directly in the sample injector loop or within the microchannel leading from the sample reservoir to the injector. They also demonstrated the pre-concentration analysis in both coated and uncoated open channels. They obtained a full separation of the protein mixture within 300 s.

Singh et al. [67, 70] presented a multi-channel chip which allowed pre-concentration of proteins and gel electrophoresis separation in a sieving monolith cast by photo polymerization. The lack of dead volume between the two polymeric structures, the size-exclusion membrane, and the separation monolith limited the band broadening that generally arises from inhomogeneous flows (coming from the zeta potential variation and/or from perturbation at the junctions). The authors showed that the size-exclusion membrane trapped not only SDS-denatured proteins but also pure micelles. This stacking of micelles could lead to a strong concentration polarization effect, and strategies were proposed to prevent this from occurring. Finally, the system was applied to the analysis of parvalbumin, trypsin inhibitor, ovalbumin, BSA, and IgG antibodies. A general improvement in both efficiency and resolution was observed upon pre-concentration.

Herr et al. [71] developed a microfluidic chip for on-chip sodium dodecyl sulfate polyacrylamide gel electrophoresis (SDS-PAGE) of proteins. They used photolithographically patterned, cross-linked gels fabricated in situ in less than 20 minutes. The effects of sieving gel composition on the migration properties of fluorescently labeled proteins (ranging in molecular weight from 14.2 to 66 kDa) were quantified, and the ability of the gels to function as a sieving matrix for biologically relevant species was studied. High performance separations were achieved in less than 30 seconds in short lengths (4 mm), which was 100 times faster than with conventional slab gel techniques.

2.3.4 Isotachophoresis

Isotachophoresis (ITP) is a common separation technique used for stacking and separating biomolecules [72]. In this technique, there are three different zones: a leading zone of higher mobility ions (LE, leading

electrolyte), a sample zone, and a terminating zone of lower mobility ions (TE, terminating electrolyte). The sample is frequently injected between the LE and TE and, upon application of an electric field, analytes are focused between the two electrolytes. The field strength in each zone is inversely related to the ion mobility, which results in separation of sample zones in the order of decreasing mobility. Each zone is defined by a sharp steady-state boundary, and these zones are sustained by the differing field strengths.

ITP is frequently compatible with high-salt samples (including urine, spinal fluid and even seawater) and has been applied to a wide range of analytes, from small ions to proteins. While open tubular ITP was a popular electrophoresis technique prior to the use of modern CZE modes, the adjacent sample zones made detection and zone identification difficult. However, interest in ITP as a pre-concentration technique prior to other CE separations has resurged. Santiago et al. achieved 500,000-fold sensitivity improvements in ITP microfluidic chips for resolving small fluorescent dyes [73].

Lin et al. coupled ITP with CGE in a glass microfluidic chip [74]. Instead of frequent substitution of buffer vials in capillary format, automatic switching of electric fields between running buffers in the chips was performed. A 5 mm SDS-protein sample plug was focused in a double T injection with a leading electrolyte of 50 mM Tris, 0.5% SDS, 2% dithiothreitol (DTT), pH 6.8, and a tailing electrolyte of 192 mM glycine, 25 mM Tris, pH 8.3; it was then sized in polymer solution of 100 mM Tris–NaH_2PO_4, 0.1% SDS, 10% glycerol, 10% dextran, pH 8.3. All of this could be completed within 300 s with an increased detectable concentration of ~40-fold compared to the CGE mode only.

Ivory et al. [75] developed a PDMS microfluidic chip for ITP of proteins. They used a 300 μm wide and 10 μm deep PDMS channel with two T-junctions for sample loading and separation. This chip was used for separating three fluorescent proteins under a constant voltage of 100 V over a 2 cm microchannel. Protein samples were initially introduced into the microfluidic chip and were successfully stacked into the adjacent zones with an estimated concentration of 40 times higher than the initial concentration. They observed a gradual reduction of the isotachophoretic velocity during ITP at a constant voltage, which was due to decreasing current as TE occupied more of the channel. A 2-D simulation of ITP was also performed to investigate the stacking and moving boundary profiles at the T-junctions.

2.3.5 Gradient Elution Isotachophoresis (GEITP)

Gradient elution isotachophoresis (GEITP) is a mode of ITP used to achieve enrichment and separation of analytes in a single step [76, 77]. Unlike conventional ITP, GEITP does not require sequential injections and relies upon continuous electrokinetic sample injection against a hydrodynamic bulk counter-flow. Similar to ITP, GEITP utilizes a dual electrolyte system with a high mobility LE in the counter-flow, and low mobility TE in the sample (either added or inherent). At first, a high counter-flow (the sum of hydrodynamic and EOF) is applied, filling the capillary or microchannel with LE, with a small amount of LE dispersing into the sample reservoir. The applied pressure (counter-flow) is then reduced and an ionic interface is formed near the separation column inlet in the sample solution. Enrichment of the analytes occurs between the LE interface and TE in the sample. This is the same process as ITP enrichment, but is initiated off-column, allowing for large sample loading in very short separation channels. Further counter-flow reduction allows the purified analyte zones to be pulled into the separation column for detection.

Danger and Ross [78] developed a GEITP system to perform chiral separations with fluorescently labeled amino acid mixtures. Capillary lengths of 3 cm were employed, and various parameters including electrolyte pH, pressure scan rate, and chiral selector concentration were manipulated to achieve high resolution separation.

Shackman and Ross [77] developed a microfluidic system for enrichment and separation of different biomolecules using GEITP. They enclosed a 3 cm fused-silica capillary with 30 μm i.d. and 360 μm o.d. between two polycarbonate sheets. One end of the device was inserted into a sample reservoir maintained at high voltage while the other end was inserted into a buffer reservoir containing leading electrolyte buffer. The buffer reservoir was connected to a pressure controller for controlling the counter-flow velocity. This device was then used for enrichment and separation of natively fluorescent proteins as well as amino acids and DNA, in less than 7 minutes.

In another study, Shackman et al. combined GEITP with CZE in a microfluidic chip [79]. They first separated analytes with GEITP at a discontinuous ionic interface through combined electroosmotic and hydrodynamic flows. The interface and enriched analytes were then pulled into a capillary or microchannel as the counter-flow was reduced for on-column detection. To transform GEITP-focused

samples to CZE-based separation, the sample solution was replaced with CZE buffer solution while maintaining hydrodynamic flow to ensure migration toward the detector. Using this system, separation of six amino acids, with limits of detection as low as 200 fM, were achieved in a total analysis time of 11 min. A glass-based microfluidic implementation was demonstrated that could perform GEITP-CZE in 1 cm effective lengths.

2.3.6 Moving Boundary Electrophoresis (MBE)

Moving boundary electrophoresis (MBE) was the first method described for electrophoretic analysis [80] and was the most commonly used method during the 1930s and 1940s. It was developed by Tiselius in 1937, who was awarded the 1948 Nobel Prize in chemistry for the separation of colloids through electrophoresis. Tiselius employed a tube network with a central U-shaped section at the middle that could be quickly inserted or removed from the network. Protein separations were performed by filling the U-tube with the sample of interest and the rest of the network with buffer. Shifting the U-tube into place completed the electrical circuit to initiate electrophoresis and introduced a sharp initial boundary between the buffer and sample. Each analyte could then be detected as a boundary between the zone containing that analyte (sample side) and the zone without that analyte (run buffer side). Using this system, Tiselius separated human serum proteins and detected distinct concentration boundaries as species entered and migrated along a buffer-filled tube.

Recently, Herr et al. developed a microfluidic system for high performance and low power protein analysis using polyacrylamide gel moving boundary electrophoresis (PAG MBE) [81]. They used a single-inlet, single-outlet microchannel (without pumps, valves, or injectors). Injection dispersion was reduced up to 85% by using a photo-patterned-free solution polyacrylamide gel (PAG) stacking interface at the head of the MBE microchannel. The chip was used to separate various model protein samples in 5 s and in a separation distance of less than 1 mm. Yet, the electrophoretic separation was powered by a 9 V battery, which was found to be the lowest power source used in protein analysis. Figure 2.6 shows the experimental procedure.
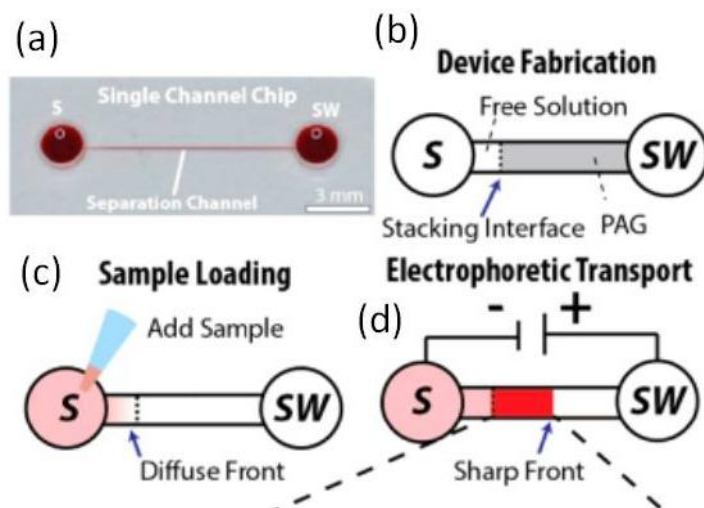
Figure 2.6 (A) Photograph of microfluidic chip scheme developed by Herr group for PAG MBE (B) Schematic illustrating the two media housed in the straight microchannel: a free-solution region abutting a PAG sieving matrix region yielding a sharp stacking interface, indicated with an arrow (C) Sample was pipette into a fluid reservoir (d) an electric field was then applied, and analytes electromigrated into the microchannel according to mobility **[81]**.

2.3.7 Gradient Elution Moving Boundary Electrophoresis (GEMBE)

Gradient elution moving boundary electrophoresis (GEMBE) was first described in 2007 [82]. GEMBE is similar to CZE, with separation based on electrophoretic mobility differences, but uses continuous sample injection and a controlled, variable counter-flow. The counter-flow can be controlled by changing the pressure applied to one end of the separation column. The analyte total velocity is a combination of the electrophoretic velocity and the counter-flow velocity. During a GEMBE separation, the counter-flow is reduced gradually, and an analyte enters the microfluidic channel for detection when its electrophoretic velocity overcomes the opposing counter-flow. This process is allowed to progress until each analyte of interest has been detected. GEMBE can use the same detectors as CZE, including UV absorption, fluorescence or conductivity. GEMBE has been successfully applied to many types of biochemical separations including proteins, DNA, and immunoassays [76, 83]. Figure 2.7 shows a schematic of the GEMBE mechanism.
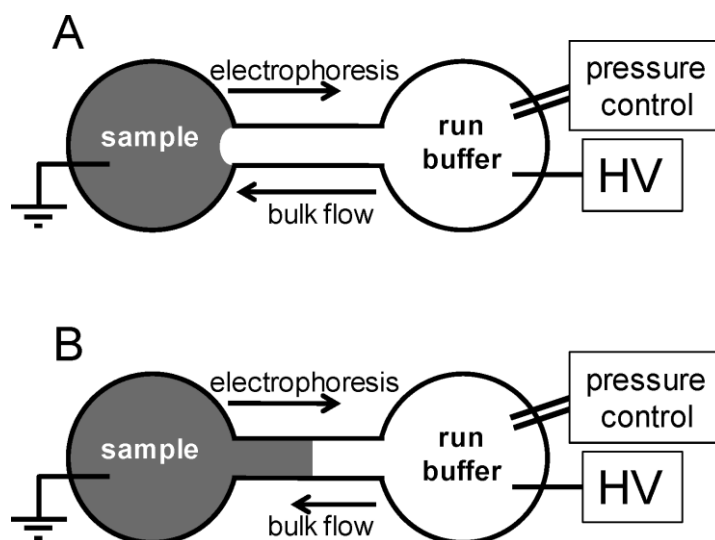
Figure 2.7 Mechanism of GEMBE (A) at high pressure, the bulk flow velocity is greater than the electrophoretic velocity of the sample analyte (B) as the applied pressure was reduced, the analyte mobility was great enough to enter the microchannel where it can be detected either optically or via changes in total current [83].

In 2008, Ross and Kralj [84] developed a GEMBE device for multiplexed electrophoresis analysis of proteins and enzymes. They used short capillaries 3 mm long, 360 μm o.d. and 5 μm i.d. both as the separation channels and as conductivity cells for detection. An array of 16 capillaries were connected to lock caps at one end and to a manifold connected to buffer reservoir at the other end and sealed using epoxy glue. High voltage and pressure control were then applied to the buffer reservoir. The current through each electrophoresis channel was monitored with a multi-channel data acquisition system connected to lock caps (Figure 2.8). Because the channels were very short, only one analyte at a time was introduced in each channel, and the measured current through each channel could therefore be used as the detector signal, with no additional detector hardware. The device was demonstrated for use with high throughput time series measurements of the activity of protein kinase A and the enzyme activity.
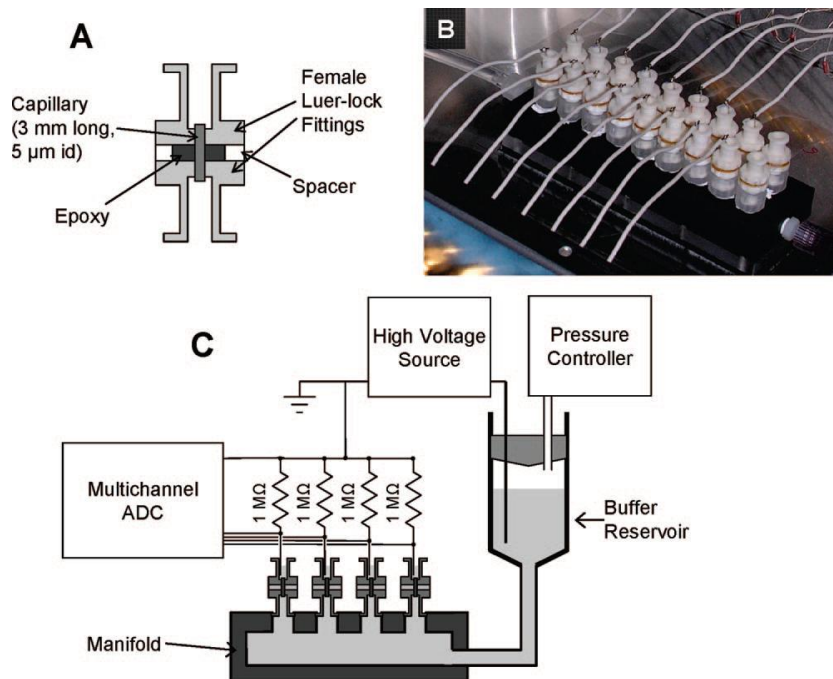
Figure 2.8 Schematic of the multiplexed system developed by Ross and Kralj. (A) Each separation capillary assembly was made of two Luer lock fittings with a 3 mm long, 5 μm i.d. and 360 μm o.d. capillary at the center. (B) The experimental setup containing an array of 16 capillaries (C) High voltage and pressure control were applied to the buffer reservoir. The current through each electrophoresis channel was monitored with a multichannel data acquisition device by measuring the voltage drop across a 1 MΩ resistor in series with each channel **[84]**.

In 2009, Ross et al. [85] developed a microfluidic device to analyse minimally prepared, complex samples containing particulates and proteins using GEMBE. A 5.5-cm fused-silica capillary with approximate outer and inner diameters of 363.5 μm and 13.5 μm was connected to plastic reservoirs through holes drilled into the sides of the reservoirs and sealed in position. A pressure controller was used to control the pressure inside the buffer reservoir while a contactless conductivity detector was used to detect the sample bands close to the capillary inlet at the sample reservoir. No sample preparation (beyond suspension or dilution in the buffer) was needed, since the sample constituents were prevented by the bulk counter-flow from entering the separation channel. The system was used for analysis of complex samples such as coal fly ash, milk, and blood serum to separate proteins and other particulates in less than 5 minutes.

In another study by the same group in 2011 [86], GEMBE was successfully applied for the analysis of whole blood and dirt to separate different anionic groups in only a few minutes. GEMBE is considered to

be one of the simplest and most capable separation techniques for proteomic analysis. Although it requires a very short microchannel or capillary to perform the separation and focusing, it has higher performance than the conventional CE and MEKC separation techniques. It can also be used to analyze complex samples with almost no sample preparation.

2.4 High Performance Focusing-Based Electrophoresis Separation Techniques

In a focusing-based separation method, different analytes are separated as they are localized and accumulated at different positions along the column. The most obvious advantage of these methods over migration-based separation methods is that with a focusing-based separation, analyte peaks become narrower and more concentrated as the separation proceeds, rather than wider and more diffused as is the case for a migration-based separation [46]. In this section, different focusing-based separation methods are addressed.

2.4.1 Capillary Isoelectric Focusing (CIEF)

Capillary isoelectric focusing (CIEF) is a powerful technique for separating proteins, peptides, and other zwitterionic biomolecules that have subtle differences in their isoelectric point (pI) – the pH at which a molecule has no charge. In this method, an axial pH gradient needs to be set up along a capillary. Under the influence of an applied electric field, samples are separated according to their different pI values [87, 88].

There are different methods for generating a pH gradient along the separation channel, the most common being to use carrier ampholytes [88]. However, because of the problems associated with carrier ampholytes such as gradient instability and poor sample loading capacity, other methods have been developed. For example, IEF with thermally generated pH gradients were studied by several groups. Pawliszyn et al. developed a system in which the temperature gradient was generated via joule heating along a tapered microchannel. They used a tapered microchannel fabricated from polyester film and glued between glass slides for focusing and separation of human, cat, and dog hemoglobin in a 25 mM Tris-HCl buffer in 6 min [89].

Immobilized pH gradients (IPG) were also used for CIEF by polymerizing cross-linked gels in capillaries [90, 91]. Sommer et al. [91] applied conventional immobilized pH gradient gels into microfluidic chips by casting a polyacrylamide gel matrix with covalently bonded acrylamido buffers (Immobilines) of different pK across the separation channel. They fabricated a glass microfluidic chip with 25 µm deep and 100 µm wide channels arranged in H geometry. To generate the pH gradient, the solutions of high pH (pH 7.0) and low pH (pH 3.8) were first injected into the chip from both ends of the channel geometry followed by the injection of monomer/Immobiline/photoinitiator solutions. After the equilibration of Immobilines along the gradient, the chip was exposed to UV light to photo-polymerize the gel containing the gradient. The chip was then used for separating several fluorescent pI markers and proteins without the addition of carrier ampholytes.

Free flow isoelectric focusing FFIEF is a derivative of CIEF in which the pH gradient is established transverse to the hydrodynamic flow by an electric field to generate a continuous separation system. In FFIEF, the sample is diluted in a carrier ampholyte solution such that a lateral pH gradient is established across the separation channel upon the application of an electric field. Analytes then separate at the outlet of the channel based on their pIs [92]. Kohlheyer et al. [93] fabricated a free flow electrophoresis micro-device with polyacrylamide barriers along the walls of the separation channel to separate the channel from the side reservoirs. These membranes restrict bulk flow while still allowing ion transport across the channel wall. The sheath flow of anolyte and catholyte was also used to help maintain a stable pH gradient by preventing diffusion of carrier ampholytes into the side reservoirs (Figure 2.9). A nearly linear pH gradient from pH 3 to 10 was generated inside 1.5 mm wide and 15 µm deep microchannels to separate several standard fluorescent markers.
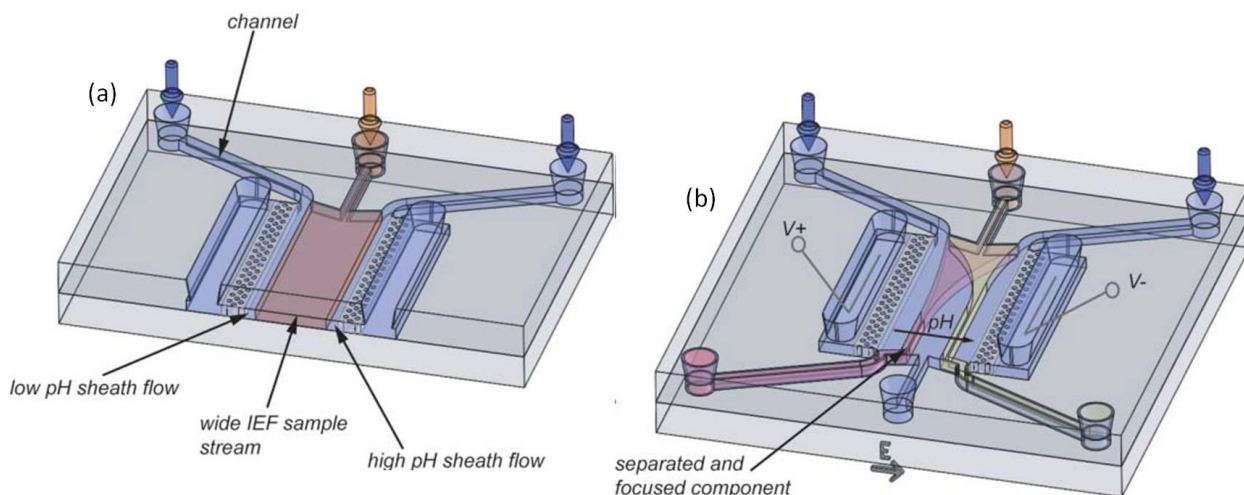
Figure 2.9 Application of free-flow isoelectric focusing: (a) a wide sample mixture with carrier ampholytes is sandwiched between two thin sheath flow streams of high and low pH values. (b) In the presence of an electrical field the ampholytes build up a linear pH gradient. Components move towards and focus at their isoelectric points **[93]**.

CIEF has been widely used for protein separation with different detection schemes, such as LIF and UV, for identifying the peaks following the separation. Many researchers used whole column imaging detection to avoid peak mobilization and dispersion [94, 35]. However, CIEF can only be used with analytes having well-defined pIs in the pH range between about 3 and 10, which, with a few exceptions, limits its use to the analysis of proteins and peptides [46]. Because of this limitation, many studies have been performed for coupling CIEF with other separation techniques (2-D separation) to achieve higher separation performances [34].

2.4.2 Counter-flow Gradient Electrofocusing Methods

Counter-flow gradient electrofocusing encompasses a family of electrophoretic separation techniques, whereby the electrophoretic motion of analytes is counter-balanced by bulk fluid flow. A key requirement for these methods is to induce an axial electrophoretic velocity gradient for each analyte so that the analyte accumulates at its unique zero velocity point and separates from other analytes as well. The major advantage of these methods is that both concentration and separation occur in one step. With

these methods, it is also possible to achieve both high resolution and low detection limits [46]. In the scanning format of these methods, the bulk counter-flow velocity varies over time. Analytes enter the channel sequentially and are focused as they traverse the temperature gradient. With this modification it is also possible to separate mixtures of several components with vastly different mobilities that cannot normally be resolved in a typical separation column at the same time [95]. The electrophoretic velocity of an analyte is given as $u_{ep} = \upsilon_{ep}E$, where υ_{ep} is the electrophoretic mobility of the analyte and E is the applied electrical field. Many methods have been developed to induce an axial electrophoretic velocity gradient along the separation column by inducing a gradient in one, or both, of the applied electrical field and electrophoretic mobility. For example, in the electric field gradient focusing method developed by Ivory et al. [96, 97], an electric field gradient is formed along the separation column; in temperature gradient focusing developed by Ross et al. [98], a temperature gradient is used that generates gradients in both electric field and electrophoretic mobility of analytes along the separation column.

2.4.2.1 Electric Field Gradient Focusing (EFGF)

Electric field gradient focusing (EFGF) uses a gradient in the electric field along the length of a separation column to generate a gradient in analyte electrophoretic mobility [46]. The electric field gradient is generated mostly by changing the cross-sectional area [99] or changing the buffer conductivity along the separation column, also known as conductivity gradient focusing (CGF) [100]. Computer-controlled arraying of individually addressable electrodes was also used to generate an electric field gradient known as dynamic field gradient focusing (DFGF) [101].

Humble et al. [99] developed a microfluidic system for EFGF with a region of changing cross-sectional area outside a fixed-width focusing channel to establish an electric field gradient. The EFGF separation channel was constructed inside an ionically conductive acrylic polymer that allowed for the transport of small buffer ions but retained proteins and other large analytes. The polymer was shaped to produce the required electric field gradient inside the separation channel (Figure 2.10). With this device, several proteins were separated and concentrated by as much as 10^4 times.
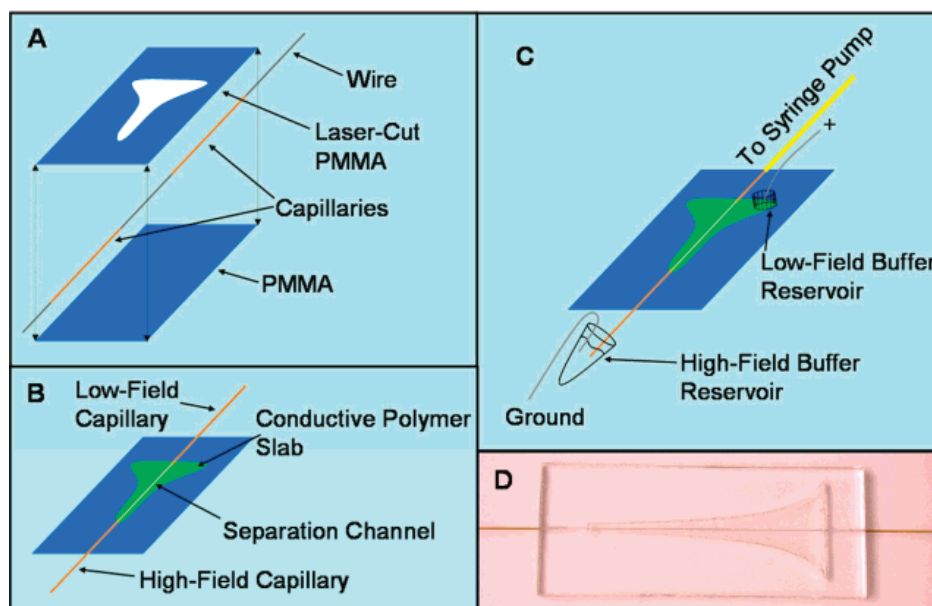
Figure 2.10 Schematics of the system developed by Humble et al. for EFGF (A) an exploded view of the components used to construct the conductive polymer-based EFGF devices (B) an assembled device (C) device with buffer reservoirs and tubing connected to the low-field capillary for syringe pump attachment (D) photograph of the actual EFGF device **[99]**.

Ivory et al. pioneered the use of a conductivity gradient along the length of the separation column to induce an electric field gradient and an electrophoretic velocity gradient, and named it conductivity gradient focusing (CGF) [96, 97]. A plastic microfluidic chip integrated with a dialysis membrane was used for separating bovine serum albumin (BSA) and bovine hemoglobin (Hb). A high-conductivity buffer was pumped through the channel on one side of the membrane and a low-conductivity buffer was pumped through on the other side. Ion diffusion across the membrane resulted in a conductivity gradient all along the channel. Application of an electric field then allowed for focusing and separation of proteins in the chamber where their electrophoretic velocity was equal to the bulk counter-flow in the gradient. They later realized that only moderate resolution of protein mixtures of BSA and hemoglobin was possible with their system, and that high resolution separations could be obtained by the addition of chromatographic packing to reduce eddy flows and Taylor dispersion.

Wang et al. [100] performed EFGF using a conductivity gradient system. In their work, the electric field gradient was formed using a dialysis hollow fiber. Fused-silica capillaries were connected to each end of a 6 cm long, 200 μm i.d. hollow dialysis fiber and the assembly was inserted coaxially inside a larger

capillary with 535 μm i.d., enabling higher conductivity buffer (100 mM Tris, pH 8.7) to be pumped through the smaller capillaries and the hollow fiber; a lower conductivity buffer (1 mM Tris, pH 8.7) was introduced through the larger capillary surrounding the exterior of the dialysis fiber. A gradient in conductivity inside the hollow fiber along its length was established as the 100 mM Tris buffer diffused to the outer capillary. A UV detector was connected to the smaller capillary at the high-field end of the device, allowing proteins to be monitored as they eluted from the hollow fiber. Using this configuration, protein focusing and pre-concentration was performed for bovine serum albumin and myoglobin.

Myers et al. [101] developed a microfluidic system for EFGF using a computer-controlled array of electrodes for controlling the electric field gradient. A PMMA chip with a 2.5 cm long, 100 μm wide, and 1 mm deep focusing channel was fabricated, while a 1 mm thick porous glass membrane separated the electrodes from the analytes, and a monolith was polymerized in the focusing channel to reduce dispersion. A syringe pump provided the opposing flow, and the electric field gradient was established by five individually controllable gold electrodes. The electrodes were in a trough with 1 mM Tris, pH 8.7 buffer, while the run buffer was 50 mM Tris, pH 8.7. On-column visualization was used for detection. With a nonlinear voltage profile, a seven protein mixture was focused and separated.

2.4.2.2 Temperature Gradient Focusing (TGF)

Temperature gradient focusing (TGF) uses a temperature gradient along the separation channel to set up a subsequent gradient in the electric field [98]. With an appropriate buffer, the temperature gradient creates a gradient in both the electric field and the electrophoretic velocity. Combined with a bulk counter-flow, ionic species concentrate at a unique point where the total velocity is zero. Figure 2.11 shows the principle of TGF separation. The critical component of TGF is a buffer that has a temperature-varying ionic strength. For most buffers, temperature changes in conductivity are associated with changes in viscosity (~2%/C). However, eletrophoretic mobility inversely depends on viscosity, which cancels out the electric field component and results in a uniform electrophoretic velocity across the channel. To induce a gradient in the electrophoretic velocity of an analyte, therefore, TGF requires a buffer solution to have temperature dependence greater than the viscous contribution. Generally, such buffers have a strongly temperature-dependent ionic strength; examples include Tris-borate [98] and Tris-phenol [102].
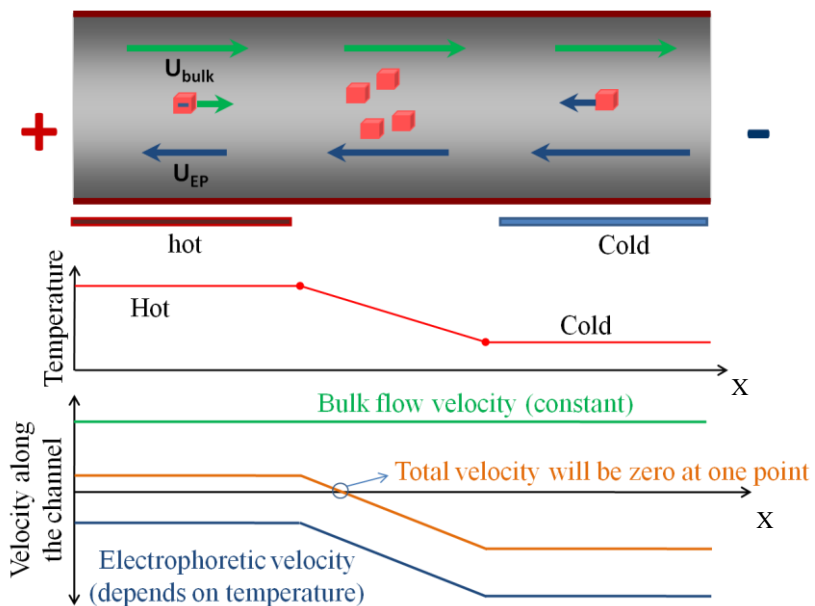
Figure 2.11 Principle of temperature gradient focusing (TGF)

Scanning TGF is a modification of the initial TGF method in which the bulk counter-flow velocity varies over time. In this case, analyte peaks enter the channel sequentially and are focused as they traverse the gradient. Fixed point detection is used at the end of the separation channel to measure the elution time of each analyte [95]. With scanning TGF, it is possible to separate mixtures of several components with vastly different mobilities that cannot normally be separated at the same time. TGF was first introduced by Ross et al. [98], and its variants have been successfully applied to separate amino acids [103, 98], proteins [98], DNA hybridization [102], and chiral separations [104]. Figure 2.12 shows the experimental setup of TGF used for separating different kinds of samples.

30
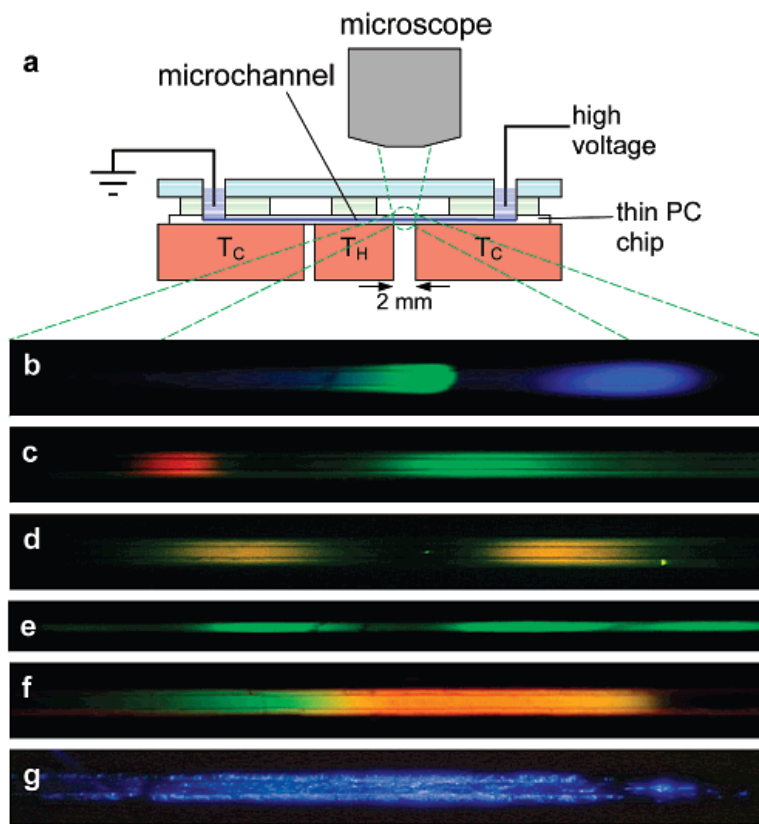
Figure 2.12 Demonstration of focusing and separation of a variety of different analytes using TGF. (a) Schematic drawing of the apparatus. The total length of each separation image is 1.9 mm. (b) Oregon Green 488 carboxylic acid and Cascade Blue hydrazide (c) The two products resulting from labeling of aspartic acid with FQ (d) Mixture of CBQCA-labeled serine and tyrosine (e) Green fluorescence protein (f) Fluorescein and TAMRA labeled DNA (g) 6 mm diameter fluorescently labeled polystyrene particles **[98]**.

More recently, Matsui et al. used a PDMS/glass hybrid microfluidic chip to perform TGF experiments. They concentrated Oregon Green 488 carboxylic acid to approximately 30 times higher than the initial concentration in 45 s at moderate electric strength of 70 V/cm and a temperature gradient of 55 °C across the PDMS/glass hybrid microfluidic chip with a 1 cm long capillary [105].

A few analytical studies have been published about TGF. The initial theoretical description of TGF was generalized by Ghosal and Horek to include axial gradients in other buffer properties and to take into account the increased band-broadening caused by Taylor dispersion from induced pressure gradients [106]. They also investigated the time evolution of the position and width of an analyte peak as they approach their steady state values. Huber and Santiago investigated the peak asymmetry caused by

induced pressure gradients in the Taylor-Aris regime and found excellent agreement between experimental measurements and their theoretical description [107].

2.4.2.3 Micellar Affinity Gradient Focusing (MAGF)

Micellar affinity gradient focusing (MAGF) [108, 109] is a microfluidic counter-flow gradient focusing technique which can separate charged, neutral, and hydrophobic analytes. MAGF combines the concepts of temperature gradient focusing (TGF) and micellar electrokinetic chromatography (MEKC). The method works by creating a gradient in the interaction strength (retention factor) between the analytes and micelles inside the separation channel. In the region of high retention, the analyte is located within the micelles and thus moves with the electrophoretic velocity of the micelles. In the region of low retention, the analyte is free and moves at its own natural mobility. In a typical MAGF separation, micelles are forced to electrophoretically migrate from a region of high retention to a region of low retention. This migration is then opposed by a counteracting bulk flow, eventually causing ionic and neutral species to concentrate at a unique point where the total velocity sums to zero [108].

The gradient in retention factor for MAGF is usually formed by applying a temperature gradient along the separation channel. The retention factor depends on two parameters: the distribution coefficient and the phase ratio. The distribution coefficient is a measure of the affinity of an analyte to partition into the hydrophobic interior of the micelle. The phase ratio is the ratio of the volume occupied by the micellar phase to the volume of the mobile phase, and therefore depends on the critical micelle concentration (CMC). Both of these terms can be temperature dependent. However, since the critical micelle concentration of most surfactant solutions is temperature dependent, the retention factor gradient can be established through the phase ratio via a temperature gradient [108]. MAGF can be accomplished in any buffer capable of supporting micelle formation [109].

MAGF can be used in a scanning format for simultaneous concentration and separation of complex mixtures by varying the bulk counter-flow velocity over time. Different analytes are focused and separated as they traverse the gradient, while fixed point detection is used at the end of the separation channel to measure the elution time of each analyte.

Kamande et al. [109] investigated the use of polymeric surfactants as the pseudostationary phase in MAGF. These covalently linked molecular micelles have several advantages over traditional surfactants like SDS, such as elimination of monomer-aggregate dynamic equilibriums, lower working concentrations due to the exclusion of a CMC, and the ability to support higher organic solvent within the medium. Using poly (sodium undecenyl sulfate) and a scanning mode of MAGF, quantitative concentration and separation of three Coumarin dyes was accomplished, with a focusing rate of 10 to 25-fold per minute within a 2 mm gradient.

2.5 Multi-Dimensional Separations

The peak capacity of a separation, *P*, describes the maximum number of components that can be resolved in any given separation [110]. The peak capacity of a single CE procedure by itself is usually not adequate for resolving complex mixtures. Therefore, attempts have been made using different CE modes in combination as (multi-dimensional separations) to achieve the required peak capacity for complex separations [111, 112]. A requirement of any successful multi-dimensional procedure is orthogonality, which means that the selected dimensions possess different, but compatible, separation mechanisms. Furthermore, a subsequent dimension in any multi-dimensional separation should not destroy the resolution achieved by a previous one [111]. The peak capacity of a multi-dimensional separation is the product of peak capacities of its constituent one-dimensional (1-D) methods (P_1 to P_n). This definition is valid only when the modes of separation are completely orthogonal [111]. This condition is rarely fulfilled, however, limiting the overall peak capacity of most multi-dimensional separations. The interfacing of two-dimensional (2-D) column-based separations, which is typically used for proteomics analyses, can be performed off-line or on-line [113]. The on-line coupled 2-D systems offer many advantages, such as minimizing the loss of analyte due to nonspecific adsorption to the walls of small-volume transfer containers, which are used with many off-line 2-D methods [114].

Moreover, poor reproducibility can result in off-line methods due to the manual sample transfer from the first to the second dimension, and peaks generated in the first dimension can be lost due to the transfer step if the transfer volume is not kept smaller than the peak volume [34]. It is obvious that microfluidic chips are good candidates as platforms for multi-dimensional analyses since they allow fluidic

connections with minimal dead volumes. The critical points when performing multi-dimensional separations in microfluidic chips are: (i) the compatibility between the buffers used for the different dimensions; (ii) the speed of the separation – for a direct coupling for instance, the second dimension has to be faster than the previous one; (iii) the ability to introduce multiple different separation media into one single microfluidic system; and (iv) the quantitative transfer of focused samples from the first to the second separation dimensions without significant loss in the resolution acquired from the first dimension. Recently, investigators have reported several on-line two-dimensional separations, which offer high column efficiencies and favorable resolution compared with single CE modes.

In 2000, Ramsey et al. first coupled MEKC (the first dimension) with CZE (the second dimension) on a glass microfluidic chip [115]. Gated injection was implemented for CZE injection, and the electric valve was switched for 0.3 s every 3–4 s to inject samples of effluent from the first dimension into the second dimension. Their system offered a peak capacity of 500–1000.

In 2003, the same team presented an optimized MEKC-CE glass microfluidic chip [58] with a similar principle: a 19.6 cm long MEKC channel was coupled to a 1.3 cm long CE channel, as shown in Figure 2.13-a. By improving the sampling rate of the CE separation, an impressive peak capacity of 4200 in less than 15 min was achieved. It was found that the efficiency of separation using serpentine devices with uniform channel cross sections suffers from a non-uniform axial electric field in the turns and an unequal path length along the inner and outer walls of the turns. This "racetrack" effect skews bands, resulting in reduced separation performance [116, 117]. In their study, they improved the performance of their microfluidic chip device for two-dimensional separations by incorporating asymmetric turns, faster sample injection of the first dimension effluent, and a decrease in the second-dimension injection plug length. The schematic of an asymmetric turn used is shown in Figure 2.13-b. To demonstrate the improved performance capabilities, the device was used to identify a peptide of an ovalbumin tryptic digest and to compare tryptic digests of human and bovine hemoglobin.
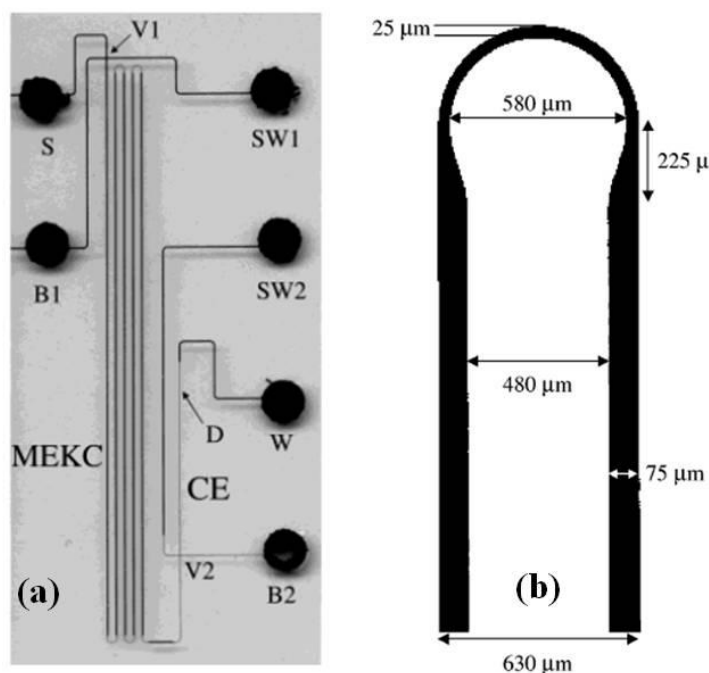
Figure 2.13 (a) Image of a microfluidic chip with a serpentine channel for two-dimensional separations. Injections were made at valve 1 (V1) for the first dimension MEKC separation and at valve 2 (V2) for the second dimension CE separation. The sample was detected 1 cm downstream from V2 at point D using laser-induced fluorescence. The reservoirs are labeled sample (S), buffer 1 (B1), sample waste 1 (SW1), buffer 2 (B2), sample waste (SW2), and waste (W). (b) Image of an asymmetric turn to avoid band broadening at the turns. The dimensions are indicated on the figure and are taken from the top of the channel **[58]**.

In 2003, Herr et al. [118] designed a PMMA chip to couple IEF with CE. IEF was run in the main channel with residual EOF, so that focusing and mobilization occur at the same time, and the CE sampling was done in an orthogonal channel, as shown in Figure 2.14. This design geometry yielded a 2-D analysis of nearly 100% of the first dimension volume. The IEF dimension showed rapid peak generation (around 1 min) and pre-concentration (70-fold), leading therefore to a high peak capacity of 1300 for the 2-D system. In their work, only a limited portion of the IEF channel was sampled in the CE dimension, so that the separation time for a complex mixture was estimated to be around an hour. The coupling of IEF with CE allowed the focused peaks to be parked while running the second dimension, as well as injection of all focused analytes in the second dimension. The associated drawback was that the first dimension was stopped during three quarters of the total separation time. The system was used for separating fluorescent species, and the 2-D on-chip separation was compared with independent relevant 1-D on-chip separations.

35
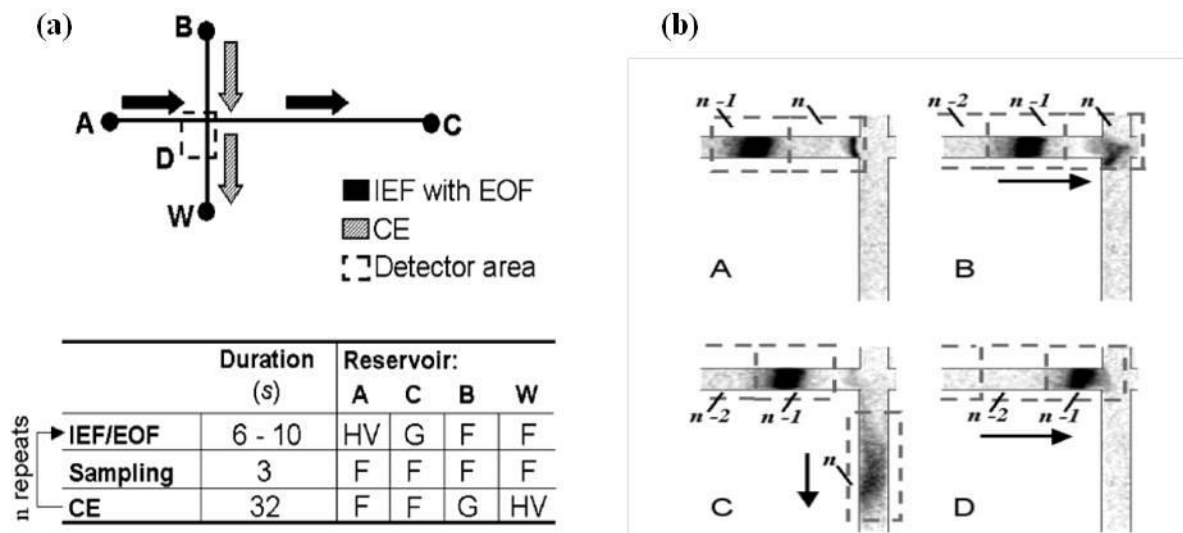
Figure 2.14 (a) Separation algorithm for the 2-D IEF-CE separation. The device geometry is shown with arrows indicating the sample motion during each serial separation step. The first dimension (IEF) extends from reservoir A (anolyte) to reservoir C (catholyte). The second dimension (CE) extends from reservoir B (buffer) to reservoir W (waste). The imaged area is indicated by the dashed box, D. The voltage applied during each step of the 2-D separation is shown in the table (HV, high voltage; G, ground; F, float). (b) CCD images during species sampling. (A) Species are focused by IEF in the first dimension (dark bands in horizontal channel). Simultaneously, the bands are mobilized toward the catholyte reservoir by low-dispersion EOF. (B) Once a fluid volume of interest, n, reach the microchannel intersection, all electrodes are switched to electrically float for 3 s. (C) High voltage is then applied at reservoir B and reservoir W is grounded, initiating sample separation in the second dimension. (D) Upon completion of the CE separation, IEF/EOF is reinitiated causing sample species to refocus and the next fluidic volume (n- 1) to migrate to the intersection. This sequence is repeated until all fluidic volumes are sampled from first dimension into the second **[118]** .

In 2006, Shadpour and Soper integrated MEKC and capillary gel electrophoresis (CGE) on a single PMMA device, achieving a peak capacity of 1121 [119]. SDS was introduced as a denaturing agent in the gel electrophoresis dimension. In a unique setup, gel electrophoresis served as the first dimension of separation before the analyte was repetitively transferred into a 10 mm MEKC separation channel. The CGE-MEKC sequence was chosen because MEKC separations were significantly faster than the SDS microfluidic chip CGE separations. The gel sieving matrix for CGE reduced the band diffusion that occurs in comparison to free solution MEKC, which helped maintain tight band widths and maximum resolution when first dimensional species were parked for sampling. The authors used a comprehensive data collection technique. Sampling of analyte from the first dimension into the second dimension was carefully controlled by current or voltage control via a programmable multi-channel high power voltage supply. In this manner, the electrokinetic direction of flow was diverted through gates which opened and

36

closed to control sampling into the second dimension. Peak capacity in the CGE separation was 19, while for the MEKC dimension was 59. In the analysis of a mixture of ten different proteins, the SR was calculated to be 2.8 and 4.9 for the CGE and MEKC separations, respectively. The sample plug from CGE was loaded into MEKC for 0.5 s with a cycle of 10.5 s. A schematic of the system configuration is shown in Figure 2.15.
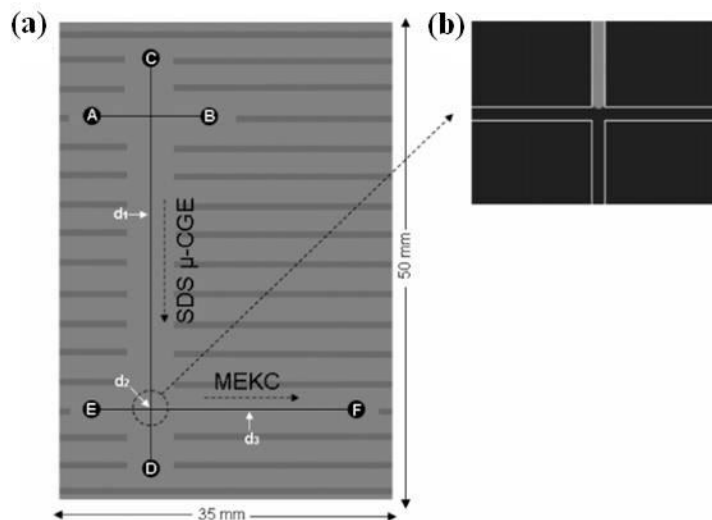
Figure 2.15 (a) Geometrical layout of the chip used for 1-D and 2-D separations. The chip was fabricated using hot embossing from a brass master into PMMA: with a channel width of 20 μm and a channel depth of 50 μm. Solution reservoirs: (A) sample reservoir, (B) sample waste reservoir, (C) SDS μ-CGE buffer reservoir, (D) SDS μ- CGE buffer waste reservoir, (E) MEKC buffer reservoir, and (F) MEKC buffer waste reservoir. (b) Fluorescence image of the sieving matrix/MEKC interface at the intersection of the SDS μ-CGE and MEKC dimensions. The fluorescence was generated by seeding the sieving matrix with fluorescein **[119]**.

In 2004, Devoe et al. integrated denaturing IEF and SDS electrophoresis in a microfluidic channel network fabricated in polycarbonate, and demonstrated the importance of separation media (Figure 2.16). The authors used different separation media in each separation dimension. A peak capacity of ~1700 was achieved using a chip with planar dimensions of 2 cm $\times$ 3 cm with capacities of approximately 10 and 170 for the IEF and CE separations, respectively [120]. Heart cutting methods work especially well with microfluidic devices for IEF-CE, as IEF-focused protein bands remain immobilized once the bands have reached their respective isoelectric points, and, therefore, many of the technical challenges that come with sampling a migrating analyte peak can be avoided. In their work, once the IEF focusing was complete, the focused proteins were simultaneously transferred using an electrokinetic method from the first dimension

microchannel into an array of second dimension microchannels for achieving parallel size-dependent separations using SDS gel electrophoresis. The use of non-native IEF further prepared denatured protein analytes for rapid and effective formation of SDS-protein complexes as required for performing electrokinetic transfer between the coupled separation dimensions and SDS gel electrophoresis.
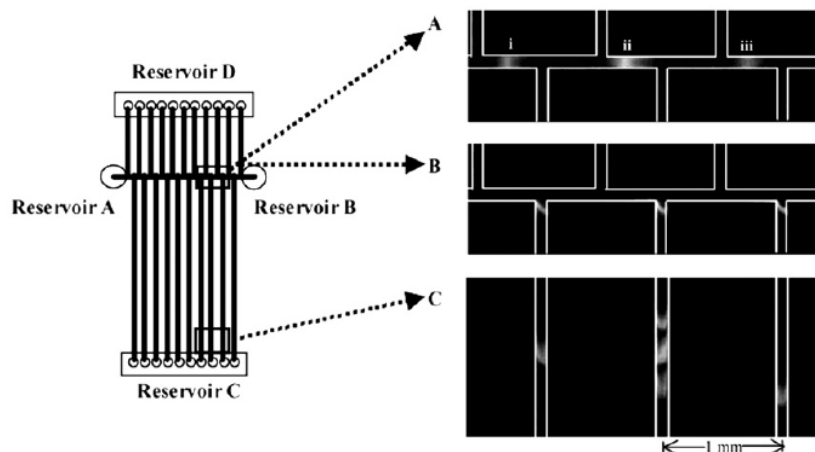
Figure 2.16 Fluorescent images of on-chip 2-D separation of five model proteins using multiple separation media. (A) Non-native IEF with focusing order of (i) actin, (ii) bovine serum albumin, ovalbumin, and trypsin inhibitor, and (iii) parvalbumin from left to right; (B) electrokinetic transfer of focused proteins; (C) SDS gel electrophoresis. Images were captured at 90 s following the initiation of IEF or SDS gel electrophoresis separations. Images were obtained using either green fluorescence of protein-fluorescein conjugates in IEF or red fluorescence of Sypro red labeled proteins during electrokinetic transfer and size-based separations **[120]**.

In a later study, in 2008, the same group tried to improve the performance of their 2-D configuration by avoiding non-uniform sample transfer between the dimensions, sample leakage, and injection plug tailing within the second dimension array during the separation [121]. In their work, numerical and analytical models suggested an optimized chip design which combined multi-dimensional back biasing and angled channel geometry to ensure leakage-free and uniform sample transfer, while minimizing the injected sample plug lengths. The optimized design was then validated experimentally using a multi-dimensional chip containing five second-dimension channels.

In 2009, the same team presented an optimized design for 2-D protein separation with the same principle [122]. In their work, a two-dimensional microfluidic system was presented for protein separation

combining isoelectric focusing (IEF) and sodium dodecyl sulfate (SDS) polyacrylamide gel electrophoresis (PAGE) using in situ photo-polymerized polyacrylamide (PAAm) gels. The IEF channel possessed an angled geometry which had been shown to minimize sample tailing in multi-dimensional microfluidic systems [121]. Additionally, the chip design employed optimized back-biasing channels which eliminated sample leakage and enabled uniform sample transfer between the separation dimensions. This was found to be essential for eliminating injection current variations which were previously degraded the overall separation resolution and the uniformity of sample bands within the second dimension. Validation of the full 2-D system was presented using fluorescently labeled E. coli cell lysate, including a comparison between chip designs containing 10 and 20 parallel SDS-PAGE microchannels. In the optimized design, The PAAm gels were used for multiple functions. In addition to serving as a highly-resolving separation medium for gel electrophoresis, discrete polyacrylamide gel plugs were used to enable the efficient isolation of different on-chip media including anolyte, catholyte, and sample/ampholyte solutions for IEF. The gel plugs were demonstrated as on-chip reagent containers, holding defined quantities of SDS for on-chip SDS-protein complexation, and enabling the use of a discontinuous buffer system for sample band sharpening during SDS-PAGE. Figure 2.17 represents the chip design and separation results from their study.
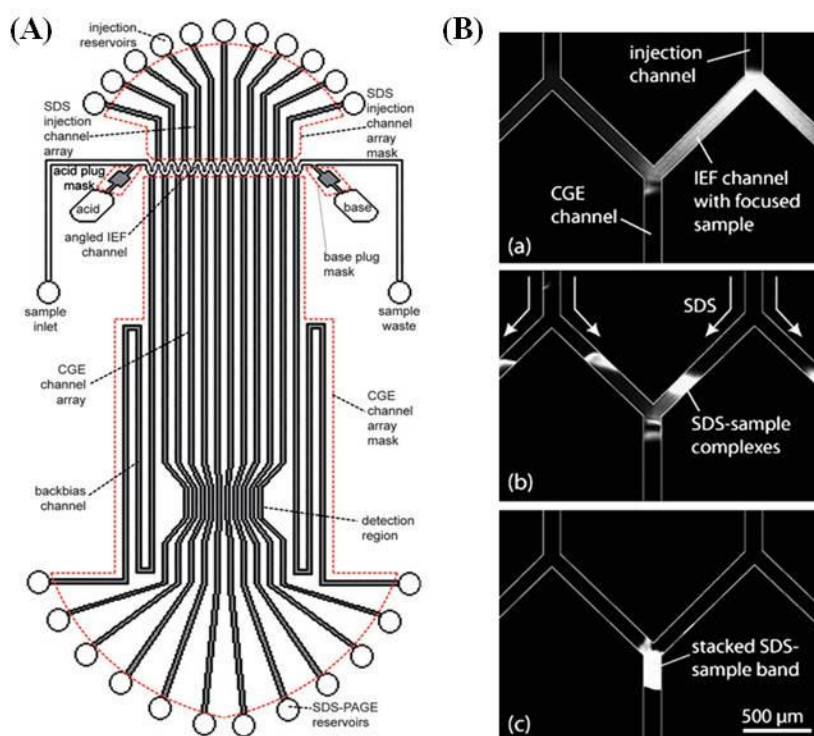
Figure 2.17 (A) Schematic of an IEF/SDS–PAGE separation chip combining PAAm sieving gel and gel plugs, an angled IEF channel design, and back biasing channels. Photolithography masks used for patterning each of the gel regions are shown (dashed contours). (B) Transfer of focused proteins showing (a) initial mobilization of SDS from the injection channels into the IEF channel, (b) real-time SDS–protein complexation, and (c) complete and uniform transfer of SDS–protein complexes to the SDS–PAGE dimension **[122]** .

Recently, Ross et al. [123] developed a simple two-dimensional microfluidic system by combining GEMBE and CZE as first and second dimensions. In their work, a glass microfluidic chip with 30 μm wide and 7 μm deep channels in a cross configuration were fabricated. The GEMBE separation took place in what would normally be the sample input arm of the chip, and analytes were transferred from the GEMBE channel to the CZE channel at the injection cross (Figure 2.18). The system was then used for chiral separations of a mixture of amino acids, and showed that the peak capacity can be improved by a factor of 3 compared with a one-dimensional CZE separation.
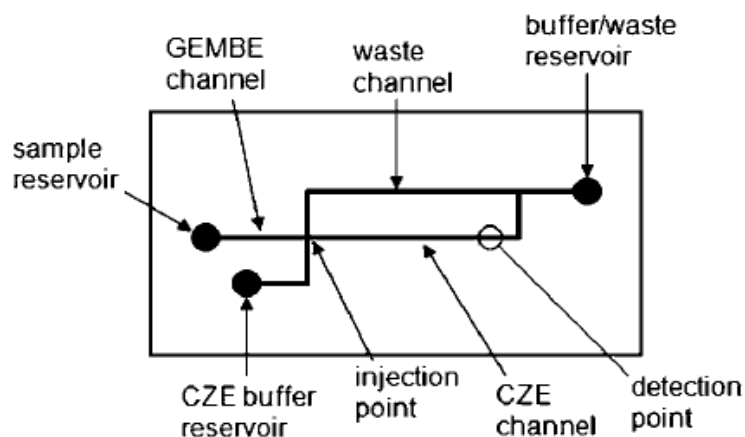
Figure 2.18 Schematic of the 2-D separation chip. Sample is loaded into the sample reservoir, and CZE buffer is loaded into the CZE buffer reservoir. Pressure control is applied to the buffer/waste reservoir. Negative high voltage is applied to the buffer/waste reservoir; the sample reservoir is grounded; and the CZE buffer reservoir is connected via a computer controlled high voltage to either ground or to a smaller, positive high voltage **[123]**.

Davis et al. [79] developed a microfluidic system that combined GEITP and CZE for separating complex mixtures. In their work, an 11 cm long capillary with 25 μm i.d. and 360 μm o.d. was first connected to sample and waste reservoirs. The sample reservoir contained the sample and TE buffer, while the waste reservoir contained the LE buffer and was connected to a pressure controller. Experiments were started by applying a high pressure to the separation column causing LE to disperse into sample reservoir by a relatively high bulk flow rate. The pressure was then gradually reduced and the analytes were enriched between LE and TE. By further decreasing the pressure, the enriched zones were introduced into the separation column. At that time, the applied pressure and voltage were discontinued, and LE replaced the TE and sample solution. The separation was then continued by applying voltage and analytes further separated based on their respective electrophoretic mobilities. The setup was also used to separate a mixture of fluorescently labeled amino acids.

2.6 Detection Systems

2.6.1 Fluorescent Detection

Fluorescent detection is the most common detection method in chip-based electrophoresis separations. Fluorescence is the emission of light by a substance that has absorbed light or other electromagnetic radiation. Fluorescence is used to illuminate a desired region of fluid or material to distinguish it from the surrounding medium. Each type of fluorophore, a fluorescent molecule, has a characteristic range of excitation frequencies at which they are excited to a higher level of energy upon exposure. At this excited S2 state, some energy is lost due to vibration, and the molecule rapidly moves into the lower energy S1 state. At this time the molecule returns to its initial ground state and releases a photon. Due to the energy losses, emission occurs at a longer wavelength (lower frequency) than the excitation spectrum. This difference in peak frequencies is called the Stokes shift, illustrated in Figure 2.19, and the time delay is called the emission time delay.
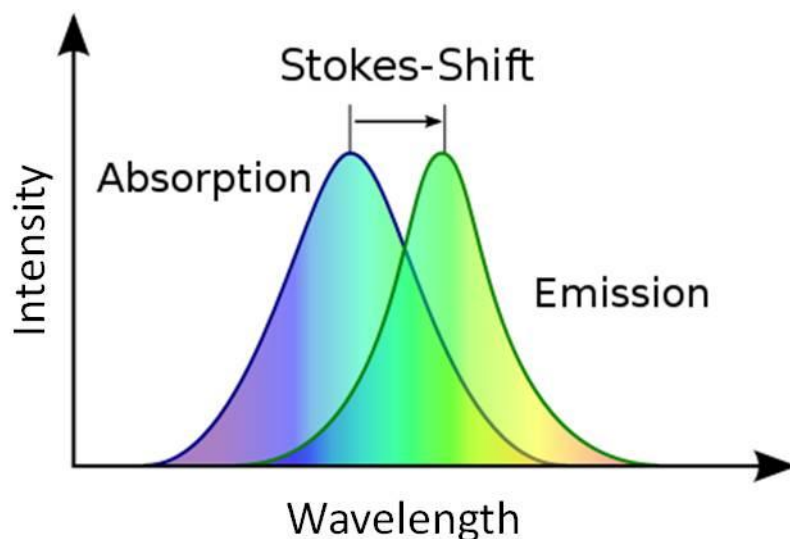
Figure 2.19 Illustration of the absorption and emission spectra for a fluorescent material. The peak intensities are separated by the Stokes shift.

A fluorescence microscope is any microscope that uses fluorescence to generate an image. All fluorescence microscopy methods share the same principle. A sample is illuminated with light of a wavelength that excites fluorescence in the sample. The fluoresced light, which is usually at a longer wavelength than the illumination, is then imaged through a microscope objective. Two filters are normally used in this technique: an illumination (or excitation) filter which ensures the illumination is at the correct wavelength, and a second emission (or barrier) filter which ensures none of the excitation light source reaches the detector. These functions may both be accomplished by a single dichroic filter. Fluorescent labels are generally used for detecting a protein or other labeled molecules with a fluorescence microscope. Fluorescent labelling is the process of covalently attaching a fluorophore to another molecule, such as a protein or nucleic acid. This is generally accomplished using a reactive derivative of the fluorophore that selectively binds to a functional group contained in the target molecule. The most commonly labeled molecules are antibodies, proteins, amino acids and peptides which are then used as specific probes for detecting a particular target [98]. Common functional groups used in fluorescent labeling include isothiocyanate derivatives such as FITC and TRITC (derivatives of fluorescein and rhodamine) which are reactive towards primary amines to form a thioureido linkage, and maleimide activated fluorophores such as fluorescein-5-maleimide, which react with sulfhydryl groups. The sulfhydryl group adds to the double bond of the maleimide.

2.6.2 UV detection

Ultraviolet detection and measurement technology can vary with the part of the spectrum under consideration. Ultraviolet light can be detected by suitable photodiodes and photocathodes, which can be tailored to be sensitive to different parts of the UV spectrum. A variety of detector options exist for UV detection between 200 and 400 nm. Proteins strongly absorb UV at 280 nm due to a number of their constituent amino acids. By using a UV microscope or micro spectrophotometer equipped for UV imaging, the sample containing the protein is imaged with 280 nm light. The protein absorbs this light more strongly than the surround sample, appears darker, and can be detected within the channel. This technique can also be used to determine protein concentrations and the relative amounts of protein to DNA or RNA. UV detection has been widely used for detecting the protein peaks in microfluidic systems [35].

2.7 Summary

The use of microfluidic technology for miniaturizing biomedical devices has been successfully demonstrated and commercialized for a variety of processes. The advantages of the chips or capillary systems over the conventional systems are the extremely small sample volume requirement, shorter analysis time, lower fabrication costs, improved sensitivity, portability and higher throughput. Electrophoresis separation plays a major role in molecular biology with the purpose of identifying and studying different biochemical samples and has been extensively used in Lab-on-a-chip devices.

There are many different types of electrophoresis, and each can be used for something different. Electrophoresis separation can be migration-based in which movement of analytes with different velocities causes the separation, or focusing-based in which different analytes focus and separate at their different zero velocity points along the separation column. Two-dimensional separations are usually used for finger printing, and when high efficiency is needed for separating complex mixtures.

Although a wide variety of designs and mechanisms have been reported for electrophoresis separation in microfluidic systems, optimization of the designs and mechanisms has not been widely studied. Higher efficiencies can still be achieved by improvements to the function, speed, and accuracy of the mechanisms, detection sensitivity, and controlling functions.

Chapter 3

Fabrication Methods and Experimental Setup

In this chapter, the experimental aspects of the thesis, as well as the equipment and procedures used, are detailed. The topics include experimental setup, materials, and techniques used for fabricating chips and performing separation experiments.

3.1 Experimental Setup

Detection system

In this research, a fluorescence microscopy system was used for sample imaging. An inverted microscope (GX-71, Olympus) with numerous dry objectives was used in various studies. The choice of the microscope objective depends on the size of the area of interest in the sample. Light illumination was performed with a 100 W halogen lamp mounted on the back of the microscope. The microscope was equipped with two Olympus filter cubes for the purpose of fluorescence imaging. Filter cubes generate a solitary band of excitation light that corresponds to the excitation and emission spectra of the fluorescent samples. The filter cubes consist of an excitation band pass filter, a long pass dichroic mirror, and an emission long pass filter. The BSWM Olympus filter cube has BP450-480 nm excitation, DM500 nm dichroic mirror, and BA515 nm long pass emission. The GSWM filter cube has BP510-550 nm excitation, LP570 nm dichroic mirror, and BA590 nm long pass emission. A mercury arc lamp is also used for fluorescence imaging in the microscope.

The imaging of the samples was performed with a CCD camera (Cool SNAP ES, 1392×1040 pixels) coupled to the microscope. The camera can acquire images at 10 frames per second in full-scale and full-depth operating conditions. The CCD sensor has 6.45×6.45 μm pixels with an imaging area of 8.77×6.6 mm and a 12 bit image depth to quantify both low and high level signals in the same image. Figure 3.1 shows a schematic of the GX-71 microscopy system.
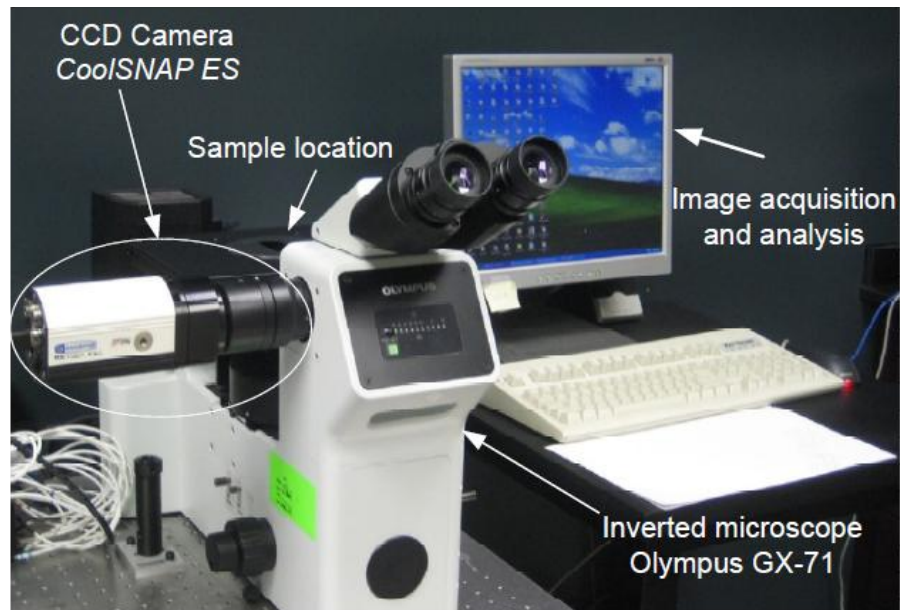
Figure 3.1 Schematic of the GX-71 fluorescent microscopy system

The image capturing and analysis was carried out with the Image-pro Plus software (Media Cybernetics). Intensity line profiling, particle tracking, data filtering, image level adjusting, and spatial measuring were commonly executed in Image Pro-Plus.

HV power sequencer

For any electrophoresis separation technique, an electric field needs to be applied along the separation channel. A Labsmith HVS448-3000 power sequencer was used for all the experiments to apply the required high voltages to the chips. The high voltage system has eight independent channels, each capable of supplying a maximum of 3000 V. The corresponding sequence software allows the channel levels to be changed manually in real time or programmed for more complex sequences. Current and voltage monitoring during experiments provides authentication of the applied potential field and helps in the discovery of system irregularities, which generally indicates disconnected electrodes or the presence of bubbles in the channels.

Samples and Buffers

Sample preparation steps are of great importance in achieving high sensitivity and specificity in any separation technique. The enrichment of the target analyte and the removal of inhibitors are two main strategies in this regard. Filters are a cost-effective and straightforward way for the rapid removal of inhibitors and insoluble particles from samples. The samples and buffers were filtered using a 0.2 μm pore size cellulose acetate syringe filter (Sartorius, Gottingen, Germany) before the experiments. Different buffers are used for different kinds of electrophoresis separation techniques. These buffers can be prepared inside the lab or directly from chemical companies. The pH of the buffer can be measured using a pH electrode. Most of the sample analytes used in this research were fluorescently labeled and were detected with the fluorescent microscopy system. Labeling of the analytes can be performed by standard lab procedures.

3.2 Device Fabrication by Soft Lithography

In this section, the basic principles of soft lithography process for fabricating multi-level polydimethylsiloxane (PDMS) devices as it is applied in this work are provided. The process begins with designing a photo mask containing the negative image of the microchannel layout. Photo masks are designed in AutoCAD and printed commercially on Mylar films with 20 k dpi resolution (CAD/Art Services). After the photo mask is received, the first step is to fabricate a reliable master for molding the PDMS microchannels. Masters are fabricated from the negative photoresist SU-8 on 4 inch silicon wafers. Three microscope-slide-size designs can fit onto one master. To fabricate the master, first the wafer (Montco Silicon, Spring-City) is dehydrated at 200 °C for 20 minutes over a hotplate. After that the wafer is cooled down to room temperature for 10 minutes.

SU-8 is spin-coated onto the silicon wafer using a spin-coating system (200 CB, Brewer Science). The thickness of the film defines the height of the microchannel and is controlled by the type of SU-8 and the spin-coating conditions such as speed and time. A layer between 1-500 μm can be deposited in a single coat. SU-8 is deposited dynamically (as the wafer is spinning) using a precision pneumatic dispensing system (Ultra 1400, Engineered Fluid Dispensing). Afterwards a soft bake is performed at 65 °C and at 95 °C on a set of level hot plates to evaporate the solvent in the photoresist and harden the film. Prior to

fabricating the multi-layer structures, SU-8 adhesion layer is usually spin-coated on the wafer with a thickness of 5 μm using SU-8 2005. This layer helps the permanent adhesion of the profiles on the wafer.

To fabricate the design, the wafer is placed in a UV exposure system (Newport) and covered with the photo mask containing the design. A vacuum mask aligner (Newport, Stratford) is used to ensure that the design is transferred on the wafer with high accuracy.

Next, the assembly is illuminated with UV light (~365nm) with the appropriate dosage where exposed regions undergo photo-polymerization and begin to cross-link. A post exposure bake at 65 °C and at 95 °C follows to complete the cross linking. The process of spin-coating, soft bake, exposure and post exposure bake can be repeated for multiple layers to produce multi-level structures. When all the layers are completed the master is placed in a large bath of SU-8 developer to dissolve the unexposed SU-8 regions. The wafer is then washed with clean SU-8 developer, isopropyl alcohol and deionized water followed by blow drying with nitrogen. To keep the photoresist from peeling off a small amount of glue (Loctite 3311) is placed around the edge of the wafer and hardened with UV light. After the master is fabricated the dimensions of the microchannels can be measured using a contact profiler (SJ-400, Mitutoyo). Figure 3.2 illustrates the steps in the soft lithography technique [2].
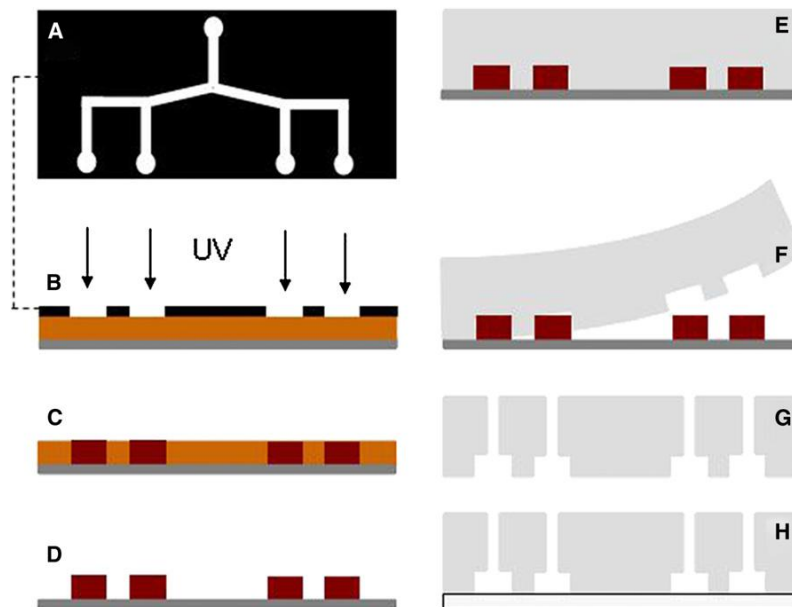
Figure 3.2 Schematic of the fabricating steps of microfluidic chips using soft lithography **[2]**

Next, the relief structures on the SU-8 master are molded in PDMS. PDMS is mixed in a ratio of base-to-curing agent of typically 10:1 by weight, and degassed in a vacuum oven to remove bubbles created when mixing. The master is placed in an aluminum dish and the PDMS is poured over the top and cured at 95 °C for 2 hours. After the mold cools, it is cut out and trimmed, and fluidic access holes are punched using a biopsy punch with a diameter that matches the tubing that connects to the chip. To complete the chip, the PDMS mold is bonded to another substrate – glass, PDMS, quartz, silicon – by oxygen plasma treatment. The system used is the PDC-001 plasma-cleaner (Harrick Plasma, Ithaca, NY). The common plasma treatment protocol is 29.6 W for 30 s. The two substrates are then placed in contact, and a permanent bond forms within a few minutes. The plasma treatment also transforms the PDMS from hydrophobic to hydrophilic, which makes it easier to fill the microchannels with liquid. To return PDMS to its natural hydrophobic state, the entire chip can be heated at 160 °C for 12 hours. The SU-8 master may be used repeatedly to replicate hundreds of PDMS microfluidic devices. The channel features fabricated by the soft lithography process have a rectangular cross section, and the width of the channels can be measured using the microscope and CCD camera and a calibrated scale that converts the number of pixels on the image into physical distances.

Many of the steps in the fabrication process are sensitive and can cause defects in the final master. Imperfections of the photomask get replicated as poor surface properties of the master at lower exposure doses. Critical imperfections, such as large scratches, can cause the chip to be unusable. Spin-coating is particularly critical, as contamination particles or inadequately cleaned slides often produce crevasses or divots, so appropriate care must be taken during the fabrication procedure.

Surface treatment of channel walls is usually required in electrophoresis separation techniques to control the electroosmotic flow inside the channel or to reduce analyte adsorption to channel walls. PDMS bears a low density of silanol groups on its surface, limiting the EOF magnitude. However, plasma treatment makes the PDMS surface more hydrophilic and simultaneously increases EOF. The increase of surface charge may be detrimental for electrophoresis separation of analytes by increasing adsorption. There are several procedures for reducing EOF in PDMS microchannels. For all the experiments in this thesis, the channels inside the chips were preconditioned using a PVP solution (1%, w/v) for 20 min to suppress electroosmotic flow and adsorption.

3.3 Sputtering and Lift-Off Procedures

Sputtering is a physical vapor deposition (PVD) method to deposit thin films of metals on substrates. This involves ejecting material from a source target onto a substrate such as a glass slide or a silicon wafer. Sputtered atoms ejected from the target have a wide energy distribution, typically up to tens of electron volts. The sputtered ions – typically only a small fraction, ~1% of the ejected particles is ionized – can ballistically fly from the target in straight lines and impact energetically on the substrates. Alternatively, at higher gas pressures, the ions collide with the gas atoms that act as a moderator and move diffusively, reaching the substrates or vacuum chamber wall and condensing after undergoing a random walk. The entire range from high-energy ballistic impact to low-energy thermalized motion is accessible by changing the background gas pressure. The sputtering gas is often an inert gas such as argon. For efficient momentum transfer, the atomic weight of the sputtering gas should be close to the atomic weight of the target material. So for sputtering light elements, neon is preferred, while for heavy elements krypton or xenon is used. The influence of many parameters on sputtering deposition make it a complex process, but also allows experts a large degree of control over the growth and microstructure of the films.

Sputtering was frequently used in this work using a sputtering device (AJA International Inc., N. Scituate, MA, USA) to fabricate heaters and temperature sensors underneath the microchannels. To fabricate a design using a sputtering system, first a design mold is fabricated using the soft lithography technique. A glass substrate (3″×1″) is first cleaned using the standard RCA cleaning procedure (Radio Corporation of America) and then dehydrated on a hot plate at 200 °C for 10 min. After dehydration, hexamethyldisilazane is spin-coated onto the glass slide at 3000 rpm for 70 s followed by spin-coating S-1813 positive photoresist at 3000 rpm for 80 s. The substrate is then baked on a hot plate at 150 °C for 75 s to remove the solvent. A positive photo mask containing the design is then used to transfer the pattern onto the chip via UV exposure. After fabrication, the substrate in the MF-319 is developed for 1 min to dissolve the unexposed S-1813. The substrate is then placed into the sputtering device perpendicular to the target at a distance of about 3 cm from the target. Before the sputtering, substrates can be cleaned with argon plasma in the sputtering chamber by applying the power to the substrate holder for 5 minutes. In this case, ionized argon atoms strike the substrate surface and etch the surface slowly to remove particles or residues. Sputtering is then performed for several hours to achieve the desired design. The thickness of the resulting sputtered layer is usually less than 500 nm. After the sputtering, a lift off process is required

to remove the sputtered region outside the design area. Lift off is performed by heating the developer solution (Remover 1165) to around 65 °C and placing the substrate inside the solution for 15 minutes. This is usually done inside a sonication bath to speed up the lift off process.

Chapter 4

Isoelectric Focusing of Proteins with Whole Channel Imaging Detection

4.1 Introduction

Several commercial CIEF instruments have been developed and available in the market as powerful separation systems. For example, the iCE280 analyzer invented by Convergent Bioscience Inc. is such an instrument utilizing CIEF for the separation of proteins and biomarkers [124, 125, 126]. This instrument has been widely adopted by the pharmaceutical industry.

Despite the success that CIEF has in both academy and industry, the use of capillary for separation has limited its throughput and its integration with other mechanisms for the separation of complex samples. In addition, capillaries have a round cross section which results in lens effects during detection [127]. These limitations have prompted the development of microfluidic chips for IEF taking advantage of the advances in photolithography technology. There have been a number of studies that successfully demonstrated IEF in chip format. Most of these studies rely on single point detection which requires the focused samples to be mobilized after separation. Hydrodynamic flow has been commonly used for pumping the focused sample bands which causes sample dispersion well documented previously [128]. Therefore, efforts have been made to explore novel pumping techniques [129]. Others have also investigated new chip materials [130] and methods for multi-dimensional separations where IEF is one of the dimensions [131, 120].

The dispersion due to mobilizing focused sample bands to a detecting point can be avoided by monitoring the entire channel or column during the separation process. In addition to no need for mobilization, whole column detection also provides several other advantages such as shorter detection time, minimized peak dispersion and consequently higher resolution. Earlier studies on whole column detection were started by several groups such as Rowlen et al. [132], Wu and Pawliszyn [94], and Wang and Hartwick [133]. Rowlen et al. [132] employed a series of diodes to detect the separation peaks of a

zone on a chromatographic column and also introduced the term of whole column detection (WCD) which was adopted later by Wang and Hartwick in their study of capillary isoelectric focusing coupled with a whole capillary scanning method. Wu and Pawliszyn [94] constructed a concentration gradient imaging detector in which a segment of capillary was illuminated by a defocused laser beam. In their study, the term of whole column imaging detection (WCID) was introduced and later UV absorbance-based WCID method was invented by Convergent Bioscience Inc. using their instrument, iCE280 analyzer. Recently, WCID has also been employed in chip format for IEF applications. For example, Das and Fan [134] evaluated the effects of separation length and voltage on IEF in a plastic microfluidic chip where fluorescence-based WCID technology was used for detection. Qiu's group [135, 136] has also developed microfluidic chips for IEF using fluorescence-based WCID technology for detection. Each method has pros and cons. Fluorescence-based detection has a much higher sensitivity than UV absorbance-based detection, however, it requires derivatization which is time consuming, expensive and more importantly may alter the pI of the analytes [137, 138].

UV-based WCID that the iCE280 analyzer employs for detecting protein or biomarker separation does not need derivatization, which will avoid any potential effects due to labelling samples. Considering the success that the iCE280 analyzer has received, the cartridge used in this analyzer therefore is employed in this study as the basis for comparing and developing chip-based IEF technology. The key features incorporated in the iCE280 analyzer include: i) a metal slit with a 65 μm opening aligned with the separation capillary to block the light outside of the separation capillary region, ii) two short hollow fiber membranes with one end connected with the separation capillary to separate the electrolytes in the reservoirs and the samples in the separation capillary, and to reduce hydrodynamic flow, and iii) two capillaries connected to the other end of the hollow fiber membranes for continuous sample injection and discharge. This cartridge is capillary-based and thus has all the disadvantages pertaining to CIEF as mentioned above. In addition, the cartridge assembly is done manually which often results in poor alignment between the separation capillary and the opening of the metal slit which in turn will lead to low detection sensitivity or even failure of the cartridge. Manually gluing cylindrical hollow fiber membranes with capillaries which have a 100 μm diameter is challenging too. Figure 4.1 shows the structure design of the commercial cartridge used in the iCE280 analyzer.
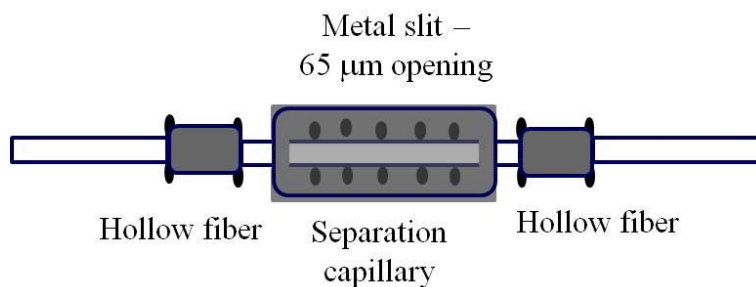
Figure 4.1 Structure design of the commercial cartridge used in the iCE280 analyzer

As a natural progression of replacing CIEF with chip-based IEF, several studies have addressed the limitations of this cartridge. For example, Liu et al. [139] first proved that IEF can be performed in a PDMS microfluidic chip coupled with UV-based WCID. Later, Ou et al. [140] demonstrated IEF in microfluidic chips with integrated dialysis membranes in replacement of the hollow fiber membrane used in the commercial cartridge. In that design, the same metal slit was used for blocking the UV light as that in the commercial cartridge. In addition, the dialysis membranes were also manually glued to the chip substrates which proved to be very difficult. In another study presented by the same group, the metal slit was replaced by a built-in SU-8 optical slit which eliminates challenging alignment between the metal slit and separation channel and manual gluing processes [141]. In this study, membranes or hollow fibers were not used which resulted in diffusion of electrolytes into the separation channel and hydrodynamic flow, causing low repeatability and low separation resolution.

The above problems can only be resolved if all the functional components can be integrated into one single chip, which include the membranes for separating electrolytes from protein samples, the SU-8 optical slit for preventing stray light, and the injection/discharge capillaries that allow continuous operation. Such a chip can potentially replace the cartridge currently being used in the iCE280 analyzer, while maintaining comparable separation performance to the commercial cartridge. In addition, it opens up the opportunity for multi-dimensional separations where IEF is one of the dimensions benefiting from the continuous flow control provided by microfluidic chips. The integration is very challenging because it involves the fabrication of different chip materials at different thickness which are prone to leakage and blockage and thus result in low separation performance. Addressing these challenges becomes the focus of this study, developing techniques which enable a fully integrated chip to be fabricated and validating the developed chips using the iCE280 analyzer.

4.2 Fabrication of the Chip

As shown in Figure 4.2, the fabrication of a fully integrated chip is done through three steps [35]. In the first step (Figure 4.2A), an open microchannel is fabricated on a quartz substrate with two side walls made of SU-8. In the second step, a PDMS substrate is fabricated with two holes (reservoirs for IEF), around which two modified porous PDMS membranes are bonded on one side of the PDMS substrate (Figure 4.2B).
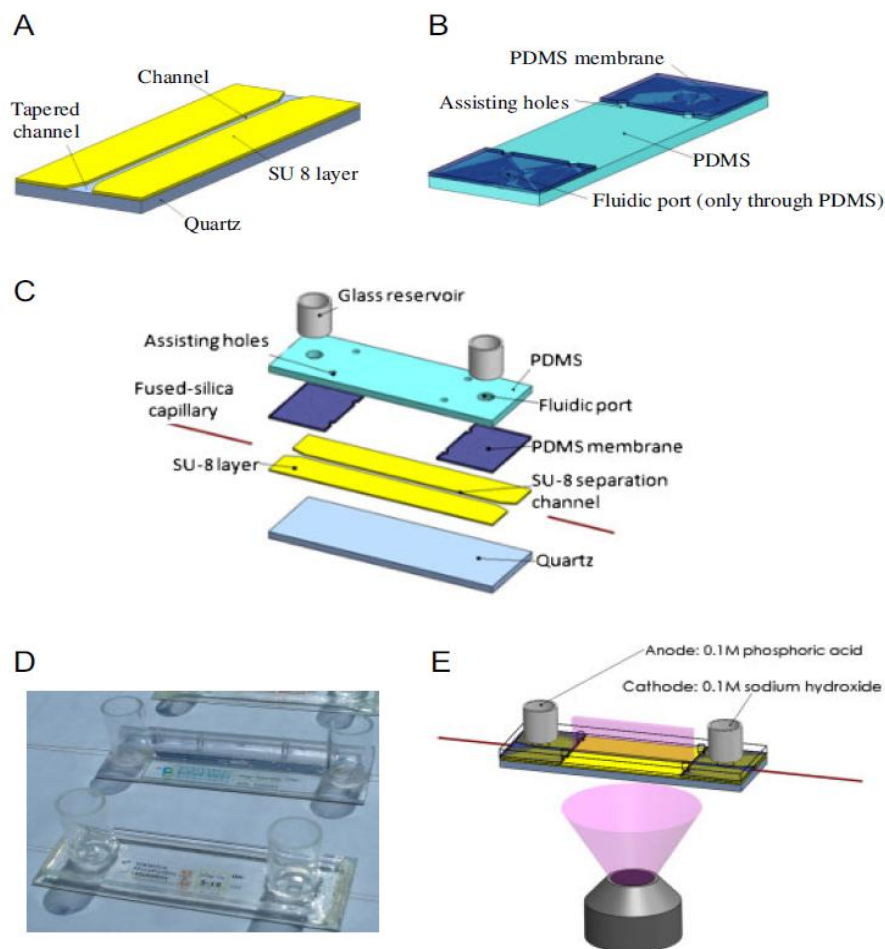
Figure 4.2 (A) quartz substrate with SU-8 channel walls, (B) PDMS substrate with membranes, (C) assembly of chips, (D) (bottom) image of the final chip (with University of Waterloo logo) and (top) commercial cartridge (courtesy of Convergent Bioscience), and (E) assembled chip with light path **[35]**.

Finally, the two substrates, Quartz substrate with an open channel made of SU-8 and PDMS substrate with modified PDMS membranes, are bonded and sealed, followed by the injection of capillaries and gluing of large glass reservoirs (Figure 4.2C).

To fabricate the SU-8 microchannel, a quartz substrate was first cleaned by RCA cleaning and then dehydrated on a hot plate at 200 °C for 30 min. A 100 μm thick SU-8 (2075) layer was spun coated onto the quartz substrate with a spin speed of 500 rpm for 25 s followed by a spin speed of 1800 rpm for 75 s. The substrate was subsequently soft baked on a hot plate at 65 °C for 5 min and at 95 °C for 12 min to remove the photoresist solvent. After the substrate was cooled to room temperature, UV exposure was performed in a UV mask aligner with a 920 mJ/cm^2 dose at a wavelength of 365 nm. In the exposure, a negative photo mask with a 100 μm wide, 5 cm long channel design was used for pattern transfer. In this design, the inlet and outlet have a gradual converging and diverging geometry for integrating the injection and discharge capillaries. Post-exposure bake was performed on a hot plate at 65 °C for 7 min and at 95 °C for 12 min successively. After cooling slowly to room temperature, the photoresist was developed in the propylene-glycol-monoether-acetate developer for 10 min to dissolve the unexposed SU-8 completing the fabrication of the bottom substrate.

The PDMS substrate partly bonded with the modified PDMS membranes was fabricated using the procedure developed by Ou et. al. [142]. Briefly, PDMS at a weight ratio of 10:1 was poured onto a blank silicon wafer and cured for 1 h at 80 °C. After curing, the PDMS layer with a thickness of 2 mm was peeled off from the silicon wafer and cut into 3″×1″ pieces. Then, two holes with a 3 mm diameter were punched through the PDMS layer with a distance of 2 inches from each other for the reservoir locations. In order to prepare the PDMS membrane, one gram of polystyrene was thoroughly dissolved in 10 mL toluene. The obtained viscous solution was spun coated on a glass slide (3″×1″) at a speed of 500 rpm for 10 s followed by a speed of 2000 rpm for 30 s. Then, the glass slide was baked at 95 °C for 10 min to deposit the polystyrene film and this slide was served as the substrate for the next step. To fabricate the porous membrane, a mixture of PDMS at a weight ratio of 10:1was diluted with toluene and the previously obtained viscous solution (containing polystyrene and toluene) by the ratio of 10:10:1 respectively. After degassing, the PDMS mixture was spun coated onto the glass side obtained previously at a speed of 500 rpm for 10 s followed by a speed of 1000 rpm for 30 s as shown in Figure 4.3. Then, the slide was soft baked on a hot plate at 95 °C for 30 min. In order to bond the PDMS membrane on the holes of the PDMS substrate, two of the resulted glass slides and the PDMS substrate obtained previously

were pre-treated by air plasma and brought into contact as shown in Figure 4.3. Only the reservoir areas of the PDMS substrate were bonded with the membranes. Then, the membranes were shaped to fit the width of the PDMS substrate and then the whole structure was immersed into toluene, acetone, and ethanol to dissolve the layer made of the viscous solution so that the PDMS substrate with the membranes could be peeled off from the glass slide. Finally, the PDMS substrate integrated with the PDMS membranes on its reservoir areas was dried in an oven under vacuum for12 h at 55 °C.
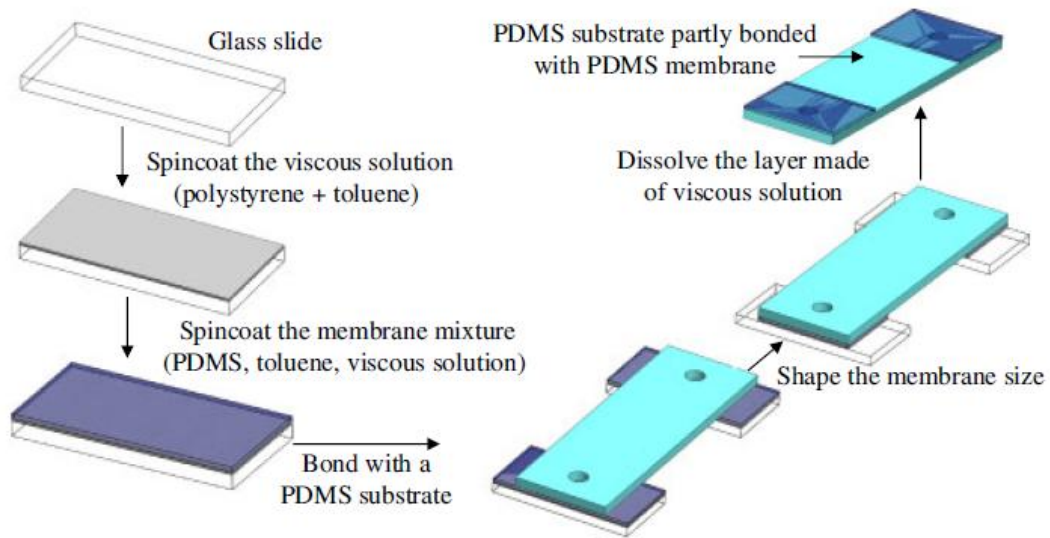
Figure 4.3 Procedure for fabricating a PDMS substrate partly bonded with the modified PDMS membranes **[35]**.

The combination of PDMS substrate integrated with PDMS membranes is shown in Figure 4.4a. The PDMS membrane has a thickness of around 10 μm and has monodisperse pores with a diameter of 1-2 μm. Figure 4.4b shows the microscope view of the membrane at the membrane boundary.
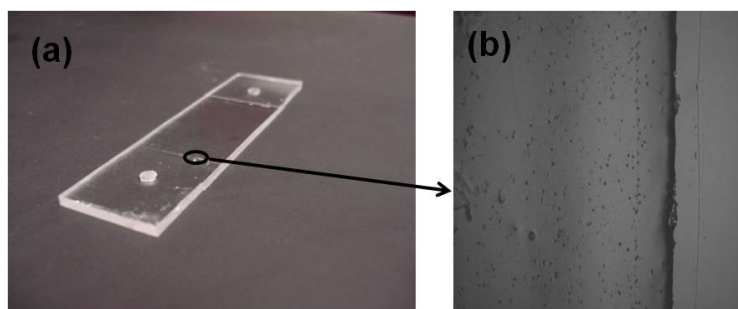
Figure 4.4 (a) PDMS substrate integrated with PDMS membranes on both reservoir locations (b) microscope view of PDMS membrane; the membrane has a thickness of around 10 µm and pores with a diameter of 1-2 µm.

Leakage has proven to be the major challenge when fabricating multi-layer microfluidic chips involving multiple different materials, which in this study involved the fabrication of PDMS, modified PDMS membrane, quartz, SU-8, and capillaries. For the initial attempt of avoiding leakage, the entire PDMS substrate was coated with the modified PDMS membrane, which indeed avoided leakage problems; however, it caused detection problems. This is because the separation channel is also covered by the membrane that caused light scattering leading to low detection sensitivity (data not shown here). Therefore, the membrane was designed to cover the reservoir area of the PDMS substrate in order to eliminate light scattering. Because of the definite thickness of the membrane (~10 mm) which made a gap between the top PDMS substrate and the bottom SU-8 layer as shown in Figure 4.5B, leakage occurred along the edge of the membrane as shown in Figure 4.5D. To solve this leakage problem, a technique involving the use of half-cured PDMS to seal the gap was developed and briefed below. After the PDMS substrate is fabricated with its reservoir areas bonded with the modified PDMS membranes, four assisting holes with a diameter of 2 mm were punched through the PDMS substrate and PDMS membrane at the membrane boundary as shown in Figure 4.2B and C. Then, the PDMS and quartz substrates obtained above were irreversibly bonded together via oxygen plasma at 29.2 W, and 300 mTorr pressure for 20 s. Immediately after bonding, half-cured PDMS (previously cured at 65 °C for 7 min) was injected into the four assisting holes, which fills the gap caused by the definite thickness of the membrane. Caution has to be paid when filling the half-cured PDMS so that it seals the gap, but does not block the channel. As a result, there is still a small gap (its length is about two channel widths) as shown in Figure 4.5C, where the liquid from the channel can fill in. It should be noted that this small gap does not affect the separation, since it neither causes appreciable liquid losses (maximum 2 nL which is around 0.4% of the total liquid volume) nor affects the applied electrical field which has been validated previously in a similar geometry

(a straight channel with a wedge along the channel length) for different applications [142]. The combined microfluidic chip was baked at 65 °C for 30 min to harden the bonding and complete PDMS curing. The fabrication was followed by the insertion of injection and discharge capillaries from the two tapered ends of the SU-8 channel, which was done under a microscope. After the insertion of capillaries, a layer of glue was applied to the capillaries around the edges of the channel to prevent leakage. Finally, the glass reservoirs were glued on top of the chip using room temperature vulcanizing silicone glue. An image of the fully integrated chip is shown in Figure 4.2D that was put side by side with a commercial cartridge from Convergent Bioscience.
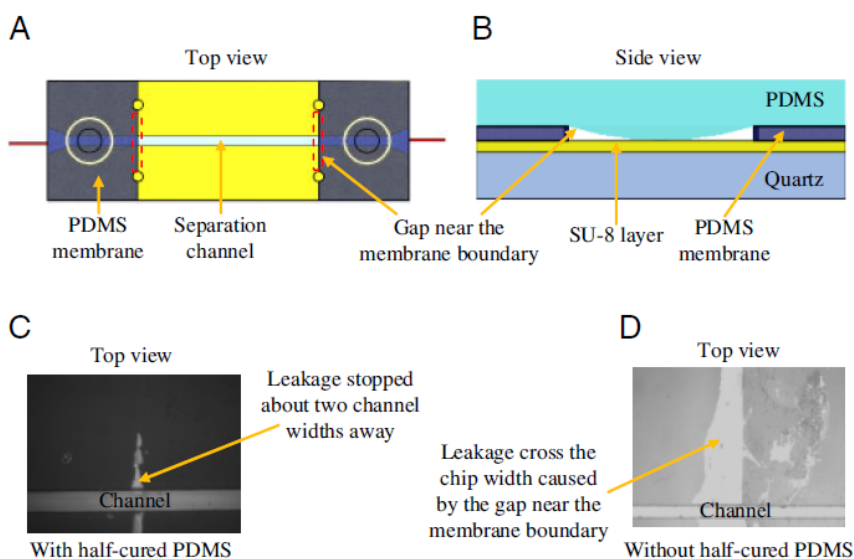
Figure 4.5 (A) top view of the chip, (B) side view of the chip showing the gap near the membrane boundary, (C) image of the top view of the chip treated with half-cured PDMS showing that leakage stopped about two channel widths away, and (D) image of the top view of the chip without introducing half-cured PDMS showing that leakage occurred cross the chip width **[35]**.

4.3 Experimental Setup

IEF experiments were performed using an iCE280 analyzer (Convergent Bioscience), which consists of a deuterium (D2) lamp as a light source and a whole channel optical absorption imaging detector operated at 280 nm. During sample focusing, the light beam from the lamp was focused onto the separation

channel by a bundle of optical fibers and a cylindrical lens as illustrated in Figure 4.2E. The UV absorption image of the whole channel was captured by a CCD camera. All the sample solutions were prepared in deionized water containing 1% PVP, 2% pharmalytes (3–10), and desired pI mixture or proteins. The anolyte and catholyte were 0.1mol/L phosphoric acid and 0.1mol/L sodium hydroxide, respectively. Experiments were performed at room temperature. All the solutions were filtered using a 0.2 μm pore size cellulose acetate filter (Sartorius, Gottingen, Germany) prior to use. The channel inside the chip was preconditioned using a PVP solution (1%, w/v) for 30 min to suppress electroosmotic flow that may cause peak relocation. Following the preconditioning, the sample mixture was injected into the channel. Focusing was performed by first applying a voltage difference of 1.5 kV for 4 min for pre-focusing and then applying a voltage difference of 3 kV for the rest of the separation that was roughly 10 min. Between each run, the channel was flushed with a 1% PVP solution for 5 min. IEF experiments were repeated three times for each sample. Prior to separation experiments, the UV blocking performance of each chip was tested. SU-8 contains eight benzene rings in its chemical structure that give it high absorption in the UV range (<300 nm). The absorbance of the SU-8 layer is expected to follow the Beer–Lambert law and increases with thickness. However, thick SU-8 layers (i.e. >100 μm using our available facility) tend to have curved side walls due to the process of multiple coatings of SU-8 (each coating gives a certain thickness). In this study, a 100 μm thick SU-8 layer was used for chip fabrication. Figure 4.6 shows a comparison of the UV light transmitted through the channel region and the 100 μm thick SU-8 region. The UV intensity is almost uniform across the separation channel length and it is six orders of magnitude higher than the UV intensity transmitted through the SU-8 layer. These results demonstrate the efficiency of the 100 μm thick SU-8 layer as an optical slit that blocks the stray UV light.
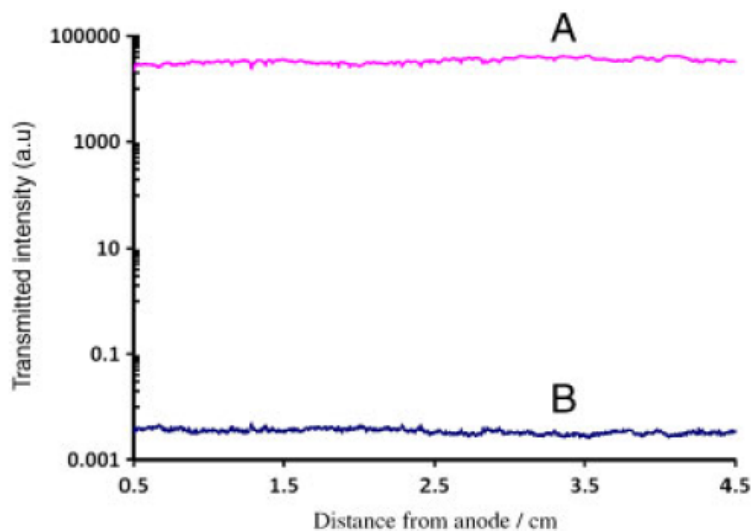
Figure 4.6 Transmitted UV intensity (A) along the separation channel and (B) along SU-8 layer **[35]**.

4.4 Results and Discussions

The fully integrated chip was evaluated based on its separation performance of pI markers and protein samples. Figure 4.7 shows the separation of 5 pI markers (4.22, 5.85, 7.00, 8.18, and 9.46) on the fully integrated chip using the IEF-UV-WCID technology and commercial cartridge, separately. As one can see, these five pI markers were successfully separated on the microfluidic chip and the peak heights and peak locations are in perfect agreement with those of the commercial cartridge. The comparison of the peak locations with the pI points of the sample mixture indicates the linear pH gradient achieved using the integrated hybrid microchip. The pH linearity was found to be 0.9978 and 0.9981 for the commercial cartridge and fully integrated chip, respectively. This also validates that the integrated membrane successfully prevents hydrodynamic flow and diffusion of electrolytes into the separation channel. The peak height achieved in the fully integrated chip (around 0.23 for 4.22 pI marker on the left axis scale) is less than the commercial cartridge (around 0.33 for 4.22 pI marker on the right axis scale). This may be due to the fact that the 100 μm -thick SU-8 optical slit cannot block 100% of stray UV light as in the metal slit.

61
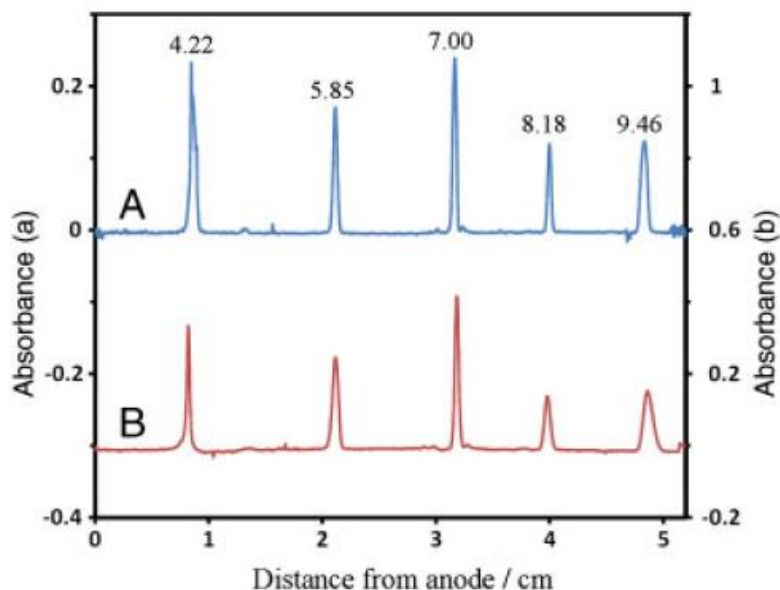
Figure 4.7 IEF profile of PI markers using (A) the fully integrated chip and (B) capillary cartridge. Separation channel: (A) 100 μm width×100 μm depth×5cm length; (B) 100 μm ID×5cm length. The sample is a mixture of five pI markers (4.22, 5.85, 7.00, 8.18, 9.46, 2% of their original concentration), pharmalytes (pH 3-10) and 1% PVP. The applied voltage was set at 1500 V for the first 4 min and then at 3000 V for the rest of separation **[35]**.

To further validate the separation performance of the fully integrated chip, it has been tested for the separation of human hemoglobin control AFSC, which contains four definite isoforms (A, 7.0; F, 7.1; S, 7.3; C, 7.5) with very close pI values. The separation results are shown in Figure 4.8 which also shows the separation results of the commercial cartridge. Four isoforms were separated very well. Based on these results it can be concluded that the microfluidic chip can achieve separation as effective as the commercial cartridge.
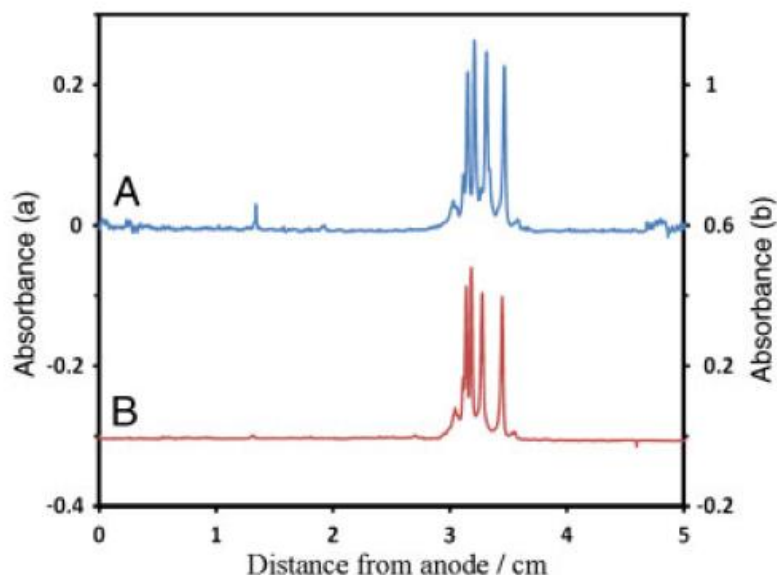
Figure 4.8 IEF profile of human hemoglobin control AFSC using (A) the fully integrated chip and (B) commercial cartridge. Separation channel: (A) 100 μm width × 100 μm depth × 5 cm length; (B) 100 μm i.d. × 5cm length. The sample contains 0.1 mg mL^{-1} human hemoglobin control, 2% pharmalytes (pH 3–10) and 1% PVP. The applied voltage was set at 1500 V for the first 4 min and then at 3000 V for the rest of separation **[35]**.

Repeatability and reproducibility of the fully integrated chip were also examined and presented in Table 4.1. Run-to-run repeatability test was performed for the fully integrated chip by comparing the peak height of pI=7.00 in the pI mixture for three runs under the same operating conditions.

Table 4.1 Repeatability and reproducibility of fully integrated chips for IEF-WCID

Parameter	Peak height ^{a}			Run-to-run	Chip-to-chip
	Run 1	Run 2	Run 3	RSD	RSD
Chip 1	0.2336	0.2296	0.2329	0.92%	
Chip 2	0.2326	0.2341	0.2371	0.97%	1.80%
Chip 3	0.2404	0.2387	0.2384	0.45%	

^{a} The peak height was the absorbance of pI 7.00 in the pI mixture samples. The IEF conditions are the same as in Figure 4.5.

The chip-to-chip reproducibility was also investigated by comparing the peak height of pI=7.00 in three different chips. As shown in Table 4.1, the relative standard deviations (RSD) are less than 1% (n=3) for run-to-run repeatability and less than 2% (n=3) for chip-to-chip reproducibility.

4.5 Conclusions

A PDMS/modified PDMS membrane/SU-8/quartz hybrid chip was developed and successfully applied for separating a protein sample and a mixture of pI markers using the IEF-UV-WCID technology. The main contributions of this study are twofold. First, this fully integrated microfluidic chip fully realizes all the functions of the commercial cartridge used in the iCE280 analyzer in a chip format, while avoiding the challenging alignment and gluing procedures associated with the commercial cartridge. In brief, in this design, the modified PDMS membranes which can be fabricated using standard micro-fabrication techniques replace the hollow fibers eliminating the need to glue two 3 mm-long, 100 μm diameter hollow fibers with 100 μm diameter capillaries including the separation capillary and sample injection and discharge capillaries, the built-in SU-8 layer replaces the metal slit avoiding the alignment needed for gluing the metal slit with the cartridge, and the square (could be rectangular) microchannel replaces the capillary reducing lens effects. In summary, the developed chip is robust and can be employed in the iCE280 analyzer with a lower cost than its current best practice. The overall cost of a fully integrated chip was estimated to be around 50$ which is far less than the 250$ selling price of the commercial cartridge.

In addition, this chip format IEF opens up the opportunity for multi-dimensional separation of complex samples, which cannot be realized easily using capillary-based separations. Second, the fabrication techniques developed in this study can be employed in other chip applications, which involve the fabrication of multilayer structures using multiple different materials. For example, the developed half-cured PDMS with assisting holes for preventing leakage problems can be applied to other fabrications where leakage is prone to happen. In addition, the modified PDMS membranes and associated fabrication techniques can be employed in other separation studies as well.

Chapter 5

Resolution Improvement in TGF and MAGF Separation Techniques

5.1 Introduction

Although the scanning format of Temperature Gradient Focusing (TGF) and Micellar Affinity Gradient Focusing (MAGF) methods are promising in separating analytes with vastly different mobilities, the use of a linear temperature gradient limits separation performance because it is not possible to obtain a sharper peak and a higher resolution simultaneously. This is because width of the peak and resolution are both inversely proportional to the square root of the field gradient. In fact, steeper gradients produce sharper peaks, but these peaks are compacted leading to lower resolutions, while shallower gradients broaden peaks but lead to higher resolutions [143]. Recently, an electric field gradient focusing (EFGF) device was developed for separating analytes using a nonlinear electric field along the separation channel [144]. It indicates that peak capacity can be improved by using a nonlinear (convex) gradient, such as the one composed of two linear gradients with differing severity [143, 144]. Analytes are first focused in the steeper gradient to form narrowly stacked bands and then moved into the shallower gradient to be resolved from each other. The aim of this study is to use a bilinear temperature gradient along the separation channel of scanning TGF and MAGF separation techniques in order to improve their separation performances. A specialized design is developed for the heaters to achieve the bilinear temperature profile using both analytical and numerical modeling. The heaters are integrated onto a hybrid PDMS/glass chip fabricated using conventional lift off and soft lithography techniques. Performance is characterized by separating several different samples which cannot be separated using single linear temperature gradients, or only with low resolution. Experiments show a dramatic improvement in peak capacity and resolution with the bilinear design in comparison to the standard single linear temperature gradients.

5.2 1-D Model of Separation

To investigate the concept of using a bilinear temperature gradient for TGF separation, numerical simulation based on a 1-D model was performed to compare the separation performance between linear and bilinear cases using the commercial software package, COMSOL Multiphysics. In this simulation, a 2cm long channel was used to separate two model analytes that have a subtle difference (i.e. 5%) in their electrophoretic mobilities using scanning TGF. The separation channel consists of two 1cm segments, where a factor F $(0<F<1)$ controls the share of gradient for the first segment such as $T_m = F \times \Delta T + T_1$, where ΔT is the temperature difference cross the entire channel and T_1 is the temperature at the cold end. When $F=0.5$ there is a linear gradient along the entire channel. By increasing the value of F, the first gradient will become sharper while the second gradient becomes shallower. In order to control the electric field gradient along the separation channel, the conductivity of each segment was defined as a linear function of the local temperature: $\sigma(T)/\sigma_1 = 1 + \alpha(T - T_1)$ while the temperature profile for the first and second segments was defined in a general heat transfer model $\nabla(-k\nabla T) = 0$ as

$T(0 \leq x \leq x_m) = T_1 + \dfrac{(T_m - T_1)}{x_m} x$ and $T(x_m < x \leq x_{end}) = T_m + \dfrac{(T_{end} - T_m)}{x_{end} - x_m} x$. Initial parameters were

defined as T_1=20 °C, T_{end}=70 °C and $\alpha = 0.6\%$ °C^{-1}. The electric field is inversely proportional to conductivity and therefore decreases by increasing temperature. The bilinear temperature profile results in a convex electric field profile. The transport of each analyte was calculated using the electrokinetic flow model $\partial c/\partial t + \nabla(-D\nabla c - \mu_{ep} c \nabla V) = -u_{bulk} \nabla c$ where c is the concentration, D is the molecular diffusion, and μ_{ep} is the electrophoretic mobility of each analyte respectively. In the model, ∇V represents the electric field gradient along the channel. To run the model, a constant electric field of 1500 V/cm was applied to the channel and a time dependent bulk flow $u_{bulk} = 0.0002 \times t - 0.001$ m/s was defined in the opposite direction. Each analyte started at the entrance of the channel with the sharp gradient. After running the model in time, the concentration of analytes as they exited the channel was recorded. The separation results for three values of F have been shown in Figure 5.1. As shown in this figure, the separation performance improves significantly with increasing F as the peaks are resolved more from each other. This confirms that using a two-step bilinear design can improve the performance of TGF.
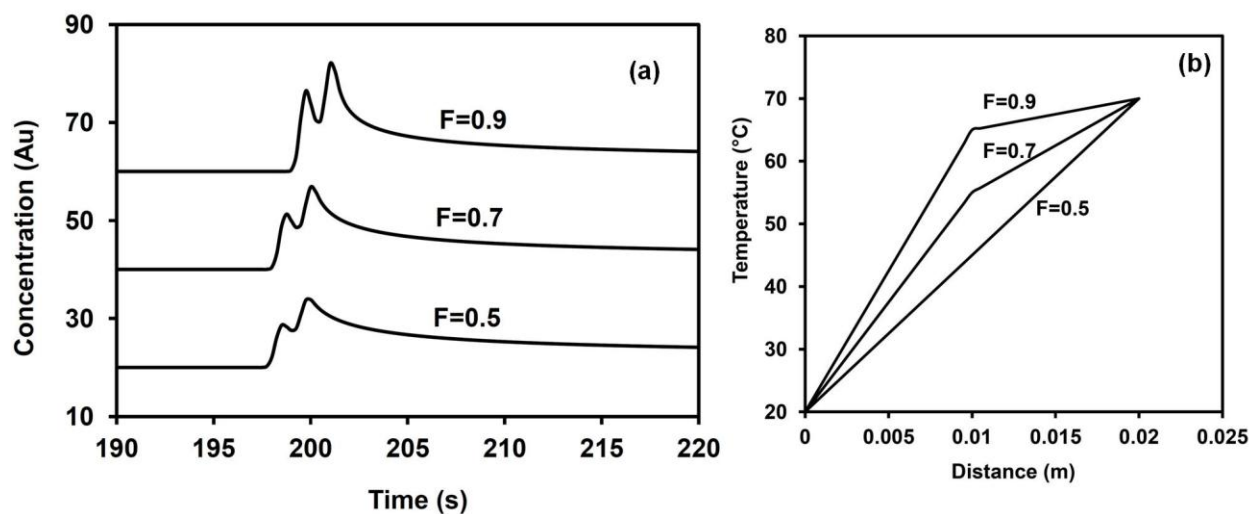
Figure 5.1 (a) Numerical results of separating two analytes with 5% difference in their electrophoretic mobilities for different values of *F* (b) Bilinear temperature gradients for different values of F

5.3 Fabrication of the chip

Figure 5.2 shows the schematic design of the chip which consists of three layers: a glass substrate on top of which are thin film aluminum resistive heaters, a PDMS substrate with the designed microchannel, and a thin PDMS layer sandwiched between the PDMS and glass substrates to separate the liquid sample in the channel and metal heaters. Details about the fabrication steps are listed below.
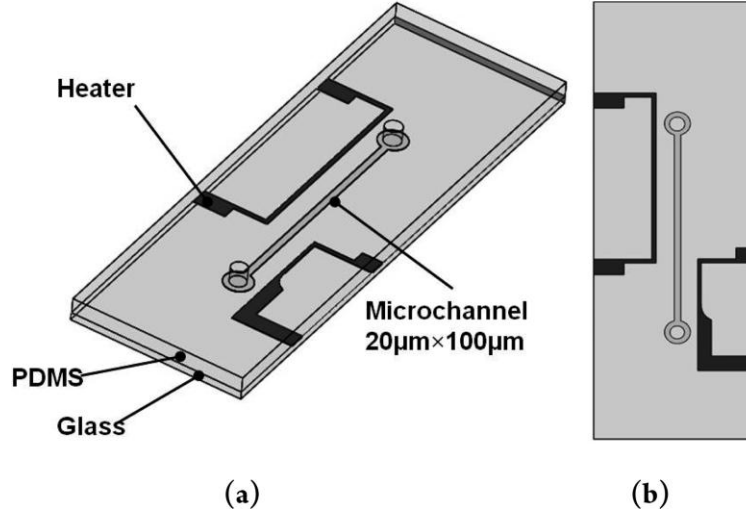
Figure 5.2 (a) Schematic of the chip integrated with heaters and (b) top view of the channel and heaters layout.

5.3.1 Analytical Model

In this work micro-heaters are fabricated on glass substrate to produce a linear temperature gradient. The heaters are embedded between the glass substrate and a PDMS cover on top. A simple 1-D steady state heat transfer model was developed as shown in Figure 5.3 to guide the heater design for generating the desired temperature gradients. The heat generated within the heater is conducted through the substrate and to the ambient through convective heat transfer. Neglecting heat radiation and assuming only radial conduction, the dominant thermal resistances are natural convection from the chip to the ambient and heat conduction through chip materials. Because the heater dimensions are much smaller compared to the chip dimensions, it is reasonable to approximate the heat transfer using a 1-D model where the left hand side is the heat generation and the right hand side the heat dissipation, as

$$\frac{I^2}{\sigma A} = \frac{(T_i - T_\infty)}{R_T{}'} \tag{5.1}$$

Where I is the current draw through the heater (A), σ the electrical conductivity of the heater (S/m), A the cross-sectional area of the heater (m^2), T_i the temperature at the heater (K) and T_∞ the ambient temperature (K). $R_T{}'$ is the overall thermal resistance of the top and bottom substrates (mK/W) which is a

68

combination of the conduction and convection resistance, $R'_{cond} = 1/kS_1$ and $R'_{conv} = 1/hS_2$, where k is the thermal conductivity of the substrate material (W/mK), h the heat convection coefficient (W/m^2K) and S_i the shape factor which depends on the geometry. Many of the parameters in these equations are temperature dependent; however, for simplicity we ignored any temperature dependence and assumed a linear system.

As shown in equation (5.1) the heat generation and temperature profile can be varied by an appropriate design of the cross-sectional area of the heater. The thickness of the heater is fixed by the fabrication technique we use, and therefore, the width is varied to achieve the desired temperature gradient $w(x) = (a+bx)^{-1}$. Using the conditions that the width is w_1 at $x=0$ and w_2 at $x=L$, the solutions for a and b are $a = 1/w_1$ and $b = [1/w_2 - 1/w_1]/L$. The temperature profile along the length of the heater can be obtained by substituting $w(x)$ into equation (5.1)

$$T_i = R'_T \frac{I^2}{\sigma h}\left(\frac{1}{w_1} + \frac{1}{L}\left(\frac{1}{w_2} - \frac{1}{w_1}\right)x\right) + T_\infty \qquad (5.2)$$

The slope of the gradient is then calculated as

$$\frac{dT}{dx} = R'_T \frac{I^2}{\sigma h}\frac{1}{L}\left(\frac{1}{w_2} - \frac{1}{w_1}\right) \qquad (5.3)$$

According to equation (5.3), the severity of the gradient can be controlled by the design of the heater $1/L(1/w_2 - 1/w_1)$ or by increasing the current I^2. Moreover, the width of the heater should be very large at one end such that there is minimal heat generation and the temperature remains close to ambient. At the other end, the heater should be very narrow to maximize the heat generation and thus the temperature range across the channel. In our design the large end is 1 mm wide and the narrow end is 25μm wide, which corresponds to a 40 times difference in heat generation between the two ends.
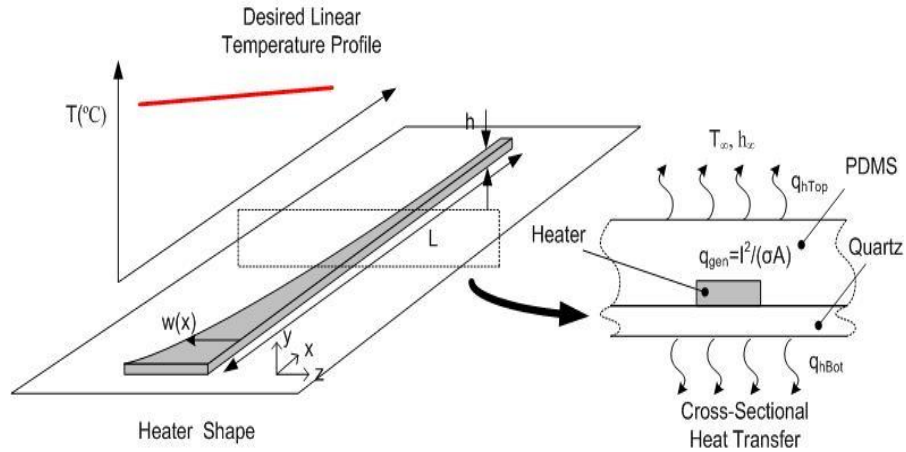
Figure 5.3 Schematic of the heater integrated to the chip and illustration of heat transfer from the heater to the surroundings.

5.3.2 Numerical Simulations

Numerical simulations were performed with the commercial finite element package (COMSOL Multiphysics) to provide guidance for the geometrical dimensions for the chip and the operation parameters such as the applied powers. Both the electrical field and temperature field were solved with coupling through the internal heat generation. Different currents were applied to the heaters using the shell conductive media DC model. This model only solves the electric field equations on the face of the heaters ($-\nabla_t\left(\sigma d\nabla_t V\right)=0$) thus saving valuable computation time since the entire model does not have to be solved. In this model σ is the electrical conductivity of the heater, d is the thickness of the heater, and V is the applied voltage. The resistive heating was then coupled to the heat transfer module through $Q_{production}=Q_{shell\_DC}\times d$ on the internal boundary of the heater face where Q_{shell_DC} is the generated heat solved from the shell conductive media DC module. Since the chip is suspended in air, natural convection conditions $-n.\left(-k\nabla T\right)=q_0+h\left(T_{inf}-T\right)$ were applied along all boundaries using standard empirical correlations. Figure 5.4 shows an example of the numerically predicted bilinear temperature profiles in the separation microchannel. The heaters are positioned 1 mm from both sides of the separation channel and use different powers to generate different temperature gradients along the channel during the simulations.

70
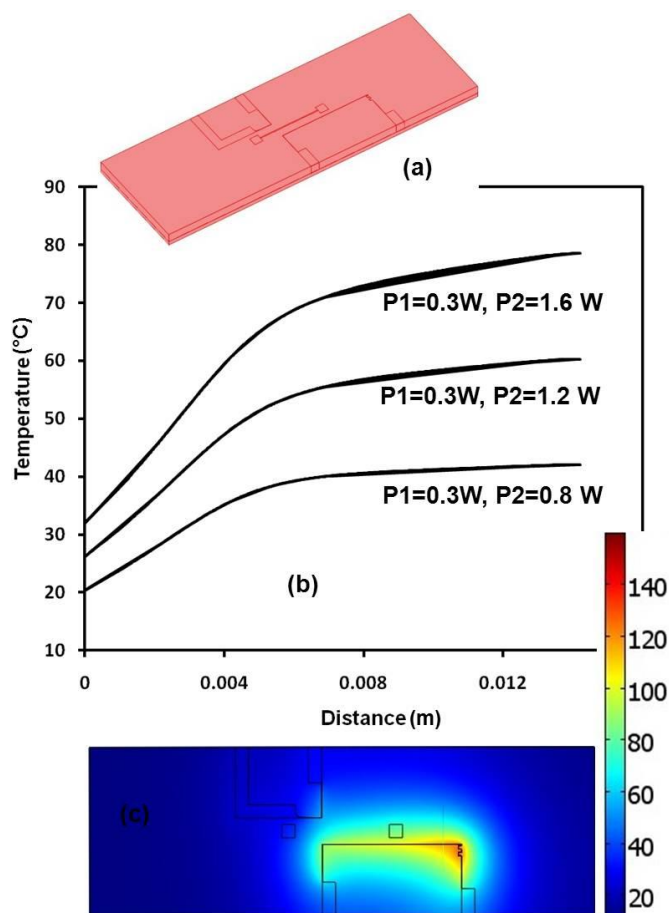
Figure 5.4 Numerical simulation of chip, (a) simulation domain; (b) temperature profiles along the microchannel for various applied powers to heaters, P1 corresponds to the short heater for the sharp gradient and P2 corresponds to the long heater for the shallow gradient. It is shown that by keeping P1 constant and slightly changing P2, one can reach to the desired bilinear temperature profiles; and (c) temperature field at the microchannel plane for P1=0.3W and P2=1.6W.

5.3.3 Fabrication Procedure

The chip consists of a glass slide on top of which are the thin film aluminum resistive heaters and a PDMS microchannel fabricated using soft lithography techniques. To fabricate the chip, first, aluminum heater designs were fabricated on a glass substrate using conventional sputtering and lift off techniques as explained in section 3.3. Briefly, a glass substrate (3″ × 1″) was first cleaned using the standard RCA cleaning procedure (Radio Corporation of America) and then dehydrated on a hot plate at 200 °C for 10

min. After dehydration, hexamethyldisilazane was spin-coated onto the glass slide at 3000 rpm for 70 s followed by spin-coating S-1813 photoresist at 3000 rpm for 80 s. The substrate was then baked on a hot plate at 150 °C for 75 s to remove the solvent. A positive photo mask containing the heater design (CAD/Art Services) was then used to transfer the pattern onto the chip via UV exposure. The fabrication was followed by developing the substrate in the MF-319 developer for 1 min to dissolve the unexposed S1813. The substrate was then placed into the sputtering device and aluminum was sputtered to achieve a final thickness of 500 nm. Lift off process was performed later to remove the sputtered region outside the heater area.

Furthermore, a protective layer of hard PDMS (EG 6301) was spin-coated onto the glass substrates at 3000 rpm for 60 s and cured at 160 °C for 2 h. The protective layer was used to prevent contact between the liquid in the microchannel and the metal heaters. Finally, the substrate was baked at 200 °C overnight to relieve internal stress from the heaters and avoid any deviations in their performance during operation.

The procedure for fabricating the PDMS microchannel is similar to section 3.2. In brief, first, a clean and dehydrated silicon wafer was spin-coated with SU-8 2025 photoresist at 500 rpm for 20 s, followed by 2500 rpm for 60 s, to achieve a 20 µm thick microchannel. The wafer was then baked at 65 °C for 2 min and at 95 °C for 6 min, and finally cooled to room temperature gradually. A straight 1.3 cm long, 100 µm wide channel was designed (CAD/Art Services) and transferred to the spin-coated wafer through UV exposure. After UV exposure, the wafer was baked again at 65 °C for 1 min and 95 °C for 6 min. Development was performed in the PGMEA developer for 4 min. The silicon wafer containing positive relief of the channel design was then dried by nitrogen gas. The mixture of PDMS prepolymer base and curing agent with a weight ratio of 10:1 was degassed under vacuum, poured onto the wafer, and then cured at 90 °C for 2 h. Two 1 mm diameter holes were then punched at the reservoir locations. After pretreatment using oxygen plasma, the PDMS substrate with the channel feature was bonded with the glass substrate integrated with the heaters. The injection and discharge capillaries were then connected to the chip from the two reservoir holes. In order to connect the heaters to the power supply, conductive glue was used to attach small aluminum electrodes to the heaters.

5.4 Measuring the Temperature Profile

5.4.1 Introduction

The temperature profile within the microchannel was experimentally measured using a new developed fluorescence thermometry technique. One of the most popular in situ temperature measurement techniques involves adding Rhodamine B to the working fluid [145, 146]. In this method, the temperature field is determined by monitoring the fluorescent intensity of the working fluid mixed with Rhodamine B using microscopy techniques. This method works well with chips made of glass materials, but does not work well with chips made of PDMS because Rhodamine B particles adsorb to and absorb into the surrounding PDMS walls as detailed in previous studies [147]. To overcome this problem, a two color thermometry technique [148] for on-chip temperature measurement was used that uses a pH sensitive fluorescent dye and Tris-HCl buffer to measure the temperature inside of the PDMS microchannel. In the new temperature measurement method, Rhodamine B is replaced with fluorescein. Generally, fluorescein is a poor candidate for thermometry measurements because its quantum efficiency shows weak temperature dependence [149]. Fluorescein does, however, possess strong pH dependence. The pH-intensity relationship of fluorescein is non-linear over a wider range of pH, i.e. 4-10, but is very sensitive and linear in the narrower range of pH value of 6-7. Therefore, using a buffer with a temperature-dependent pH, the pH-dependent fluorescent intensity can be correlated to the change in temperature. A particularly useful buffer for this task is Tris-HCl, which possesses an approximately linear pH-temperature relationship over the pH range of 6-7 [148]. Tris-HCl is often used to replace carrier ampholytes in establishing a temperature controlled pH gradient in isoelectric focusing applications [150, 151]. Thus, to perform the measurements, a working solution of 10 mM Tris-HCl adjusted to a pH of 7.1 at 22 °C was prepared. Figure 5.5 shows the pH-temperature relationship of 10 mM Tris-HCl with pH of 7.1 at room temperature.
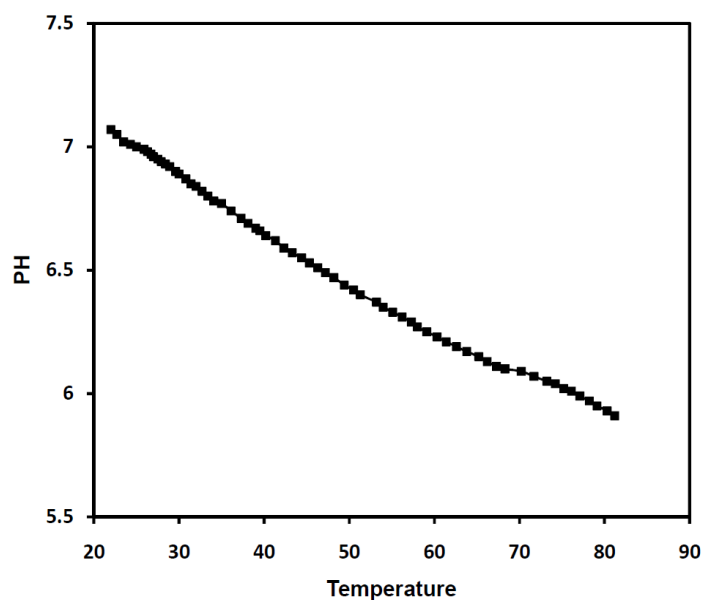
Figure 5.5 Variation of pH with temperature for 10 mM Tris-HCl with a pH value of 7.1 at room temperature to 5.9 at 65 °C.

It is well known that fluorescein has a relatively high rate of photobleaching [152]. In order to avoid the photobleaching effect in the experiments, the dye solution was pumped through the channel continuously at a low flow rate (1μL/min) and numerical simulations showed that the chosen flow rate did not influence heat transfer much within the chip. Also, to avoid intensity measurement errors, another fluorescent dye which must be weakly dependent on pH and temperature was added to the solution as the background [153]. In this study, Alexa Fluor 546 C5-maleimide was chosen as the background dye.

5.4.2 Temperature Calibration

A new temperature calibration method was also used for generating the temperature calibration curve. A hybrid PDMS/glass microfluidic chip with the same conditions of the separation chip was used for the calibration. The chip contains a 5 cm long, 100×100 μm microchannel in the middle surrounded by several parallel 100×500 μm microchannels, as shown in Figure 5.6. The dye solution is pumped to the middle channel while water with constant temperature is pumped quickly through the surrounding channels. It is expected that the temperature of the dye solution in the middle channel is the same as that

of the water passing through the other channels. To ensure the accuracy of the temperature of the dye solution, it is also measured using a resistance temperature detector (RTD). The RTD was calibrated prior to the experiments.
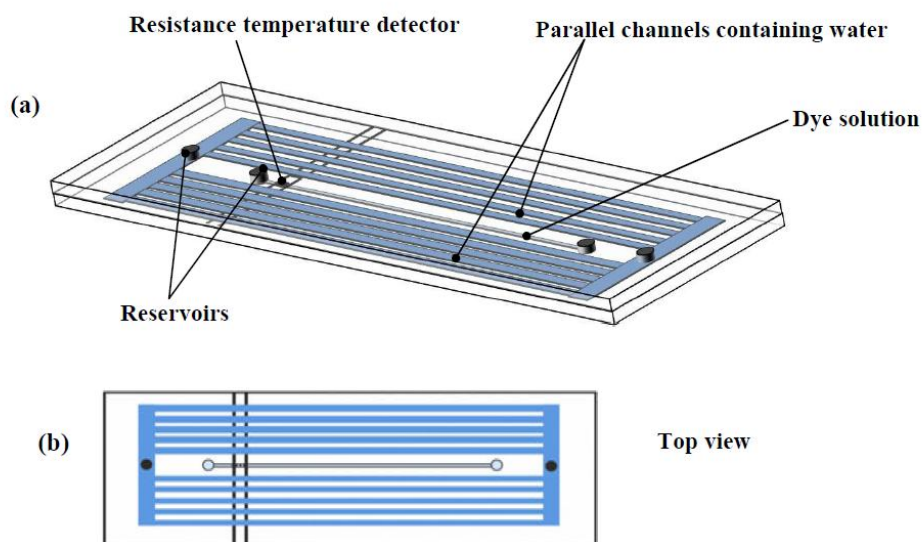
Figure 5.6 (a) Illustration of the calibration chip; and (b) top view of the channel layout.

After reaching steady state, images were taken at different temperatures from several points of the channel close to the RTD using an epi-fluorescence microscope (OLYMPUS GX-71) and a CCD camera (Photometrics Cool SNAP ES). During each measurement, images were taken with two different filters BP450-480 nm and BP510-550 in order to measure the intensity of fluorescein and Alexa Fluor 546, respectively. Figure 5.7 shows the measured intensity versus temperature for fluorescein and Alexa Fluor dyes. The intensity values were normalized by that at room temperature. The final calibration curve (Figure 5.7c) is the ratio of intensity for the two dyes and follows the equation $y = -7E\text{-}0.5x^2 - 0.0029x + 1.0992$. This calibration curve was used for further temperature measurements during the experiments.
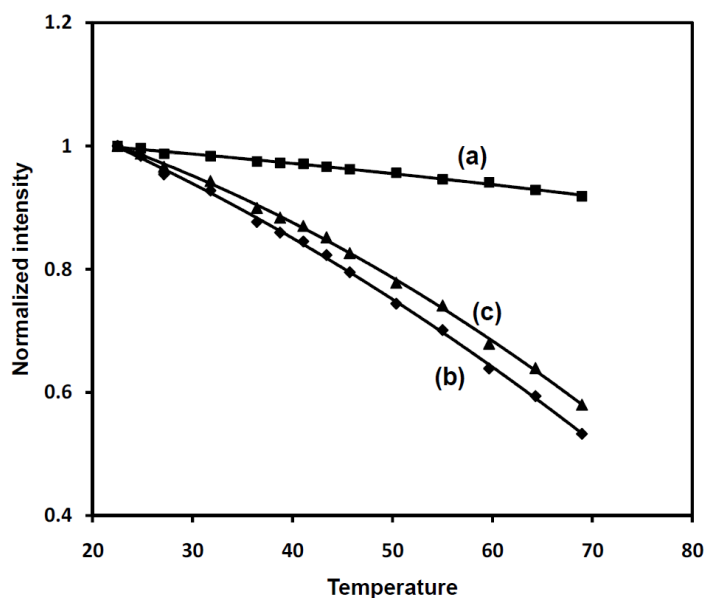
Figure 5.7 Temperature calibration data of 10 µM fluorescein and 10 µM Alexa Fluor in 10 mM Tris-HCl. (a) Intensity change versus temperature for Alexa Fluor 546, (b) Intensity change versus temperature of fluorescein dye, and (c) Intensity ratio of the two dyes versus temperature.

5.4.3 Temperature Measurement Results

The temperature profile within the microchannel was experimentally measured using the developed fluorescence thermometry technique and the above calibration curve. In order to generate a larger temperature gradient, the entire chip was cooled to below room temperature by placing it on an aluminum plate that is cooled by a thermoelectric cooler. The temperature distribution was controlled by adjusting the applied power to the heaters. After reaching steady state, images were taken from different points of the channel using the fluorescent imaging system described above. Figure 5.8 shows the temperature profile along the separation channel for both linear and bilinear heaters. Each data point corresponds to an average of ten images. As shown in Figure 5.8, both linear and bilinear gradients are in a range of about 44 ∘C/13 mm. The bilinear gradient consists of a sharp gradient of 30 ∘C/4 mm followed by a shallow gradient of 14∘C/9 mm. Here, the factor F for the bilinear gradient is 0.68.
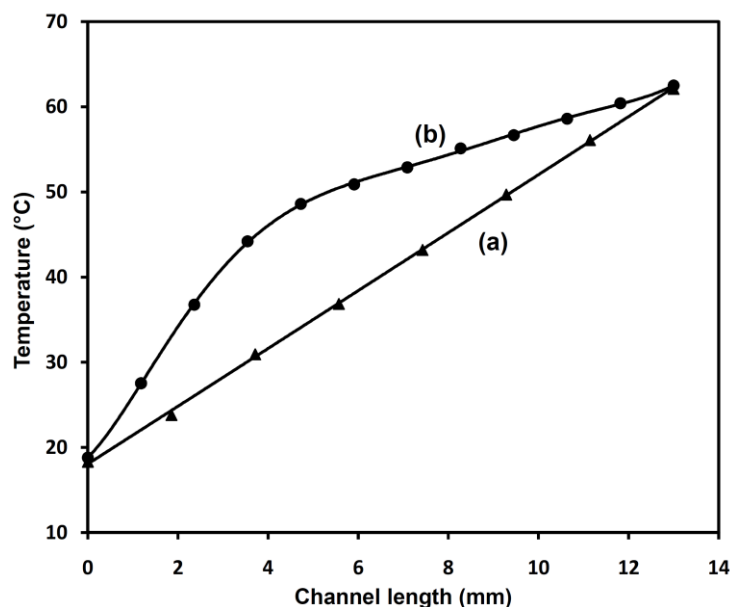
Figure 5.8 Temperature profile along the separation channel (a) Linear heater (b) Bilinear heaters, bilinear profile consists of a sharp gradient for the first 4 mm of the channel followed by a shallow gradient for the rest of the channel.

5.5 Experimental Setup and Sample Preparation

5.5.1 Temperature Gradient Focusing Separation Experiments

To investigate the effect of bilinear temperature gradient on separation performance, analytes should have electrophoretic mobilities that are close enough so that they are present in the channel at the same time. For all the experiments, Tris-phenol was used as a buffer because it has greater temperature-ionic strength dependence than Tris-borate. On the basis of the ionic strength change of Tris-phenol in the given temperature range, the electric field differs by 50% from the cold end of the channel to the hot end. Therefore the difference in the electrophoretic mobility of two analytes should be less than 50% for both to appear in the channel simultaneously.

The experimental setup is illustrated in Figure 5.9. Since Tris-phenol has a lower ionic strength at a higher temperature, negatively charged samples were injected inside the chip from the cold side by pressure while the positive voltage was applied to the sample vial connected to the cold reservoir.

Counteracting bulk flow was created by changing the relative pressure head between the two vials using a linear stage. The pressure scan rate can be controlled by adjusting the elevation speed of the linear stage. The flow directions are also illustrated in Figure 5.9.
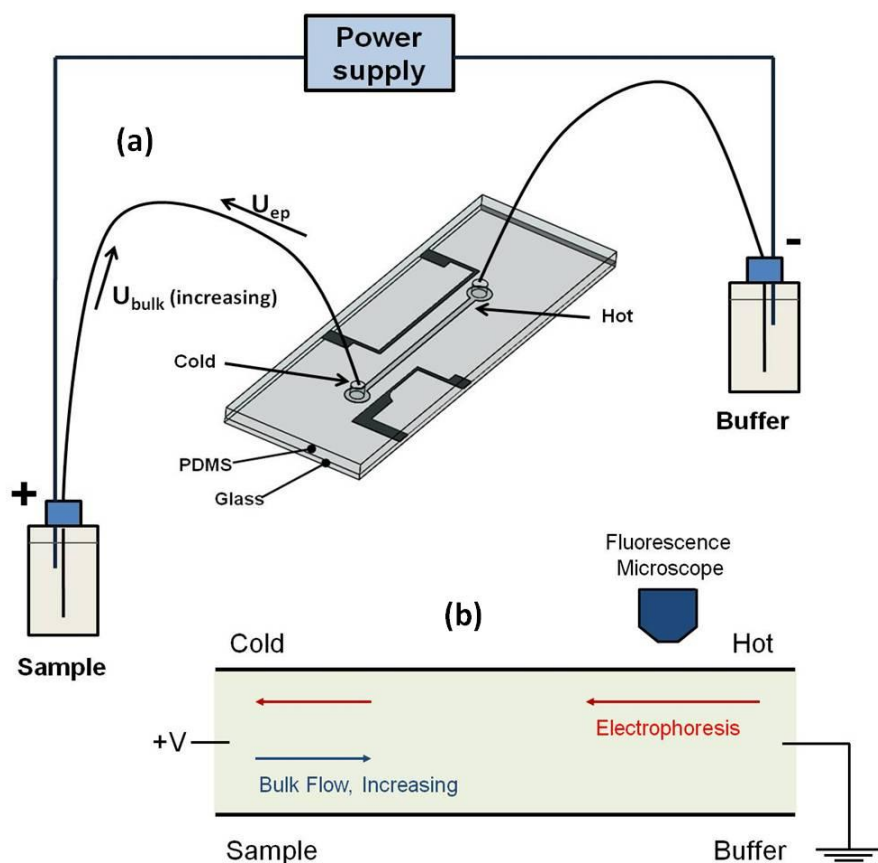
Figure 5.9 (a) Schematic of the experimental setup of TGF with the chip; and (b) flow directions in the microchannel.

The schematic of the scanning TGF with a bilinear temperature profile in the microchannel using Tris-phenol as the buffer is given in Figure 5.10. The application of a temperature gradient gives rise to a corresponding gradient in the ionic strength and applied electrical field as shown in Figure 5.10a. Experiments started with a zero counter-flow velocity. When the counter-flow velocity is gradually increased, the analytes are focused and concentrated at the sharper gradient where separation is not clear as shown in Figure 5.10b. When the counter-flow velocity is further increased, the sample bands are

transported through the shallower gradient towards the detection point (close to the hot end). Then separation is clearly observed via fluorescence microscopy as shown in Figure 5.10c.
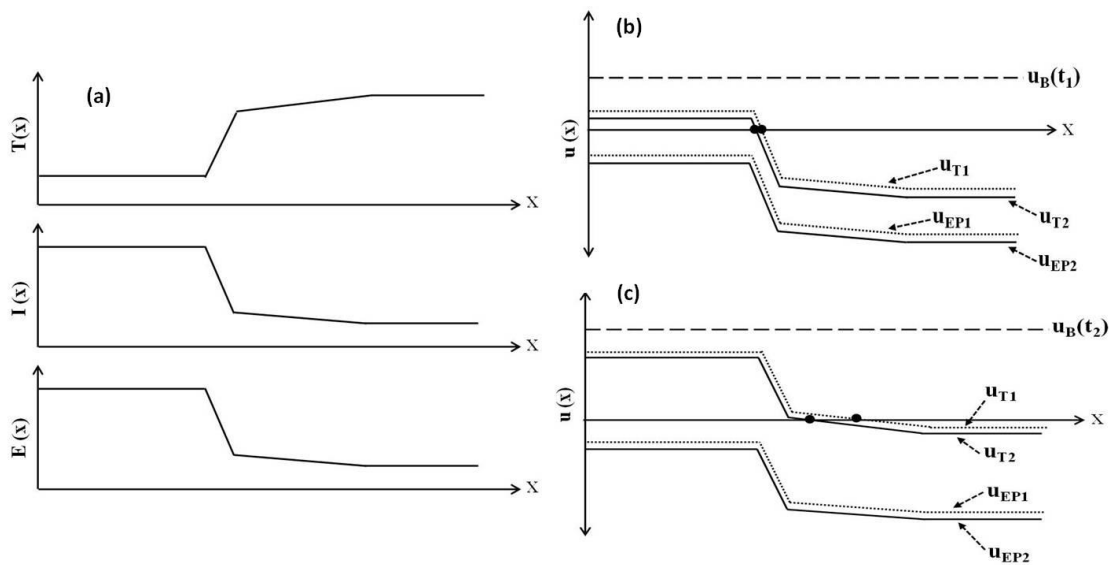
Figure 5.10 Schematic of the scanning TGF: (a) gradients in temperature, T (x), ionic strength, I(x) and applied electrical field, E(x); (b) and (c) illustration of electrophoretic velocity, u_{ep}, counter-flow velocity u_B and the total velocity u_T for two analytes at the sharper and shallower gradients, respectively.

Prior to experiments, the microchannels were treated with 0.5% PVP solution for 10 min in order to decrease the effect of electroosmotic flow. A high voltage difference (2500 V) was applied to the two ends of the channel (Labsmith, HVS448-3000). Since the dyes are negatively charged, the samples were injected to the chip from the hot reservoir which is grounded. The samples were then pumped to the cold reservoir where a high voltage is applied by electrophoretic flow while the counteracting bulk flow was created from the cold end to the hot end by a head difference. Experiments started with a zero difference in head and increased at a predetermined rate, so that the samples were focused while pumping down to the detection point which is close to the hot end. Separation performance can be controlled by adjusting the voltage, the pressure scanning rate and temperature gradient. Generally, higher voltages, slower scanning rates and larger temperature gradients resulted in better separations.

5.5.2 Micellar Affinity Gradient Focusing Separation Experiments

The schematic of the principle of MAGF is illustrated in Figure 5.11. The temperature gradient creates a corresponding gradient in the interaction strength (retention factor) between the analytes and micelles inside the separation channel. In the region of high retention (cold reservoir), the analyte is located within the micelles and thus moves with the electrophoretic velocity of the micelles. In the region of low retention, the analyte is free and moves at its own natural mobility. The analyte velocity is opposed with a bulk counter-flow so that species concentrate at a unique point along the channel where the total velocity sums to zero.
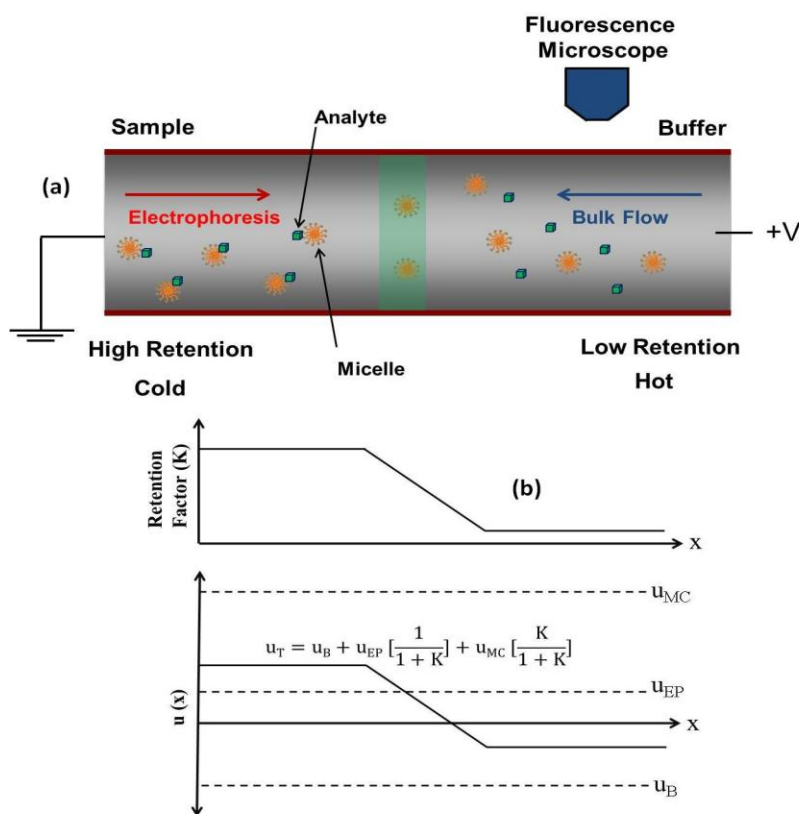
Figure 5.11 (a) Schematic of the experimental setup of MAGF in the chip and flow directions in the microchannel. (b) In the region of high retention, the analyte is located within the micelles and therefore moves with the electrophoretic velocity of the micelles (u_{MC}). In the region of low retention, the analyte is free and moves at its own mobility (u_{EP}). Opposed by a bulk fluid flow (u_B), the total velocity (u_T) therefore sums to zero at a unique point along the channel and the analyte will be focused at that point. In the equation, K is the retention factor for the miceller phase.

The experimental setup for MAGF separation using the fabricated chips is similar to Figure 5.9a. Sample and buffer vials were connected to the chip using fused-silica capillaries with 200 μm i.d. and 350 μm o.d. and counteracting bulk flow was created by changing the relative pressure head (h) between the two vials using a linear stage. Experiments started by positioning the buffer vial about 8 cm above the sample vial to create a positive pressure of around 800 Pa at the buffer reservoir. Negatively charged analytes were then electrically injected into the chip from the cold reservoir by applying a positive high voltage of 2500V to the buffer vial connected to the hot reservoir. The difference in head decreased at a predetermined rate so that the samples focused, and moved along the microchannel toward the hot exit where they were detected using the fluorescent imaging system.

5.6 Results and Discussions

5.6.1 Bilinear Temperature Gradient Focusing

TGF Experiments were performed using an ideal set of analytes (fluorescent dyes): Alexa Fluor 546 C5-maleimide, Alexa Fluor 532 C5-maleimide, and Alexa Fluor 555 C5-maleimide. These dyes have similar molecular structures and therefore their electrophoretic mobilities are expected to be close. These dyes were dissolved in 0.1 M Tris-phenol at a 1 μM concentration and placed in the sample vial. Separation results of the fluorescent dyes are shown in Figure 5.12 for two different temperature profiles (linear and bilinear) and two pressure scanning rates (1 Pa/s and 2 Pa/s). The total channel length was 13 mm. The applied voltage difference was 2500 V and the temperature range was 19 $^{\mathrm{o}}$C (T_1) - 64 $^{\mathrm{o}}$C (T_2) over a 13 mm length.

Figure 5.12 Separation of 3 Alexa Fluor dyes (Alexa Fluor 546 C5-maleimide, Alexa Fluor 532 C5-maleimide and Alexa Fluor 555 C5-maleimide), (a) and (b): bilinear and linear temperature profiles with a scanning rate of 1 Pa/s respectively, and (c) and (d) bilinear and linear temperature profiles with a scanning rate of 2 Pa/s respectively. Sample was 1 µM of each dye into 0.1 M Tris-phenol buffer. The applied voltage was 2500 V and the temperature range was 19 ◦C (T_1) - 64 ◦C (T_2) over a 13 mm length.

The bilinear design shows a significant improvement in the separation results. Resolution is calculated using the following equation [154]:

$$R_S = \frac{\Delta P}{0.85\left(w_1 + w_2\right)} \qquad\qquad (5.4)$$

where ΔP is the pressure difference between the two adjacent peaks and w_i is the peak width at the half peak height. Table 5.1 shows the peak to peak resolution for the dye separation in both linear and bilinear chips. One can see that the peak resolution can be improved using a bilinear gradient profile.

Table 5.1 Peak resolution obtained from separation of 3 Alexa Fluor dyes using both linear and bilinear chips. Peaks are number from right to left.

		Resolution	
		1 pa/s	2 pa/s
PeakID	Linear	1.36	1.31
1−2	Bilinear	3.01	2.53
PeakID	Linear	2.04	0.58
2−3	Bilinear	2.71	0.98

Subsequently, experiments were performed to separate 3 amino acids (glycine (Gly), alanine (Ala), and valine (Val)) labelled by fluorescein isothiocyanate isomer I (FITC). Although FITC-labeled amino acids have been well separated in capillary electrophoresis [155, 156], these amino acids were selected as test analytes because they are expected to have similar electrophoretic mobilities based on their molecular structures. Stock solutions of amino acids were 20 mM in 40 mM sodium bicarbonate buffer (pH 9). FITC dye stock was 0.1 M in DMSO. For labeling, 20 μL of dye stock solution was added to 980 μL of amino acid stock solution and incubated at room temperature for 12 h in the dark. Following incubation, labeled amino acid solutions were stored in the fridge until used. These solutions were used without removal of free dye. Amino acids were diluted into 0.1 M Tris-phenol buffer by the ratio of 1:20, for the experiments. The separation results for two different temperature profiles (linear and bilinear) and two pressure scanning rates (0.5 Pa/s and 1 Pa/s) are shown in Figure 5.13.
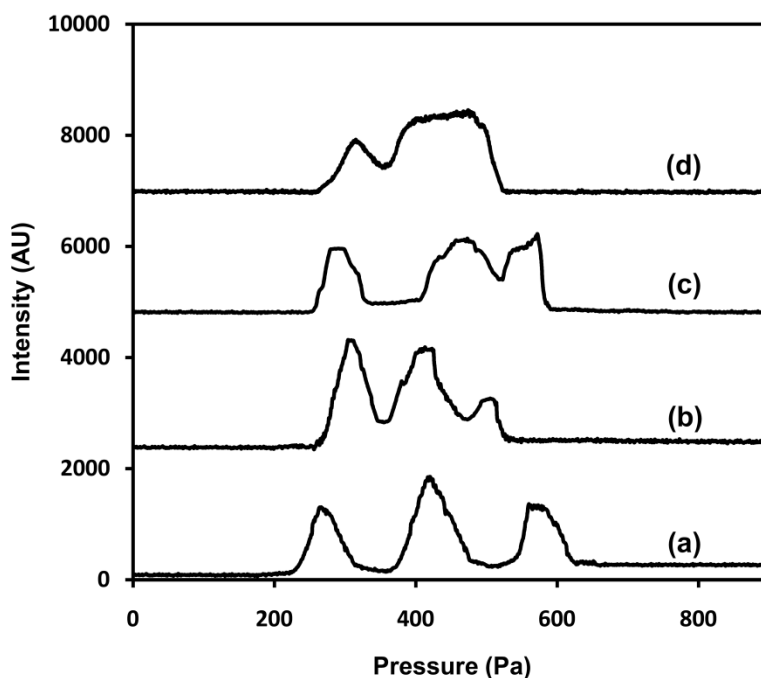
Figure 5.13 Separation of 3 fluorescently labeled amino acids (glycine (Gly), alanine (Ala), and valine (Val)): (a) and (b): bilinear and linear temperature profiles with a scan rate of 0.5 Pa/s, and (c) and (d) bilinear and linear temperature profile with a scan rate of 1 Pa/s. Sample was prepared the day before each experiment and diluted into 0.1 M Tris-phenol buffer by the ratio of 1:20. The applied voltage was 2500 V and the temperature range was 18 ∘C (T1) - 64 ∘C (T2) over a 13 mm length.

The separation resolution of bilinear profile is significantly higher than the linear profile in this case. It can be seen that two of the peaks are merged together for the linear case with a higher scanning rate (Figure 5.13d), while the three peaks are almost completely resolved for the bilinear case (Figure 5.13c). Table 5.2 summarizes the peak to peak resolution for the amino acids results. Again the resolution increases with the bilinear profile.

Table 5.2 Peak resolution obtained from separation of 3 labeled amino acids using both linear and bilinear chips. Peaks are number from right to left.

		Resolution	
		0.5 pa/s	1 pa/s
PeakID 1−2	Linear	0.72	n/a
	Bilinear	1.09	0.64
PeakID 2−3	Linear	0.71	0.59
	Bilinear	1.2	1.12

5.6.2 Bilinear Micellar Affinity Gradient Focusing

To quantify the separation performance of MAGF using bilinear temperature profiles, different analytes including Alexa Fluor dyes and fluorescently labeled pI markers were focused and separated using both linear and bilinear temperature profiles. The average temperature gradient was kept constant at 50 °C/13 mm for both linear and bilinear profiles. Separation of 3 Alexa Fluor dyes (Alexa Fluor 546 C5-maleimide, Alexa Fluor 532 C5-maleimide and Alexa Fluor 555 C5-maleimide) is shown in Figure 5.14 for two different temperature profiles (linear and bilinear) and two pressure scanning rates (0.5 Pa/s and 1.0 Pa/s). In the experiments, the buffer was 5 mM carbonate buffer with a pH of 9.4, containing 20 mM SDS and 25% (v/v) ethanol. The dyes were dissolved in the buffer at a 2 μM concentration and placed in the sample vial.
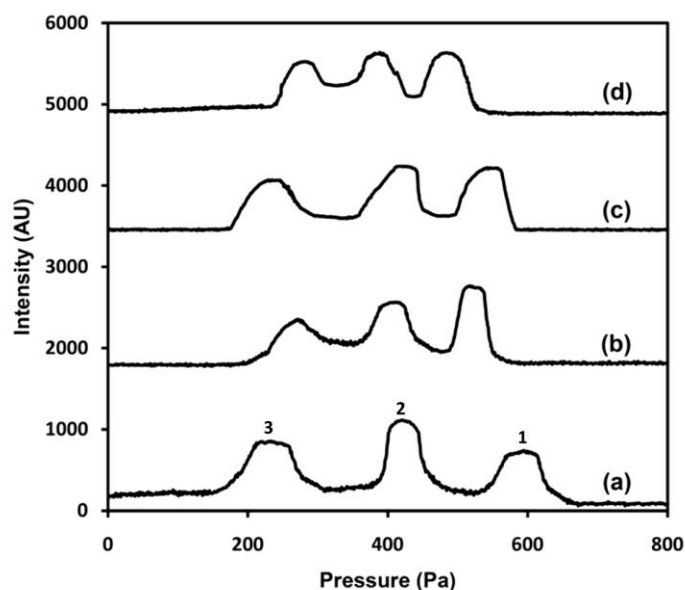
Figure 5.14 Separation of 3 Alexa Fluor dyes (Alexa Fluor 546 C5-maleimide, Alexa Fluor 532 C5-maleimide and Alexa Fluor 555 C5-maleimide), (a) bilinear and (b) linear temperature profiles with a scanning rate of 0.5 Pa/s; (c) bilinear and (d) linear temperature profiles with a scanning rate of 1.0 Pa/s. Sample was 2 µM of each dye into 5 mM carbonate buffer, pH 9.4, containing 20 mM SDS and 25% (v/v) ethanol. The applied voltage was 2500 V and the temperature range was 15 °C (T1)-65 °C (T2) over a 13 mm length.

Lower scanning rates generally lead to higher resolution in separation. One can see that the separation performance can be improved by using a bilinear temperature profile over a linear profile. To quantify the improvement, peak-to-peak resolution was calculated for the separation results using equation (5.4).

The peak-to-peak resolution results for the separation of Alexa Fluor dyes with two different scanning rates are presented in Table 5.3 for both linear and bilinear profiles. It can be seen that peak-to peak resolution increases by approximately 50–100% when the bilinear design is used.

Table 5.3 Peak resolution obtained from separation of three Alexa Fluor dyes using both linear and bilinear chips and SDS surfactant. Peaks order is from right to left.

Resolution			
		0.5 pa/s	1 pa/s
PeakID 1−2	Linear	1.13	0.84
	Bilinear	1.88	1.46
PeakID 2−3	Linear	1.03	0.80
	Bilinear	1.92	1.6

85

Additional separations were performed with three pI markers (4.2, 6.0, 7.3) labeled by 5-carboxytetramethylrhodamine (5-TAMRA). The samples were dissolved in the buffer at a 5 µM concentration and placed in the sample vial. The separation results for two different temperature profiles (linear and bilinear) and two pressure scanning rates (0.4 Pa/s and 0.8 Pa/s) are presented in Figure 5.15.
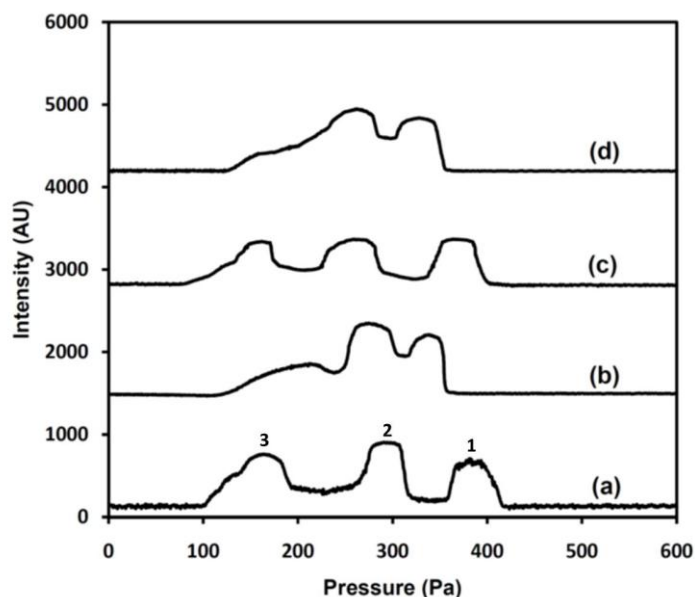
Figure 5.15 Separation of 3 fluorescently labelled pI markers, (a) and (b): bilinear and linear temperature profiles with a scanning rate of 0.4 Pa/s respectively, and (c) and (d) bilinear and linear temperature profiles with a scanning rate of 0.8 Pa/s respectively. Sample was 5 µM of each marker into 5 mM carbonate buffer, pH 9.4 in approximately 25% ethanol by weight, 75% water, with a 20 mM concentration of sodium dodecyl sulfate (SDS). The applied voltage was 2500 V and the temperature range was 15 °C (T_1) - 65 °C (T_2) over a 13 mm length.

Table 5.4 summarizes the peak-to-peak resolution for the separation results. Again, the resolution increases with the bilinear profile by nearly two-fold.

Table 5.4 Peak resolution obtained from separation of three fluorescently labeled pI markers using both linear and bilinear chips and SDS surfactant. Peaks order is from right to left.

Resolution			
		0.4 Pa/s	0.8 Pa/s
PeakID 1−2	Linear	0.73	0.7
	Bilinear	1.25	1.18
PeakID 2−3	Linear	0.69	n/a
	Bilinear	1.50	1.09

In order to validate the presented scanning MAGF separation method, another different surfactant (poly-SUS) was employed to perform the separation of the three pI markers (4.2, 6.0, 7.3) and compared with the separation results using SDS surfactant. Poly-SUS has several advantages over traditional surfactants such as elimination of monomer–aggregate dynamic equilibriums, lower working concentrations due to the exclusion of a CMC, and the ability to support higher organic solvent content within the media. These advantages make this surfactant an ideal candidate for the separation of samples that are moderately to highly hydrophobic [157]. In order to perform the experiments using poly-SUS surfactant, the buffer was prepared according to the previous work by Kamande et al. [109]. A solution of 12.5 mM sodium phosphate dibasic and 12.5 mM sodium borate into 10% methanol was prepared and the pH was adjusted to 9.2 using 1 M NaOH. Poly-SUS surfactant was then added to the prepared solution at 0.125% w/v. The samples were dissolved in the buffer at a 5 µM concentration and placed in the sample vial. Experiments were performed using the same setup as before. The bulk flow pressure was applied from the buffer reservoir and started from a high value while decreased by time during the separation process. The separation results for both linear and bilinear profiles and two pressure scanning rates (0.4 Pa/s and 0.8 Pa/s) are presented in Figure 5.16.
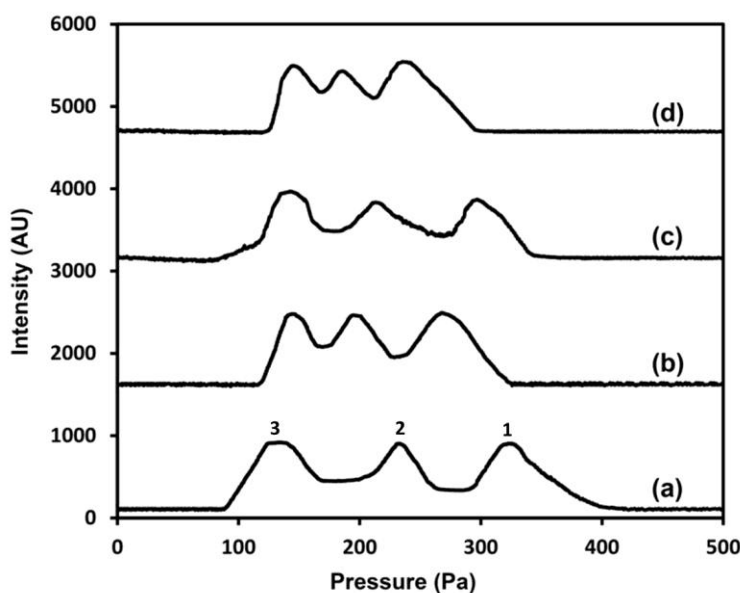
Figure 5.16 Separation of 3 fluorescently labelled pI markers, (a) and (b): bilinear and linear temperature profiles with a scanning rate of 0.4 Pa/s respectively, and (c) and (d) bilinear and linear temperature profiles with a scanning rate of 0.8 Pa/s respectively. Sample was 12.5 mM Sodium phosphate dibasic and 12.5 mM Sodium borate into 10% MeOH with a 0.125% w/v concentration of poly-SUS surfactant as the micellar phase (pH 9.2). The applied voltage was 2500 V and the temperature range was 15 °C (T_1) - 65 °C (T_2) over a 13 mm length.

The peak-to-peak resolution for the separation results is summarized in Table 5.5. It is shown that the resolution increases with the bilinear profile.

Table 5.5 Peak resolution obtained from separation of three fluorescently labeled pI markers using both linear and bilinear chips and Poly-SUS surfactant. Peaks order is from right to left.

Resolution			
		0.4 Pa/s	0.8 Pa/s
PeakID 1−2	Linear	0.72	0.58
	Bilinear	1.14	0.98
PeakID 2−3	Linear	0.76	0.54
	Bilinear	1.24	0.93

According to Figure 5.15 and Figure 5.16, the separation results of the three pI markers using SDS and poly-SUS surfactants are similar. However, poly-SUS is better than SDS in separation performance for the single linear temperature profile. It can be seen in Figure 5.15d that peak 2 and peak 3 are barely distinguishable from each other for higher scanning rates using SDS surfactant while all three peaks are almost the same height when using poly-SUS even at higher scanning rates. Overall, the peaks are more compact when using poly- SUS than using SDS. In both cases, the use of a bilinear temperature gradient improved the separation resolution. A comparison between Table 5.4 and Table 5.5 indicated that the bilinear temperature profile improves the resolution about nearly two times for SDS surfactant and about 1.6 times for poly SUS surfactant, respectively.

Repeatability and reproducibility of the experimental results were also examined and are presented in Table 5.6. Run-to-run repeatability test was analyzed by comparing the resolution of peak ID 1–2 for separation of Alexa Fluor dyes at 0.5 Pa/s scanning rate and the pI markers at 0.4 Pa/s scanning rate using the bilinear experiments. Chip-to-chip reproducibility was also investigated by comparing the resolution of peak ID 1–2 for three different chips. As shown in Table 5.6, the RSD are less than 3% ($n = 3$) for run-to-run repeatability, and less than 7% ($n = 3$) for chip-to-chip reproducibility indicating stable operation of the device and experimental system.

Table 5.6 Repeatability and reproducibility of the MAGF experiments; Resolution was calculated for peak ID 1-2 in separation of Alexa Fluor dyes at 0.5 Pa/s scan rate and the pI markers at 0.4 Pa/s scan rate using the bilinear chip for experiments.

Experiment	Parameter	Resolution			Run-to-run RSD	Chip-to-chip RSD
		Run 1	Run 2	Run 3		
Alexa Fluor separation	Chip 1	1.883	1.931	1.845	2.28%	4.70%
	Chip 2	1.752	1.741	1.796	1.65%	
	Chip 3	1.967	1.926	1.903	1.68%	
pI marker separation using SDS	Chip 1	1.248	1.286	1.303	2.20%	6.17%
	Chip 2	1.204	1.235	1.228	1.33%	
	Chip 3	1.376	1.422	1.342	2.91%	
pI marker separation using poly-SUS	Chip 1	1.143	1.095	1.126	2.17%	5.90%
	Chip 2	1.233	1.202	1.184	2.05%	
	Chip 3	1.264	1.234	1.286	2.07%	

5.7 Conclusion

This work investigated the use of bilinear temperature gradients to improve the separation performance of the scanning temperature gradient focusing and micellar affinity gradient focusing methods. In this chapter, a separation scheme where a bilinear temperature gradient along the separation channel was employed with scanning TGF and MAGF was presented. The temperature profile along the channel consists of a very sharp gradient used to pre-concentrate the sample, followed by a shallow gradient that increases separation resolution. A specialized design was developed for the heaters to achieve the bilinear profile using both analytical and numerical modeling. Separation experiments were performed for different dyes, amino acids and pI markers that have close electrophoretic mobilities. Experiments show a dramatic improvement in peak capacity and resolution of both techniques with bilinear design in comparison to the standard linear profile.

Chapter 6

Theory of Bilinear Scanning Counter-Flow Gradient Electrofocusing Methods

6.1 Introduction

As discussed in section 2.4.2, in counter-flow gradient electrofocusing methods, the electrophoretic motion of analytes is counter-balanced by a bulk fluid flow to accumulate or focus analytes at stationary points along a separation column. To achieve this, a gradient has to be made for one or both of the forces that affect the analytes along the column in order to generate a gradient in the total analyte velocity (the sum of electrophoretic and counter-flow velocities) with a zero-velocity point somewhere along the gradient [158, 41]. In most of these techniques, a gradient is made in the electrophoretic velocity of the analyte, while the bulk counter-flow is kept constant [41]. The electrophoretic velocity of an analyte is given as $u = E\upsilon_{ep}$, where υ_{ep} is the electrophoretic mobility of the analyte and E is the applied electrical field. By changing one of the applied electrical field and electrophoretic mobility, or both, one can reach a gradient in the electrophoretic velocity of the analyte along the separation column [41]. For example, in the temperature gradient focusing method [98], a temperature gradient is used that generates gradients in electric field, electrophoretic mobility and electrophoretic velocity of analytes along the separation column.

As discussed in Chapter 5, the use of a bilinear temperature gradient along the separation channel can improve separation resolution of TGF and MAGF techniques. Similar studies have also shown that using a bilinear electrophoretic velocity gradient along the separation column, improves both peak capacity and separation resolution of EFGF technique [144, 143]. A bilinear gradient consists of a sharp gradient to pre-concentrate the sample, followed by a shallow gradient that increases separation resolution.

Despite previous studies, the effect of changing parameters such as the geometry of bilinear gradients or the bulk counter-flow scan rate on separation performance of counter-flow gradient electrofocusing methods has not been studied yet. In this work, an analytical model is developed to calculate the

separation resolution of scanning counter-flow gradient electrofocusing methods with any bilinear gradient at different scan rates. The effect of bilinear gradient combination and bulk counter-flow scan rate has been studied on the equation of motion of analytes as well as the 1-D convection-diffusion equation along the separation channel. The results indicate that any bilinear gradient provides a higher separation resolution (up to 100%) than the linear case. Additionally, for some scanning rates, an optimum bilinear gradient can be found that maximizes separation resolution. A one-dimensional COMSOL simulation was also developed to validate some of the results.

6.2 Analytical Model

6.2.1 Model Definition

In order to investigate the effect of using a bilinear electrophoretic velocity gradient on separation performance, in this section an analytical model is developed for calculating the separation resolution of scanning counter-flow gradient electrofocusing techniques with different bilinear gradients and scan rates. In this work, it is assumed that transport and separation of analytes occur only in the x dimension along the column. According to the theory of counter-flow gradient electrofocusing methods [41], the velocity of an analyte in the separation column is given by the sum of its electrophoretic velocity and the counter-flow velocity of the buffer

$$u_T = u_{ep} + u_B \qquad (6.1)$$

Here we assume that for a linear gradient, the electrophoretic velocity along the separation column is defined as

$$u_{ep} = E_0 \upsilon_0 f(x) \qquad (6.2)$$

where E_0 and υ_0 are the electric field and the electrophoretic mobility of the analyte at the inlet x=0 and $f(x)$ corresponds to the electrophoretic velocity gradient along the separation column. Considering the gradient in equation (6.2), the bulk counter-flow velocity can be adjusted so that the total velocity is equal to zero at a single point along the channel and the analyte is focused at that point. By using a constant

bulk counter-flow, the focusing point will be stationary and the peak capacity will be limited and only very few analytes with similar electrophoretic mobilities can be focused and separated in the column at the same time. In the scanning format, the applied bulk counter-flow starts from a very low (high) value and increases (decreases) with time. Therefore, analytes with a wide range of electrophoretic mobilities can enter the separation column sequentially and be focused as they traverse the column. The general equation for the bulk counter-flow velocity can be expressed as

$$u_B = at + u_{B0} \qquad (6.3)$$

where a is the counter-flow scan rate, t is time, and u_{B0} is the initial bulk counter-flow value. Figure 6.1 shows a schematic of the analytical model. A long, straight, buffer-filled microchannel with length L is used in which a factor F $(0.5 \leq F \leq 1)$ controls the share of the first segment from the overall electrophoretic velocity difference along the channel, such as

$$f(L/2) = f_0 + F(f(L) - f(0)) \qquad (6.4)$$

When $F = 0.5$, there is a linear gradient along the entire channel. By increasing the value of F, the first gradient becomes sharper while the second becomes shallower.
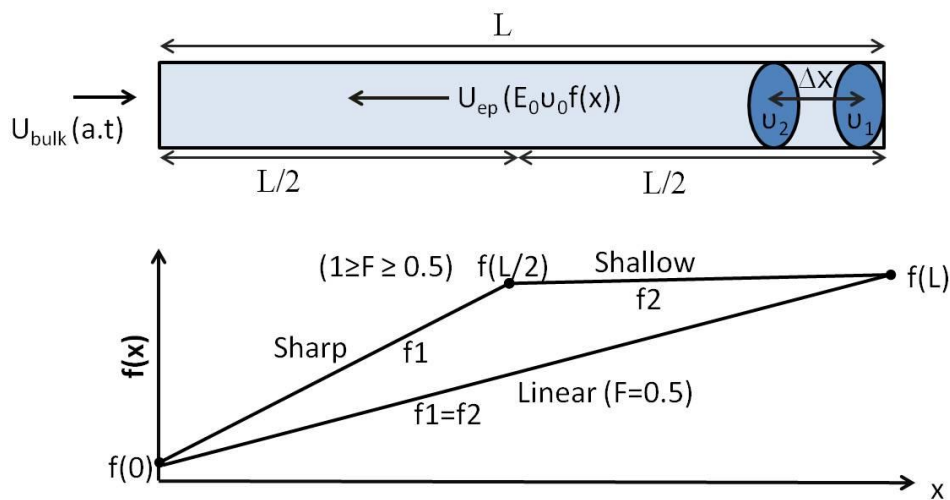
Figure 6.1 Schematic of the analytical model. Separation starts when the electrophoretic velocity of the first analyte is equal to the bulk counter-flow velocity at the channel inlet $u_{B0} = E_0 \upsilon_{01} f(0)$. The factor F $(0.5 \leq F \leq 1)$ controls the share of the first half of the channel from the overall electrophoretic velocity difference along the channel. Separation resolution is calculated once the first peak reaches at the channel outlet.

Here, we assume that the minimum and maximum electrophoretic velocities along the channel (electrophoretic velocity at $x=0$ and $x=L$ respectively) for each analyte are constant for any value of F. Therefore the values of $f(0)$ and $f(L)$ are constant and $f(x)$ can be defined at any point along the channel

$$0 \leq x \leq L/2 \qquad f(x) = f(0) + f_1 x$$
$$L/2 \leq x \leq L \qquad f(x) = f(0) + f_1 \times L/2 + f_2(x - L/2)$$
(6.5)

where f_1 and f_2 are the slopes of the first and second gradients and are defined as

$$f_1 = \left(f(L/2) - f(0)\right)/(L/2)$$
$$f_2 = \left(f(L) - f(L/2)\right)/(L/2)$$
(6.6)

The separation of two sample analytes with electrophoretic mobilities υ_{01} and υ_{02} is also shown at the channel exit in Figure 6.1. It is assumed that separation starts when the electrophoretic velocity of the first analyte is equal to the bulk counter-flow velocity at channel inlet, and therefore,

$$u_{B0} = E_0 \upsilon_{01} f(0)$$
(6.7)

According to the analytical setup, the bulk counter-flow increases with time in order to perform the separation and analytes can enter the separation channel only when the bulk counter-flow velocity is higher than the electrophoretic velocity of the analyte at the channel inlet. Therefore it is obvious that $\upsilon_{01} < \upsilon_{02}$. In general, the analyte with the lowest electrophoretic mobility enters the channel first and requires less time to traverse the channel, while the analyte with the highest electrophoretic mobility enters the channel at last and also requires the highest time to traverse the channel. The separation resolution for these two analytes at the end of the channel can be defined as [41]

$$R_s = \frac{\Delta x}{2(\sigma_1 + \sigma_2)}$$
(6.8)

where Δx is the distance between the center of the peaks and σ_1 and σ_2 are the standard deviation of the first and second peak, respectively. In order to find Δx in equation (6.8), the position of the analyte peaks

at any time along the separation channel has to be known. The equation of motion of an analyte along the separation channel can be found by solving the following differential equations

$$dx/dt = at - p_1 x \qquad x(0) = 0 \qquad 0 \le x \le L/2$$
$$dx/dt = at - p_2(x - L/2) + u_T(L/2) \qquad x(0) = L/2 \qquad L/2 \le x \le L$$

(6.9)

where $p_1 = E_0 \upsilon_0 f_1$, $p_2 = E_0 \upsilon_0 f_2$ and $u_T(L/2)$ is the total velocity of the analyte at the middle of the channel. The solution for the position, overall velocity, and passing time of the analyte in each gradient can be written as

For $0 \le x \le L/2$

$$x = \frac{a(p_1 t - 1)}{p_1^2} + \frac{a}{p_1^2} e^{-p_1 t} = \frac{1}{2} a t^2 - \frac{1}{6} a p_1 t^3 + \frac{1}{24} a p_1^2 t^4 - \ldots$$

$$u = \frac{dx}{dt} = \frac{a}{p_1}\left(1 - e^{-p_1 t}\right) = at - \frac{1}{2} a p_1 t^2 + \frac{1}{6} a p_1^2 t^3 - \ldots$$

(6.10)

$$t_1 = \frac{aW(-e^{\frac{-Lp_1^2}{2a}-1}) + a + Lp_1^2/2}{a p_1}$$

For $L/2 \le x \le L$

$$x - L/2 = \frac{a(p_2 t - 1)}{p_2^2} + \frac{a}{p_2^2} e^{-p_2 t} + \frac{u(L/2)}{p_2}\left(1 - e^{-p_2 t}\right)$$

$$u = \frac{dx}{dt} = \frac{a}{p_2}\left(1 - e^{-p_2 t}\right) + u(L/2) e^{-p_2 t}$$

(6.11)

$$t_2 = \frac{cW(-\frac{(c-d)e^{d/c - L/2c - 1}}{c}) + c - d + L/2}{c p_2}$$

where $c = \dfrac{a}{p_2^2}$, $d = \dfrac{u_T(L/2)}{p_2}$, W is the product log function and t_1, t_2 are the times required for the analyte to pass the first and second half of the channel. Using equations (6.10) and (6.11), the value of

94

Δx in equation (6.8) can be calculated at the end of the separation channel for any value of F and counter-flow scan rate a as

$$\Delta x = L/2 - \left(\frac{a\left(p_{22}t_{22}^* - 1\right)}{p_{22}^2} + \frac{a}{p_{22}^2} e^{-p_{22}t_{22}^*} + \frac{u_{T2}\left(L/2\right)}{p_{22}} \left(1 - e^{-p_{22}t_{22}^*}\right) \right) \tag{6.12}$$

where $p_{22} = E_0 \upsilon_{02} f_2$, $u_{T2}\left(L/2\right)$ is the total velocity of the second analyte at the middle of the channel, and t_{22}^* is the time that the second peak spends in the second gradient before the first peak reaches the channel outlet

$$t_{22}^* = \left(t_{11} + t_{12}\right) - t_{21} - E_0 f\left(0\right)\left(\upsilon_{02} - \upsilon_{01}\right)/a \tag{6.13}$$

In equation (6.13), t_{11} and t_{12} correspond to the times required for the first peak $\left(\upsilon_1\right)$ to pass the first and second gradients, and can be calculated from equations (6.10) and (6.11). Similarly, t_{21} corresponds to the time required for the second peak $\left(\upsilon_2\right)$ to pass the first gradient in the channel. The last term in equation (6.13) corresponds to the difference in times that the analytes first enter the separation channel.

6.2.2 Convection-Diffusion Equation

To calculate the standard deviation σ of the peaks in equation (6.8), we first need to solve the 1-D convection-diffusion equation for our counter-flow gradient electrofocusing problem. Here, we solve the convection-diffusion equation for a system that has a linear electrophoretic velocity gradient with a slope f and an increasing bulk counter-flow with scan rate a, and then we use the solution for each of our gradients explicitly. The general form of the 1-D convection-diffusion equation with respect to Fokker-Plank diffusivity law [159, 107] can be written as

$$\frac{\partial c}{\partial t} = -\frac{\partial}{\partial x}\left(u_T c\right) + \frac{\partial^2}{\partial x^2}\left(D_{eff} c\right) \tag{6.14}$$

where $u_T = u_{ep} + u_B$ is the sum of all analyte displacement velocities, D_{eff} is the effective diffusion around the focusing point, c is analyte concentration, and t is time. To solve equation (6.14) for our scanning counter-flow gradient electrofocusing system, we first need to change the coordinate so that the new

coordinate moves with the focusing location and its basis is located on the center of gravity of the focused peak at any time [160]. By defining $\tilde{x} = x - x_{foc}$ and rewriting equation (6.14) with $x = \tilde{x} + x_{foc}$, we obtain

$$\frac{\partial c}{\partial t} + \frac{\partial c}{\partial \tilde{x}} \times \frac{\partial \tilde{x}}{\partial t} = -\frac{\partial}{\partial \tilde{x}}\left(\left(u_B - p\left(\tilde{x} + x_{foc}\right)\right)c\right) + \frac{\partial^2}{\partial \tilde{x}^2}\left(D_{eff}c\right) \qquad (6.15)$$

where $p = E_0 \upsilon_0 f$ corresponds to the gradient along the channel. By using Taylor series expansion, we can rewrite D_{eff} around the focusing point as

$$D_{eff} = D_{foc} + D_1 \tilde{x} \qquad (6.16)$$

where D_1 is a constant and D_{foc} is the overall diffusion at the focusing point and can be defined as [107]

$$D_{foc} = D\left(1 + \frac{2}{105}Pe^2\right) \qquad (6.17)$$

where D and Pe are the molecular diffusivity and the Peclet number at the focusing point, respectively. Considering the fact that both the terms $-\frac{\partial \tilde{x}}{\partial t}$ and $\left(u_B - px_{foc}\right)$ in equation (6.15) correspond to the total velocity of the analyte at the focusing point u_{foc}, and using $D_{eff} = D_{foc} + D_1 \tilde{x}$, the equation will become

$$\frac{\partial c}{\partial t} = p\frac{\partial}{\partial \tilde{x}}\left(c\tilde{x}\right) + D_{foc}\frac{\partial^2 c}{\partial \tilde{x}^2} + 2D_1\frac{\partial c}{\partial \tilde{x}} + D_1\tilde{x}\frac{\partial^2 c}{\partial \tilde{x}^2} \qquad (6.18)$$

In order to find the variance of the focused peak in equation (6.18), we use the method of statistical moments [160, 161, 106]. The nth moment of the distribution function about the mean is defined as

$$M_n = \int_{-\infty}^{\infty} \tilde{x}^n c\left(\tilde{x}, t\right) d\tilde{x} \qquad (6.19)$$

Similar to the work of Ghosal et al. [106], with multiplying equation (6.18) by $\tilde{x}^n$ and integrating, we get

$$\frac{\partial}{\partial t}\int_{-\infty}^{\infty}c\tilde{x}^{n}d\tilde{x} = p\int_{-\infty}^{\infty}\left(c\tilde{x}^{n} + \frac{\partial c}{\partial \tilde{x}}\tilde{x}^{n+1}\right)d\tilde{x} + D_{foc}\int_{-\infty}^{\infty}\left(\frac{\partial^{2}c}{\partial \tilde{x}^{2}}\tilde{x}^{n}\right)d\tilde{x} +$$

$$+ D_{1}\left(\int_{-\infty}^{\infty}\left(2\frac{\partial c}{\partial \tilde{x}}\tilde{x}^{n} + \frac{\partial^{2}c}{\partial \tilde{x}^{2}}\tilde{x}^{n+1}\right)d\tilde{x}\right)$$

(6.20)

By simplifying the integrations and using the definition of statistical moments, equation (6.20) further becomes

$$\frac{dM_{n}}{dt} = \left(1-(n+1)\right)pM_{n} + D_{foc}n(n-1)M_{n-2} + D_{1}\left(-2n+n(n+1)\right)M_{n-1} = -npM_{n} +$$

$$+ D_{foc}n(n-1)M_{n-2} + D_{1}n(n-1)M_{n-1}$$

(6.21)

Setting $n=$ 0, 1, and 2 in equation (6.21), we can find the first three moments and use them to calculate the mean and variance of the peak [106]

$$n=0: \quad \frac{dM_{0}}{dt} = 0 \rightarrow M_{0} = const$$

$$n=1: \quad \frac{dM_{1}}{dt} = -M_{1}p \rightarrow M_{1} = M_{1}(0)e^{-pt}$$

$$n=2: \quad \frac{dM_{2}}{dt} = -2pM_{2} + 2D_{foc}M_{0} + 2D_{1}M_{1} \rightarrow M_{2} = M_{2}(0)e^{-2pt} +$$

$$+ \frac{D_{foc}M_{0}}{p}\left(1-e^{-2pt}\right) + \frac{2D_{1}M_{1}}{p}\left(1-e^{-pt}\right)$$

(6.22)

From equation (6.22), the mean or the position of the center of gravity of the peak can be calculated as [160, 106]

$$m = \frac{M_{1}}{M_{0}} = \frac{M_{1}(0)}{M_{0}}e^{-p.t}$$

(6.23)

where $M_{1}(0)$ corresponds to the initial value of M_{1} at $t=0$. Similarly, the variance can be calculated as [160, 106]

$$v = \sigma^2 = \frac{M_2}{M_0} - m^2 = \frac{M_2(0)}{M_0} e^{-2.p.t} + \frac{D_{foc}}{p}\left(1 - e^{-2.p.t}\right) + \frac{2D_1 m}{p}\left(1 - e^{-p.t}\right) \tag{6.24}$$

The mean value calculated in equation (6.23) is always zero for our case because the basis of the coordinate system is arbitrarily fixed at the center of gravity of the peak [160]. Therefore, the variance can be simplified as

$$v = \sigma^2 = \sigma_0^2 e^{-2.p.t} + \frac{D_{foc}}{p}\left(1 - e^{-2.p.t}\right) \tag{6.25}$$

Here, σ corresponds to the peak width used in equation (6.8) and σ_0 is the initial peak width which is considered equal to the channel length L at the channel inlet. For a bilinear gradient, the equations for the sharp and shallow gradients are different because the values of p and σ_0 in equation (6.25) are different in each gradient. In general, when a peak moves from the sharp gradient into the shallow gradient, the value of p changes in the equation, and σ_0 for the second gradient becomes the standard deviation at the end of the first gradient.

6.2.3 Resolution Calculation

The separation resolution for two analytes at the end of the channel can be defined by equation (6.8) for any bilinear gradient at different scan rates.

Using equation (6.25), the values of σ_1 and σ_2 at the end of the separation channel can be calculated as

$$\sigma_1^2 = \left(L^2 e^{-2p_{11}t_{11}} + \frac{D_{foc,11}}{p_{11}}\left(1 - e^{-2p_{11}t_{11}}\right)\right) e^{-2p_{12}t_{12}} + \frac{D_{foc,12}}{p_{12}}\left(1 - e^{-2p_{12}t_{12}}\right)$$

$$\sigma_2^2 = \left(L^2 e^{-2p_{21}t_{21}} + \frac{D_{foc,21}}{p_{21}}\left(1 - e^{-2p_{21}t_{21}}\right)\right) e^{-2p_{22}t_{22}^*} + \frac{D_{foc,22}}{p_{22}}\left(1 - e^{-2p_{22}t_{22}^*}\right) \tag{6.26}$$

where $p_{11} = E_0 \upsilon_{01} f_1$, $p_{12} = E_0 \upsilon_{01} f_2$, $p_{21} = E_0 \upsilon_{02} f_1$, $D_{foc,11}$ and $D_{foc,12}$ are the overall diffusion of the first analyte at the end of the first and second gradient respectively and can be calculated from equation (6.17). Similarly, $D_{foc,21}$ and $D_{foc,22}$ correspond to the overall diffusion of the second analyte at the end of the first and second gradients respectively. Using equations (6.12),(6.13), and (6.26), the final equation

for the resolution of two analytes at the end of the separation column with any bilinear gradient and scan rate can be expressed as

$$R_s = \frac{L/2 - \left(\dfrac{a\left(p_{22}t_{22}^* - 1\right)}{p_{22}^2} + \dfrac{a}{p_{22}^2}e^{-p_{22}t_{22}^*} + \dfrac{u_{T2}\left(L/2\right)}{p_{22}}\left(1 - e^{-p_{22}t_{22}^*}\right) \right)}{2\left(\sqrt{\left(L^2 e^{-2p_{11}t_{11}} + \dfrac{D_{foc,11}}{p_{11}}\left(1 - e^{-2p_{11}t_{11}}\right)\right)e^{-2p_{12}t_{12}} + \dfrac{D_{foc,12}}{p_{12}}\left(1 - e^{-2p_{12}t_{12}}\right)} + \sqrt{\left(L^2 e^{-2p_{21}t_{21}} + \dfrac{D_{foc,21}}{p_{21}}\left(1 - e^{-2p_{21}t_{21}}\right)\right)e^{-2p_{22}t_{22}^*} + \dfrac{D_{foc,22}}{p_{22}}\left(1 - e^{-2p_{22}t_{22}^*}\right)} \right)} \qquad (6.27)$$

6.3 Numerical Model

To validate our analytical results, a 1-D numerical simulation similar to section 5.2 was performed using the commercial software package, COMSOL Multiphysics. In the numerical simulation, a 2 cm long channel was used to separate two model analytes that have a 5% difference in their electrophoretic mobilities. An electrophoretic velocity gradient $u_L = 1.4u_0$ was defined along the channel together with a time-dependent bulk counter-flow $u_{bulk} = a \times t - 0.001$ to perform the focusing and separation along the channel. The transport of each analyte was calculated using the electrokinetic flow model $\partial c / \partial t + \nabla\left(-D\nabla c - \mu_{ep}c\nabla V\right) = -u_{bulk}\nabla c$ where c is the concentration, D is diffusion, and μ_{ep} is the electrophoretic mobility of each analyte respectively. In the model, ∇V represents the electric field gradient along the channel. A constant electric field of 3000 V was applied over the length of the separation channel and the diffusion was calculated along the channel length using equation (6.17) and was used in the simulations. All the other parameters, such as mobilities, scan rates, and etc. were used the same as in our analytical model. After the separation of analytes at the end of the second segment, the resolution was calculated for each case using the formula $R_s = \Delta x / 0.85\left(w_1 + w_2\right)$, where Δx is the distance between the two peaks and w_1, w_2 are the peak width measured at half height [36]. Using equation above, the resolution was calculated to validate some of the analytical results.

6.4 Results and Discussions

A Matlab program was developed to calculate the resolution from equation (6.27) for any value of F, scan rate a, diffusion D, electric field E_0, and mobility v. In the model, it was assumed that the channel length L is 0.02 m with $L_1=L_2=0.01$ m and that the two analytes have 5% difference in their electrophoretic mobilities for all cases. The electrophoretic mobility of the first analyte, v_1, the electric field over the length of the channel E_0/L, $f(0)$, and $f(L)$ were set to be 2×10^{-8}, 3000, 1, and 1.4, respectively. Figure 6.2 shows the calculated resolution at the end of the channel for any value of F $(0.5 \le F \le 1)$ and different scan rates. The scan rate values are normalized with the electrophoretic velocity of the first analyte at the beginning of the separation channel $u_0 = E_0 v_{01} f(0)$. The results were calculated for diffusion rate $D = 5\times10^{-9}$ m^2/s, which corresponds to the effective diffusion of $D_{eff} = 1.2\times10^{-8}$ m^2/s at the end of the separation channel. The dashed lines in Figure 6.2 show the COMSOL simulation results for the resolution at the two scan rates $a/u_0 = 0.02$ and $a/u_0 = 0.002$. These results agree well with the results of theoretical work.

It is possible to calculate the resolution for other values of D_{eff} at the end of the separation channel with reasonable accuracy from Figure 6.2, given the fact that for a steady state Gaussian profile, the peak variance and resolution are proportional to and inversely proportional to, respectively, the square root of the effective diffusion at the focusing point [107, 98]. Therefore, using the formula at the vertical axis of Figure 6.2, for D_{eff} higher than the initial value of 1.2×10^{-8} m^2/s and lower than it, the resolution decreases and increases, respectively, with a factor of $\left(1.2\times10^{-8}/D_{eff}\right)^{1/2}$.

As seen in Figure 6.2, the resolution for bilinear gradients $(0.5 < F \le 1)$ is higher than the equivalent linear gradient for different scan rates and, in some cases, the resolution can be improved over 100% by using an appropriate bilinear gradient. Starting from the high scan rate $a/u_0 = 0.1$, the resolution increases by increasing the value of F until $F = 1$. For high scan rates, the focused analytes spend less time in the shallow gradients, and the diffusion cannot exceed convection even for $F = 1$. By reducing the scan rate, analytes spend more time in the shallow gradient and the rate of dispersion increases, which

affects the resolution especially for higher values of F. For $a/u_0 = 0.01$, the resolution does not significantly change from $F = 0.8$ to 1, which corresponds to the case in which diffusion and convection are of the same order. By further reducing the scan rate, resolution increases from $F = 0.5$ to around 0.84, where it reaches to its maximum value. For higher values of F until $F = 1$, resolution decreases, which indicates that diffusion rate is higher than convection for these cases. Therefore, an optimum value of F around 0.84 can be found for moderate to low scan rates to be used in counter-flow gradient electrofocusing methods in order to maximize the resolution. It can also be seen that by further decreasing the scan rate, the resolution cannot exceed the value of around 2.5 for the linear gradient, but it can be further increased by using a bilinear gradient.
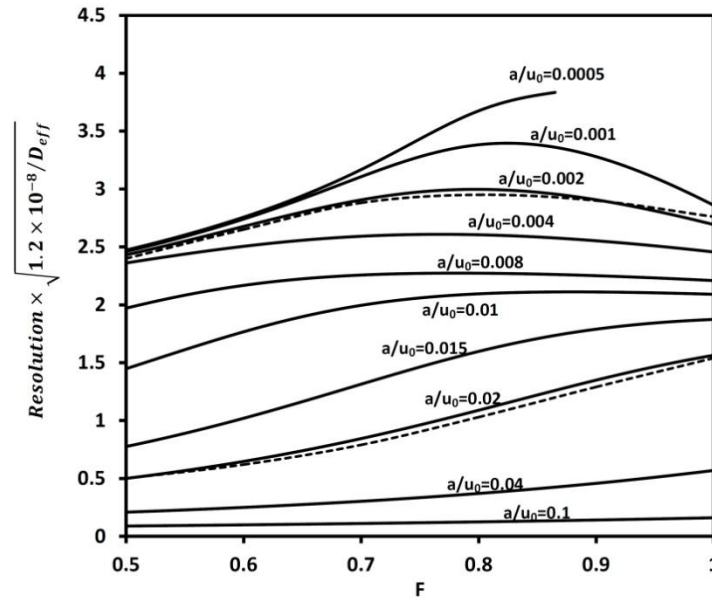
Figure 6.2 Resolution results for different values of F at different scan rates. In the calculations, it was assumed that the channel length L is *0.02 m* with $L_1=L_2=0.01$ m and that the two analytes have 5% difference in their electrophoretic mobilities. The electrophoretic mobility of the first analyte υ_1, the electric field over the length of the channel E_0/L, $f(0)$, and $f(L)$ were set to be 2×10^{-8}, 3000, 1, and 1.4 respectively. The scan rate values are normalized with the electrophoretic velocity of the first analyte at the beginning of the channel $u_0 = E_0\upsilon_{01}f(0)$. The results were calculated for diffusion rate $D = 5\times10^{-9}$ m^2/s, which corresponds to the effective diffusion of $D_{eff} = 1.2\times10^{-8}$ m^2/s at the end of the separation channel. The dashed lines correspond to a 1-D COMSOL simulation performed with the same initial values and for scan rates $a/u_0 = 0.02$ and $a/u_0 = 0.002$. Resolution results for other values of D_{eff} can be estimated from the figure by using the formula presented at the vertical axis.

The discontinuity in Figure 6.2 for $a/u_0 = 0.0005$ and $F=0.86$ corresponds to the case in which the first analyte exits the channel before the second analyte enters the shallow gradient. Although it is still possible to calculate the resolution for higher values of F, we consider this case as a stop point for our bilinear separation study.

To investigate the effect of gradient length on separation performance, the resolution was also calculated for the case in which $L_1=0.3L$ while all other parameters were used the same and the results are shown in Figure 6.3. It is obvious that in this case, $F=0.3$ corresponds to the linear gradient along the channel and by increasing the value of F, the first gradient becomes sharper while the second becomes shallower.
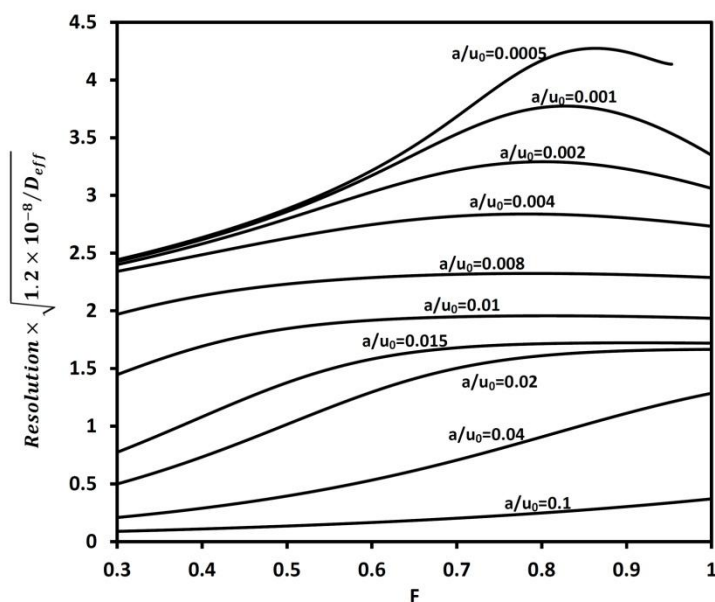
Figure 6.3 Resolution results for all values of F at different scan rates. In the calculations, it was assumed that the channel length L is 0.02 m with $L_1=0.3L= 0.006$ m and that the two analytes have 5% difference in their electrophoretic mobilities. The electrophoretic mobility of the first analyte υ_1, the electric field over the length of the channel E_0/L, $f(0)$, and $f(L)$ were set to be 2×10^{-8}, 3000, 1, and 1.4 respectively. The scan rate values are normalized with the electrophoretic velocity of the first analyte at the beginning of the channel $u_0 = E_0\upsilon_{01}f(0)$. The results were calculated for diffusion rate $D=5\times10^{-9}$ m^2/s, which corresponds to the effective diffusion of $D_{eff} =1.2\times10^{-8}$ m^2/s at the end of the separation channel.

A simple comparison between Figure 6.2 and Figure 6.3 indicates that although the results are very similar, the separation resolution is slightly higher in Figure 6.3 especially for higher values of F and

102

lower scan rates. This can be due to the fact that in this case, the two analytes can spend more time together inside the shallow gradient and therefore separate more from each other. It is also shown that for this case, the limit in which the two analytes can still appear inside the shallow gradient is shifted to $F=0.95$ for $a/u_0 = 0.0005$. Furthermore, an optimum value of F for moderate to low scan rates can still be found around 0.84 in this case.

It is noteworthy that for those counter-flow gradient electrofocusing methods in which a temperature gradient is used along the channel to generate the electrophoretic velocity gradient such as TGF, the calculated resolution can be different from that found with techniques without a temperature gradient in the same conditions. The reason is, the diffusion D in equation (6.17) is temperature dependent and changes along the separation channel, which gives rise to a different D_{eff} along the channel.
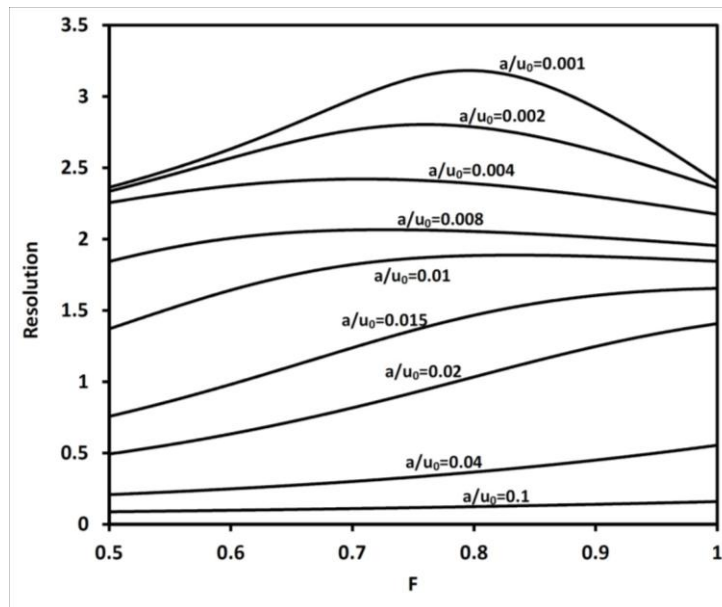
Figure 6.4 Resolution results for all values of F at different scan rates for temperature gradient focusing method (TGF) with temperature gradient 20 °C-80 °C over the channel length. In the calculations, it was assumed that the channel length L is 0.02 m with $L_1=L_2=0.01$ m and that the two analytes have 5% difference in their electrophoretic mobilities for all cases. The electrophoretic mobility of the first analyte υ_1, the electric field over the length of the channel E_0/L, $f(0)$, and $f(L)$ were set to be 2×10^{-8}, 3000, 1, and 1.4 respectively. The scan rate values are normalized with the electrophoretic velocity of the first analyte at the beginning of the channel $u_0 = E_0 \upsilon_{01} f(0)$. The results were calculated for diffusion rate $D = 5 \times 10^{-9}$ m^2/s at channel inlet which corresponds to the effective diffusion of $D_{eff} = 1.8 \times 10^{-8}$ m^2/s at the end of the separation channel.

Figure 6.4 shows the calculated resolution for the TGF method with a temperature gradient of $20^{\circ}C - 80^{\circ}C$ along the separation channel, with peaks located at the hot end of the channel and all the other conditions the same as Figure 6.2. Here, it was assumed that the defined temperature gradient leads to the same electrophoretic velocity gradient – same values for $f(0)$ and $f(L)$ – along the separation channel. For such a case, the effective diffusion was $D_{eff} = 1.8 \times 10^{-8} \ m^2/s$ at the end of the channel, and the resolution was slightly lower than the results shown in Figure 6.2.

6.5 Conclusion

An analytical model was developed to calculate the separation resolution of scanning counter-flow gradient electrofocusing methods with different bilinear gradients and scan rates. The results indicate that a bilinear gradient combination provides a higher separation resolution than the linear system. Depending on the scan rate and the bilinear gradient shape, this increment can be up to 100%. It was observed that for moderate to low scan rates, an optimum bilinear gradient with F around 0.84 can be found that maximizes the separation resolution. Results were agreed well with those of equivalent numerical simulations performed in a 1-D COMSOL model.

Chapter 7

Development of a Two-Dimensional Separation System Combining TGF and SDS-PAGE

7.1 Introduction

According to section 2.5, the peak capacity of a separation, *P*, describes the maximum number of components that can be resolved in any given separation [110]. However, the peak capacity of a single CE procedure is, by itself, usually not adequate for resolving complex mixtures. Attempts have therefore been made to combine different methods (multi-dimensional separations) to generate the required peak capacity for complex separations [111, 112]. A requirement of any successful multi-dimensional procedure is orthogonality, which means that the selected dimensions possess different, but compatible, separation mechanisms. Furthermore, the subsequent dimension in any multi-dimensional separation should not destroy the resolution achieved by the previous one [111]. The peak capacity of a multi-dimensional separation is the product of peak capacities of its constituent one-dimensional (1-D) methods (P_1 to P_n), a definition valid only when the modes of separation are completely orthogonal [111]. It is obvious that microfluidic chips are good candidates as platforms for multi-dimensional analyses since they allow fluidic connections with minimal dead volumes, making multiple separation channels easily coupled. The critical points when performing multi-dimensional separations in microfluidic chips are: (i) the compatibility between the buffers used for the different dimensions; (ii) the speed of the separation – for a direct coupling, for instance, the second dimension has to be faster than the previous one; (iii) the ability to introduce multiple different separation media in one single microfluidic system; and (iv) the quantitative transfer of focused samples from the first separation dimension to the second without significant loss in the resolution acquired from the first dimension.

So far, there is no 2-D configuration that uses TGF as one of the dimensions. However, scanning TGF has the potential to be used in multi-dimensional separations because of its ease of use and its high peak capacity [95, 36]. In this section, a two-dimensional microfluidic system is presented for protein

separation that combines temperature gradient focusing (TGF) and sodium dodecyl sulfate (SDS) polyacrylamide gel electrophoresis (PAGE). Denatured proteins are first focused and separated based on their electrophoretic mobility, in a 15 mm separation channel using scanning the TGF method with a temperature range of 15-50 °C and the relatively low pressure scan rate of -0.5 Pa/s. By gradually reducing the bulk flow, the focused bands are subsequently transferred toward the end of the first dimension, where they are continuously introduced into a 25 mm channel filled with polyacrylamide gel. A side channel is used at the beginning of the second dimension to continuously inject SDS into the gel, allowing defined volumes of SDS to be mixed into the focused bands [122]. The proteins are further separated along the second dimension based on molecular size using SDS-PAGE. Figure 7.1 shows a schematic of the two-dimensional separation system.
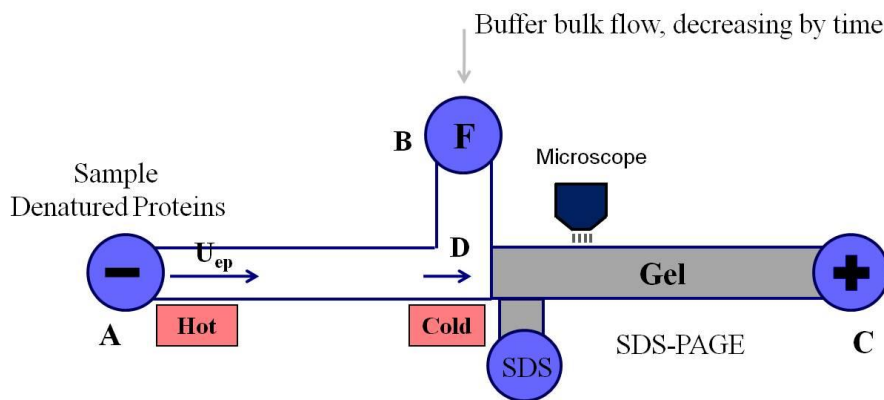
Figure 7.1 Schematic of the proposed 2-D system. Samples are first separated by scanning TGF and the focused peaks move slightly toward the intersection D. Following the separation, the focused peaks move inside the gel and are further separated based on size.

This is a novel configuration that offers several advantages over the previously developed systems, such as continuous separation without the need to switch between the dimensions, simplicity, ease of fabrication which leads to stable performance, and low fabrication cost which facilitates commercialization. Additionally, in this configuration, samples are highly concentrated when entering the gel, which significantly improves SDS-PAGE performance [162]. Separation experiments are performed to separate several Alexa Fluor 488 conjugated proteins ranging in size from 12 to 66 kDa, with a fluorescent single point detection located 5 mm from the gel entrance. Experimental results show a

dramatic improvement in separation performance and peak capacity over each of the 1-D separation techniques.

7.2 Fabrication of the Chip

To perform the 2-D separation experiments, a PDMS/glass microfluidic chip was first fabricated using soft lithography techniques as described in section 3.2. Briefly, a clean and dehydrated silicon wafer was first spin-coated with SU-8 2025 photoresist at 500 rpm for 20 s followed by 2500 rpm for 60 s, to achieve a 20 µm thick microchannel. The wafer was then baked at 65 °C for 2 min and at 95 °C for 6 min, and finally cooled to room temperature. The 2-D configuration as shown In Figure 7.1 with 100 µm wide channels was designed (CAD/Art Services) and transferred to the spin-coated wafer through UV exposure. After UV exposure, the wafer was baked again at 65 °C for 1 min and 95 °C for 6 min. Development was performed in the PGMEA developer for 4 min. The silicon wafer containing positive relief of the design was then dried by nitrogen gas. The mixture of PDMS prepolymer base and curing agent with a weight ratio of 10:1 was degassed under vacuum, poured onto the wafer, cured at 90 °C for 2 h, and punched to form 1 mm diameter holes at the reservoir locations. After pretreatment with oxygen plasma, the PDMS substrate with the design feature was bonded with a glass substrate coated with a thin layer of PDMS (~30 µm) to achieve uniform surface conditions. Immediately after the plasma bonding, a 2:3:5 mixture of 3-(trimethoxysilyl) propyl methacrylate, glacial acetic acid, and deionized water was used for channel conditioning [71]. The mixture was introduced to the chip for 10 min from reservoir C using a syringe pump with 2 µL/min flow rate. Following the channel conditioning, the channels were flushed and purged with air using a syringe pump with 5 µL/min flow rate. Next, all conditioned channels were filled with the unpolymerized acrylamide solution using a syringe pump with 2 µL/min flow rate. The separation gel consisted of 6% T, 3.3% C acrylamide/bis-acrylamide (29:1), 1× Tris-glycine native buffer, 1% (wt/vol) SDS, and 0.4% (wt/vol) VA-086 photoinitiator. Notations % T and % C indicate the percentage of total acrylamide (wt/vol) and cross-linker (wt/wt), respectively, which can be adjusted by mixing with buffer (e.g., 1× Tris-glycine) to define the gel pore size [34]., The gel also served as a container for defined quantities of SDS for mixing with denatured proteins and to form SDS/protein complexes. For optimized photoinitiation, 0.4% (wt/vol) VA-086 was used in the gel as it is soluble in water and is an attractive choice for this system, given its non-ionic groups and rapid photodecomposition [163, 164].

An inverted epi-fluorescence microscope (GX-71) equipped with a 100W mercury arc lamp was used to photopolymerize the highlighted region of the chip, as shown in Figure 7.1. Step-by-step photopolymerization was performed by visualizing the channel region using a 10x objective, while an x–y translation stage was used to slowly move the UV beam along the channel. The target channels were exposed under the microscope for a total time of about 20 min. After that, DI water was injected to the chip for 10 min from reservoir A using a syringe pump with 1μL/min flow rate to ensure that all the uncured acrylamide solution was flushed out. The chip was then placed in a UV exposure system (Newport) and illuminated with UV light (~365nm) for an additional 5 min to ensure full polymerization of gel-filled channels. To complete the chip design, injection and discharge capillaries were connected to the chip from reservoir holes A and B respectively, while plastic reservoirs were glued on top of the other two reservoir holes.

To apply the temperature gradient along the TGF channel, Peltier thermoelectric heater/coolers (TE-35-0.6-1) were glued on an aluminum holder with a distance of 5 mm from each other to generate a temperature range (15-50 °C) along the channel. The holder contains a 4 mm wide slit at the middle to enable channel visualization using the inverted GX-71 microscope. The chip was then placed on the holder and taped on the heater/cooler configuration.

7.3 Experimental Setup

Before performing the experiments, reservoir C was filled with 1× Tris-glycine native buffer and the SDS reservoir was filled with 1× Tris-glycine containing 2% (wt/vol) SDS. Alexa Fluor 488 conjugated protein samples (Bovine Serum Albumin (66 kDa), Ovalbumin (45 kDa), Parvalbumin (12 kDa) and Trypsin Inhibitor (21 kDa)) were denatured without SDS using the previously reported procedure [122].

Briefly, a total of 0.4 mg protein sample (0.1 mg per protein) was dissolved into 400 mL DI water, and urea and DTT were thoroughly mixed with the sample solution in a vial with final concentrations of 8 M and 100 mM, respectively. The reaction was allowed to proceed in the dark overnight at room temperature. Subsequently, iodoacetamide (IAM) was added to the solution to a concentration of 120 mM and the vial was placed in the dark for 1 h at room temperature. The resulting solution was diluted 10 times with 0.1M Tris-phenol solution for use in TGF separation experiments.

To perform the separation experiments, sample and buffer vials were connected to the chip through reservoirs A and B respectively using fused-silica capillaries with 200 μm i.d. and 350 μm o.d. and a counteracting bulk flow was created by changing the relative pressure head (h) between the two vials using a linear stage. Experiments started by filling the TGF channel with Tris-phenol buffer and positioning the buffer vial about 6 cm above the sample vial to create a positive pressure of around 600 Pa at the buffer reservoir. TGF separations were then performed by applying a negative high voltage of -2000 V (Labsmith, HVS448–3000) to the sample reservoir while keeping reservoir C grounded. The difference in head decreased at a predetermined rate so that the samples focused, and moved along the microchannel toward the intersection D where they entered the second dimension.

To perform SDS-PAGE separation, denatured proteins need to be mixed with SDS inside the gel, so it is important to have a high concentration of SDS inside the gel during the experiments. In this study, the current along the channel was measured during the experiments and additional SDS was electrically injected into the gel from SDS reservoir as needed. An epi-fluorescence microscope (GX-71, OLYMPUS, Melville, NY, USA) equipped with a 10× objective, a 100 W mercury lamp (Olympus), and a CCD camera (CoolSnap HQ, Roper Scientific, Trenton, NJ, USA) were used to take images of an area of approximately 0.5×0.5 mm both at the end of the TGF channel and at 5 mm from the gel entrance inside the gel. Electropherograms were then generated by cropping the images and measuring the fluorescent intensity at the smaller area of 10×50 μm inside the microchannel.

7.4 Results and Discussions

Before the experiments, the temperature gradient along the TGF channel was measured using the previously reported two-color thermometry technique [36]. The same power was applied to the Peltier thermoelectric heater/coolers for all the experiments and the temperature gradient was measured to confirm it was in an approximate range of 15-50 °C over 5 mm along the channel. SDS was electrically injected into the gel from SDS reservoir by applying a negative voltage of -1200 V to the SDS reservoir while reservoir C stayed grounded. Experiments started by applying a negative high voltage of -2000 V to the sample reservoir containing the denatured proteins while reservoir C was kept grounded. A positive pressure of around 600 Pa was applied at the buffer reservoir and the difference in head decreased at a predetermined rate to generate a scanning rate of -0.5 Pa/s during the separation. To investigate the

efficiency of the proposed 2-D configuration, separation of labeled proteins was recorded both at the end of the TGF separation (point D) and at 5 mm from the gel entrance inside the gel.
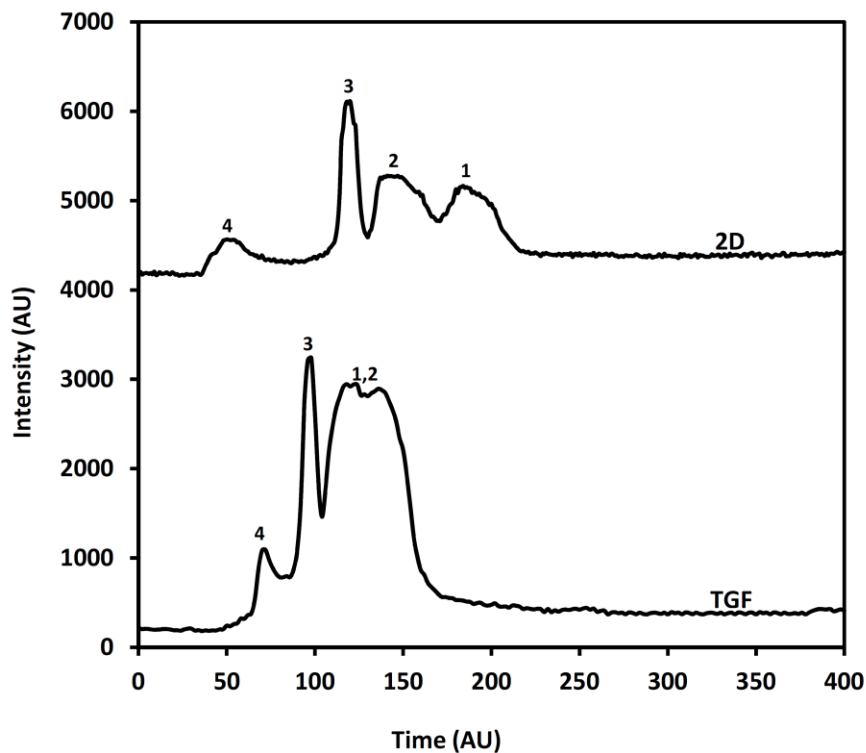
Figure 7.2 Separation of four Alexa Fluor 488 conjugated proteins ((Bovine Serum Albumin (66 kDa), Ovalbumin (45 kDa), Parvalbumin (12 kDa) and Trypsin Inhibitor (21 kDa)) using both TGF and proposed 2-D separation methods. Separation was recorded inside the developed microfluidic system both at the end of the TGF separation channel (point D) and at 5 mm from the gel entrance inside the gel.

Figure 7.2 shows the separation results of four Alexa Fluor 488 conjugated proteins at the end of the TGF separation (point D) and at 5 mm from the gel entrance inside the gel. The separation performance is higher for the 2-D separation system than for the TGF separation results. Furthermore, it is shown that peaks 1 and 2 are not distinguishable from each other by TGF separation, while all the peaks are separated from each other using the 2-D separation system.

To quantify the improvement, peak-to-peak resolution was calculated for the separation results using the following equation

110

$$R_S = \frac{\Delta t}{0.85\left(w_1 + w_1\right)} \qquad (7.1)$$

where Δt is the distance between the two adjacent peaks and w_i is the peak width at the half-peak height.

Equation (7.1) was used to calculate the resolution since the half height width of the peaks is much easier to measure than the baseline width when the peaks are not fully separated.

Peak-to-peak resolution results for the separation of Alexa Fluor conjugated proteins are presented in Table 7.1 for both TGF and 2-D separation techniques. Results indicate that overall resolution significantly increases when the 2-D design is used.

Table 7.1 Peak resolution obtained from separation of four Alexa Fluor 488 conjugated proteins ((Bovine Serum Albumin (66 kDa), Ovalbumin (45 kDa), Parvalbumin (12 kDa) and Trypsin Inhibitor (21 kDa)) using both TGF and 2-D separation methods. Peaks order is from right to left.

	Resolution	
	TGF	2-D
Peak ID 1−2	n/a	0.77
Peak ID 2−3	0.63	0.65
Peak ID 3−4	1.1	1.87

Reproducibility of the experimental results for the 2-D separation system was also examined and is presented in Table 7.2. Chip-to-chip reproducibility was investigated by comparing the peak-to-peak resolution of the 2-D separation experiments for three different chips. As shown in Table 7.2, the RSD are less than 8% ($n = 3$) for chip-to-chip reproducibility indicating stable operation of the device and experimental system.

Table 7.2 Chip to chip reproducibility of the 2-D separation experiments for separation of four Alexa Fluor 488 conjugated proteins ((Bovine Serum Albumin (66 kDa), Ovalbumin (45 kDa), Parvalbumin (12 kDa) and Trypsin Inhibitor (21 kDa)). Peaks order is from right to left.

	Resolution			Chip-to-chip
Parameter	Chip 1	Chip 2	Chip 3	RSD
Peak ID 1−2	0.77	0.68	0.73	6.21%
Peak ID 2−3	0.65	0.69	0.71	4.47%
Peak ID 3−4	1.87	1.61	1.70	7.65%

7.5 Conclusions

A PDMS/glass microfluidic chip was designed and developed for two-dimensional separation of proteins, combining temperature gradient focusing (TGF) and sodium dodecyl sulfate (SDS) polyacrylamide gel electrophoresis (PAGE). In this system, denatured proteins are first focused and separated, based on their electrophoretic mobility, in a 15 mm separation channel using the scanning TGF method, and the focused bands are gradually transferred toward the end of the first dimension while they are continuously introduced into a 25 mm channel filled with polyacrylamide gel. A photopolymerization technique was used to fabricate the sieving gel inside a portion of the chip for size-based separation. A side channel is used at the beginning of the second dimension to continuously inject SDS into the gel, allowing defined volumes of SDS to be composed within the focused bands. The proteins are further separated along the second dimension based on their molecular sizes, using SDS-PAGE. The temperature gradient along the TGF channel was created using Peltier thermoelectric cooler/heaters under the chip surface. The scanning bulk flow was created by adjusting the head difference between the sample and buffer reservoirs using a motorized linear stage. Separation of four Alexa Fluor conjugated proteins was performed using the developed 2-D configuration, and the results were recorded both at the end of the TGF separation (first dimension) and at 5 mm from the gel entrance. The results show a dramatic improvement in peak capacity and resolution with the proposed 2-D system compared with the 1-D TGF separation results.

Chapter 8
Conclusions and Recommendations

8.1 Conclusions

Electrophoresis separation corresponds to the motion and separation of dispersed particles under the influence of a constant electric field. In molecular biology, electrophoresis separation plays a major role in identifying, quantifying and studying different biological samples, such as proteins inside cells. In electrophoresis separations, different characteristics of the particles, such as charge to mass ratio, size or pI values, can be used to separate and isolate those particles. For very complex samples, two or more characteristics can be combined to form a multi-dimensional electrophoresis separation system, significantly improving separation efficiency. Employing microfluidic technology for electrophoresis separation provides several advantages, such as improved transport control, reduced reagent consumption, simplicity of operation, portability, improved sensitivity, and reduced cost. The aim of this study was to develop microfluidic systems for high performance separation of biochemical samples using electrophoresis methods. In this case, the design, mechanism and performance of three currently used separation methods were improved to achieve a higher separation resolution and better efficiency. A new, continuous, two-dimensional separation mechanism was also introduced for high performance separation of complex mixtures.

The first part of the thesis concerned the development of a fully integrated microfluidic chip (PDMS/modified PDMS membrane/SU-8/quartz) for isoelectric focusing separation of proteins with whole-channel imaging detection. The motivation for this work was the need to develop low-cost, fully automated chips that have similar performances to currently used commercial products that are much more expensive and difficult to fabricate. All the challenges posed in fabricating and integrating the chip were addressed. The chip was tested by performing protein and pI marker separations, and the separation results obtained for the chip were compared with those obtained for commercial cartridges. Side-by-side comparison of the results validated the chip and fabrication techniques.

The second part of the thesis focused on counter-flow gradient electrofocusing separation methods. In these methods, the electrophoretic motion of analytes is counter-balanced by a bulk fluid flow to accumulate or focus analytes at stationary points along a separation column. The research focused on improving the peak capacity and separation resolution of two counter-flow gradient electrofocusing methods – Temperature Gradient Focusing and Micellar Affinity Gradient Focusing – by using a bilinear temperature gradient along the separation channel. The temperature profile along the channel consists of a sharp gradient used to pre-concentrate the sample followed by a shallow gradient that increases separation resolution. Simple numerical modeling was performed to validate the resolution improvement by using a bilinear gradient. Then a hybrid PDMS/glass chip integrated with planar micro heaters for generating the desired bilinear temperature gradients was fabricated using conventional sputtering and soft lithography techniques. A specialized design was developed for the heaters to achieve the bilinear profile using both analytical and numerical modeling. To confirm the temperature profile along the channel, a two-color thermometry technique was developed for measuring the temperature inside the chip. Separation performance was characterized for each of the techniques by separating several different dyes, amino acids and peptides. Experiments showed a dramatic improvement in peak capacity and resolution of both techniques over the standard linear temperature gradients.

Subsequently, an analytical model was developed to investigate the effect of bilinear gradients in counter-flow gradient electrofocusing methods. The model solves the convection-diffusion equation, and equation of motion, of the focused peaks along the separation channel and provides a general equation for calculating the resolution for different gradients, diffusion coefficients, and bulk flow scan rates. The results indicate that any bilinear gradient provides up to 100% improvement in separation resolution compared with the linear case. Additionally, for some scanning rates, an optimum bilinear gradient can be found that maximizes separation resolution. Numerical modeling was also developed for validating some of the results.

The final part of the thesis focused on the development of a two-dimensional separation system for protein separation, combining temperature gradient focusing (TGF) and sodium dodecyl sulfate (SDS) polyacrylamide gel electrophoresis (PAGE) in a PDMS/glass microfluidic chip. An experimental study was performed to separate a mixture of four fluorescently labeled proteins using two characteristics: charge to mass ratio and size. By using this configuration, experimental results showed a dramatic improvement in peak capacity and resolution over the 1-D TGF separation method.

The knowledge gained in this thesis will push the forefront of our understanding of electrophoresis separation and advance the development of LOC devices for separation analysis to achieve higher separation efficiency and better reproducibility. The information obtained in this research will be of interest to researchers in fluid mechanics, analytical chemistry and bioengineering.

8.2 Recommendations for future work

The findings from this work lead to several recommendations for additional research. For instance, the fully integrated IEF-WCID chip fully realizes all the functions of the commercial cartridge used in the iCE280 analyzer in a chip format, while avoiding the challenging alignment and gluing procedures associated with the commercial cartridge. Further, this chip format IEF presents the opportunity for multi-dimensional separation of complex samples, which cannot be realized easily using capillary-based separations. It is possible, therefore, to develop a two-dimensional separation system using the IEF-WCID technique established in this thesis as one of the dimensions. In addition, the fabrication techniques developed for this chip can be used in other chip applications that involve the fabrication of multilayer structures using different materials. For example, the half-cured PDMS with holes that prevent leakage can be applied to other fabrication work where leakage is prone to occur. The modified PDMS membranes and associated fabrication techniques can be used in other separation studies as well.

This research has shown that using bilinear gradients improves the resolution and peak capacity of any counter-flow gradient focusing method over the conventional linear gradients. It is usually possible to generate bilinear gradients in chip-based systems, providing the opportunity to improve the efficiency of different counter-flow gradient focusing systems for analysis of different biochemical samples in very short microchannels. These bilinear systems are also excellent candidates for multi-dimensional separation since they can provide high-performance separation without the use of long microchannels and, therefore, reduce the size and complexity of the chips. The microheaters developed in this work can be used in other chip applications that require temperature gradients or temperature sources inside the chip. In addition, the two-color thermometry technique developed in this work can be used for temperature measurement studies in PDMS microchannels. When using confocal microscopy systems,

this measurement technique can be used for temperature measurements of the whole chip volume by applying thin layers of dye across the whole platform.

The two-dimensional separation system developed here offers several advantages over the previously developed systems, such as continuous separation without the need to switch between the dimensions, simplicity, ease of fabrication which leads to stable performance, and low fabrication cost which facilitates commercialization. In addition, this system provides reproducible results – an important consideration when working with multi-dimensional separation systems. This configuration can be modified for separation of other biochemical samples, such as DNA samples. In addition, it is possible to perform western blotting and similar analyses following the SDS-PAGE inside the gel.

Bibliography

[1]   Feng, X., Du, W., Luo, Q., Liu, B.F., Analytica Chimica Acta 2009, 650, 83-97.

[2]   Vyawahare, S., Griffiths, A.D., Merten, C.A., Chemistry and Biology 2010, 17, 1052-1065.

[3]   Becker, H., Locascio, L.E., Talanta 2002, 56, 267-287.

[4]   Chen, Y., Zhang, L., Chen, G., Electrophoresis 2008, 29, 1801-1814.

[5]   Foudeh, A.M., Fatanat Didar, T., Veres, T., Tabrizian, M., Lab on a Chip 2012, 12, 3249-3266.

[6]   Gupta, K., Kim, D.-H., Ellison, D., Smith, C., Kundu, A., Tuan, J., Suh, K.-Y., Levchenko, A., Lab on a Chip 2010, 10, 2019-2031.

[7]   Haeberle, S.,Zengerle, R., Lab on a Chip, 2007, 7, 1094-1110.

[8]   Nguyen, N. T.,Wereley, S. T., Fundamentals and Applications of Microfluidics, Artech House Publishers, 2006.

[9]   Whitesides, G. M., Nature, 2006, 442, 368-373.

[10]   Manz, A., Effenhauser, C. S., Burggraf, N., Harrison, D. J., Seiler, K.,Fluri, K., Journal of Micromechanics and Microengineering, 1994, 4, 257-265.

[11]   Chin, C. D., Linder, V.,Sia, S. K., Lab on a Chip, 2007, 7, 41-57.

[12]   Abgrall, P.,Gue, A. M., Journal of Micromechanics and Microengineering, 2007, 17, 15-49.

[13]   Dittrich, P. S., Tachikawa, K.,Manz, A., Analytical Chemistry, 2006, 78, 3887-3907.

[14]   Yi, C. Q., Li, C. W., Ji, S. L.,Yang, M. S., Analytica Chimica Acta, 2006, 560, 1-23.

[15]   "http://www.agilent.com/about/newsroom/lsca/imagelibrary/images/lsca_62_4labchips.jpg".

[16]   "http://www.sonydadc.com/typo3temp/pics/1dc42f86fa.jpg".

[17]   "http://www.genengnews.com/Media/images/Article/Fluidgm_Digital487701554542517.jpg".

[18]   "http://www.mhra.gov.uk/Publications/Safetywarnings/MedicalDeviceAlerts/CON152632".

[19]   Duffy, D. C., McDonald, J. C., Schueller, O. J. A.,Whitesides, G. M., Analytical Chemistry, 1998, 70, 4974-4984.

[20]   Duffy, D. C., Schueller, O. J. A., Brittain, S. T.,Whitesides, G. M., Journal of Micromechanics and

Microengineering, 1999, 9, 211-217.

[21] Xia, Y. N.,Whitesides, G. M., Annual Review of Materials Science, 1998, 28, 153-184.

[22] Rogers, J.A., Nuzzo, R.G., Materials Today 2005, 8, 50-56.

[23] Lee, J. N., Park, C.,Whitesides, G. M., Analytical Chemistry, 2003, 75, 6544-6554.

[24] McDonald, J. C.,Whitesides, G. M., Accounts of Chemical Research, 2002, 35, 491-499.

[25] McDonald, J. C., Duffy, D. C., Anderson, J. R., Chiu, D. T., Wu, H. K., Schueller, O. J.
      A.,Whitesides, G. M., Electrophoresis, 2000, 21, 27-40.

[26] de Jong, J., Lammertink, R. G. H.,Wessling, M., Lab on a Chip, 2006, 6, 1125-1139.

[27] Kane, R.S., Takayama, S., Ostuni, E., Ingber, D.E., Whitesides, G.M., Biomaterials 1999, 20, 2363-
      2376.

[28] Cho, W.C.S., proteomics & bioinformatics 2007, 5, 77-85.

[29] Bodzon-Kulakowska, A., Bierczynska-Krzysik, A., Dylag, T., Drabik, A., Suder, P., Noga, M.,
      Jarzebinska, J., Silberring, J., Journal of Chrom. B 2007, 849, 1-31.

[30] Chen, H., Fan, Z.H., Electrophoresis 2009, 30, 758-765.

[31] Lion, N., Rohner, T.C., Dayon, L., Arnaud, I.L., Electrophoresis 2003, 24, 3533-3562.

[32] Wu, D., Qin, J., Lin, B., Journal of Chromatography A 2008, 1184, 542-559.

[33] Peng, Y., Pallandre, A., Tran, N.T., Taverna, M., Electrophoresis 2008, 29, 157-178.

[34] Tia, S., Herr, A.E., Lab on a Chip 2009, 9, 2524-2536.

[35] Shameli, S.M., Elbuken, C., Ou, J., Ren, C.L., Pawliszyn, J., Electrophoresis 2011, 32, 333-339.

[36] Shameli, S.M., Glawdel, T., Liu, Z., Ren, C.L., Analytical Chemistry 2012, 84, 2968-2973.

[37] Shameli, S.M., Glawdel, T., Fernand, V.E., Ren, C.L., Electrophoresis 2012, 33, 2703-2710.

[38] Ledur Kist, T.B., Mandaji, M., Electrophoresis 2004, 25, 3492-3497.

[39] Kasicka, V., Electrophoresis 2009, 30, 40-52.

[40] Skoog, D.A., Holler, F.J., Crouch, S.R, Principles of Instrumental Analysis 6th ed. Chapter 30
      Thomson Brooks/Cole Publishing: Belmont, CA 2007.

[41] Shackman, J. G., Ross, D., Electrophoresis 2007, 28, 556–571.

[42] Jabasini, M., Murakami, Y., Kaji, N., Tokeshi, M., Baba, Y., Biological & pharmaceutical bulletin,

2006, 29, 595-604.

[43]   Pauling, L., Corey, R.B., Branson, H.R., Proc. Natl. Acad. Sci. 1951, 37, 205–211.

[44]   Murzin, A. G., Brenner, S., Hubbard, T., Chothia, C., Molecular Biology 1995, 247, 536–540.

[45]   Kosmulski, M., Saneluta, C., Colloid and Interface Science 2004, 280, 544–545.

[46]   Shackman, J.G., Ross, D., Electrophoresis 2007, 28, 556-571.

[47]   Dolník, V., Electrophoresis 2006, 27, 126-141.

[48]   El Rassi, Z., Electrophoresis 2010, 31, 174-191.

[49]   Shafaati, A, Capillary Electrophoresis, 2005,
       http://www.docstoc.com/docs/108040687/CAPILLARY-ELECTROPHORESIS.

[50]   Jacobson, S. C., Hergenroder, R., Koutny, L. B., Ramsey, J. M., Anal. Chem. 1994, 66, 1114-1118.

[51]   Schulze, P., Ludwig, M., Kholer, F., Belder, D., Anal. Chem. 2005, 77, 1325–1329.

[52]   Lacher, N. A., Rooij, N. F., Verpoorte, E., Lunte, S. M., J. Chromatogr. A, 2003, 1004, 225-235.

[53]   Fu, L. M., Yang, R. J., Electrophoresis, 2003, 24, 1253-1260.

[54]   Abad-Villar, E. M., Tanyanyiwa, J., Fernadez-Abedul, M. T., Costa-Garcia, A., Hauser, P. C., Anal. Chem., 2004, 76, 1282-1288.

[55]   Abad-Villar, E. M., Kuban, P., Hauser, P. C., Electrophoresis 2005, 26, 3609-3614.

[56]   Popa, T.V., Mant, C.T., Hodges, R.S., Electrophoresis 2003, 24, 4197-4208.

[57]   Popa, T.V., Mant, C.T., Hodges, R.S., Journal of Chromatography A 2006, 1111, 192-199.

[58]   Ramsey, J. D., Jacobson, S. C., Culbertson, C. T., Ramsey, J. M., Anal. Chem. 2003, 75, 3758-3764.

[59]   Terabe, S., Miyashita, Y., Shibata, O., Barnhart, E.R., Alexander, L.R., et. al., Journal of Chromatography, 1990, 516, 23-31.

[60]   Terabe, S., Annual Review of Anal. Chem. 2009, 2, 99-120.

[61]   Otsuka, K., Terabe, S., Ando, T., Journal of Chromatography, 1985, 332, 219-226.

[62]   Fujiwara, S., Iwase, S., Honda, S., Journal of Chromatography, 1988, 447, 133-140.

[63]   Kaneta, T., Tanaka, S., Taga, M., Yoshida, H., Analytical Chemistry, 1992, 64, 798-801.

[64]   Yashima, T., Tsuchiya, A., Morita, O., Analytical Chemistry, 1992, 64, 2981-2984.

[65] Culbertson, C. T., Jacobson, S. C., Ramsey, J. M., Anal. Chem., 2000, 72, 5814-5819.

[66] Kutter, J. P., Jacobson, S. C., Ramsey, J. M., Anal. Chem., 1997, 69, 5165-5171.

[67] Han, J., Singh, A. K., J. Chromatogr. A, 2004, 1049, 205-209.

[68] Tabuchi, M., Kuramitsu, Y., Nakamura, K., Baba, Y., J. Proteome Res., 2003, 2, 431-435.

[69] Foote, R.S., Khandurina, J., Jacobson, S.C., Ramsey, J.M., Analytical Chemistry, 2005, 77, 57-63.

[70] Song, S., Singh, A. K., Kirby, B. J., Anal. Chem. 2004, 76, 4589-4592.

[71] Herr, A.E., Singh, A.K., Anal Chem 2004, 76, 4727-4733.

[72] Persat, A., Marshall, L. A., Santiago, J. G., Anal. Chem. 2009, 81, 9507-9511.

[73] Jung, B., Bharadwaj., R., Santiago. JG., Anal. Chem. 2006, 78, 2319–2327.

[74] Huang, H., Xu, F., Dai, Z. P., Lin, B. C., Electrophoresis 2005, 26, 2254–2260.

[75] Cui, H., Dutta, P., Ivory, C.F., Electrophoresis 2007, 28, 1138-1145.

[76] Vyas, C.A., Flanigan, P.M., Shackman, J.G., Bioanalysis 2010, 2, 815-827.

[77] Shackman, J.G., Ross, D., Anal. Chem. 2007, 79, 6641–6649.

[78] Danger, G., Ross, D., Electrophoresis 2008, 29, 4036–4044.

[79] Davis, N.I., Mamunooru, M., Vyas, C.A., Shackman, J.G., Anal. Chem. 2009, 81, 5452-5459.

[80] Tiselius, A., Trans. Faraday. Soc. 1937, 33, 524−531.

[81] Duncombe, T.A., Herr, A.E., Anal. Chem. 2012, 84, 8740-8747.

[82] Shackman, J.G., Munson, M.S., Ross, D., Anal. Chem. 2007, 79, 565–571.

[83] Ross, D., Romantseva, E.F., Anal. Chem. 2009, 81, 7326-7335.

[84] Ross, D., Kralj, J.G., Anal. Chem. 2008, 80, 9467-9474.

[85] Strychalski, E.A., Henry, A.C., Ross, D., Anal. Chem. 2009, 81, 10201-10207.

[86] Strychalski, E.A., Henry, A.C., Ross, D., Anal.Chem. 2011, 83, 6316-6322.

[87] Sommer, G.J. , Hatch, A.V. , Electrophoresis 2009, 30, 742-757.

[88] Yang, C., Wang, S., Chang, C., Wang, Y. , Hu, X. , Anal. Chem. 2010, 82, 1580-1583.

[89] Huang, T., Pawliszyn, J., Electrophoresis 2002, 23, 3504–3510.

[90] Liang, Y., Cong, Y., Liang, Z., Zhang, L., Zhang, Y., Electrophoresis 2009, 30, 4034-4039.

[91]   Sommer, G. J., Singh, A. K., Hatch, A. V., Anal. Chem. 2008, 80, 3327–3333.

[92]   Albrecht, J. W., Jensen, K. F., Electrophoresis 2006, 27, 4960-4969.

[93]   Kohlheyer, D., Besselink, G. A. J., Schlautmann, S., Schasfoort, R. B. M., Lab Chip 2006, 6, 374–380.

[94]   Wu, J., Pawliszyn, J., Anal Chem 1992, 64, 224-227.

[95]   Hoebel, S. J., Balss, K. M., Jones, B. J., Malliaris, C. D., Munson, M. S., Vreeland, W., Ross, D., Anal. Chem. 2006, 78, 7186-7190.

[96]   Greenlee, R. D., Ivory, C. F., Biotechnol. Prog. 1998, 14, 300– 309.

[97]   Koegler, W. S., Ivory, C. F., Biotechnol. Prog. 1996, 12, 822– 836.

[98]   Ross, D., Locascio, L. E., Anal. Chem. 2002, 74, 2556-2564.

[99]   Humble, P. H., Kelly, R. T., Woolley, A. T., Tolley, H. D., Lee, M. L., Anal. Chem. 2004, 76, 5641-5648.

[100] Wang, Q., Lin, S. L., Warnick, K. F., Tolley, H. D., Lee, M. L., J. Chromatogr. A 2003, 985, 455-462.

[101] Myers, P., Bartle, K. D., J. Chromatogr. A 2004, 1044, 253-258.

[102] Balss, K. M., Ross, D., Begley, H. C., Olsen, K. G., Tarlov, M. J., J. Am. Chem. Soc. 2004, 126, 13474-13479.

[103] Munson, M.S., Danger, G., Shackman, J.G., Ross, D., Anal. Chem., 2007, 79, 6201-6207.

[104] Balss, K. M., Vreeland, W. N., Phinney, K. W., Ross, D., Anal. Chem., 2004, 76, 7243–7249.

[105] Matsui, T., Franzke, J., Manz, A., Janasek, D., Electrophoresis, 2007, 28, 4606-4611.

[106] Ghosal, S., Horek, J., Anal. Chem. 2005, 77, 5380–5384.

[107] Huber, D.E., Santiago, J.G., Electrophoresis 2007, 28, 2333–2344.

[108] Balss, K. M., Vreeland, W. N., Howell, P. B., Henry, A. C., Ross, D., J. Am.Chem. Soc. 2004, 126, 1936–1937.

[109] Kamande, M.W., Ross, D., Locascio, L.E., Lowry, M., Warner, I.M., Anal. Chem. 2007, 79, 1791-1796.

[110] Giddings, J. C., Anal. Chem., 1967, 39, 1027-1028.

[111] Giddings, J. C., J. High-Resolut. Chromatogr., 1987, 10, 319-323.

[112] Cortes, H. J., J. Chromatogr., 1992, 626, 3-23.

[113] Stroink, T., Schravendijk, P., Wiese, G., Teeuwsen, J., Lingeman, H., et. al., Electrophoresis 2003, 24, 1126-1134.

[114] Stroink, T., Ortiz, M. C., Bult, A., Lingeman, H., de Jong, G. J., et. al., J. Chromatogr. B, 2005, 817, 49-66.

[115] Rocklin, R.D., Ramsey, R.S., Ramsey, J.M., Analytical Chemistry, 2000, 72, 5244-5249.

[116] Jacobson, S. C., Hergenroder, R., Koutny, L. B., Warmack, R. J., Ramsey, Anal. Chem., 1994, 66, 1107-1113.

[117] Zubritsky, E., Anal. Chem., 2000, 72, 687-690.

[118] Herr, A.E., Molho, J.I., Drouvalakis, K.A.,Mikkelsen, J.C., Utz, P.J., Santiago, J.G.,Kenny, T.W., Analytical Chemistry, 2003, 75, 1180-1187.

[119] Shadpour, H., Soper, S.A., Analytical Chemistry, 2006, 78, 3519-3527.

[120] Li, Y., Buch, J.S., Rosenberger, F., DeVoe, D.L., Lee, C.S., Analytical Chemistry, 2004, 76, 742-748.

[121] Liu, J., Yang, S., Lee, C.S., DeVoe, D.L., Electrophoresis, 2008, 29, 2241-2250.

[122] Yang, S., Liu, J., Lee, C.S., DeVoe, D.L., Lab on a Chip, 2009, 9, 592-599.

[123] Ross, D., Shackman, J.G., Kralj, J.G., Atencia, J., Lab on a Chip 2010, 10, 3139-3148.

[124] Wu, X. Z., Huang, T. , Liu, Z., Pawliszyn, J. , Trends in Anal Chem, 2005, 24, 369-382.

[125] Liu, Z. , Pawliszyn, J. , J. Proteome Research, 2004, 3, 567-571.

[126] Wu, X. Z. , Asai , S. , Yamaguchi , Y. , Electrophoresis, 2009, 30, 1552-1557.

[127] Tsuda, T., Sweedler, J. V., Zare, R. N., Anal Chem, 1990, 62, 2149-2152.

[128] Karniadakis, G., Beskok, A., Aluru, N., Microflows and Nanoflows: Fundamentals and Simulation, Springer, 2005.

[129] Guillo, C., Karlinsey, J. M., Landers, J. P., Lab Chip, 2007, 7, 112-118.

[130] Li, C., Yang, Y. N., Craighead, H. G., Lee, K. H., Electrophoresis, 2005, 26, 1800-1806.

[131] Kim, K.H. , Moon, M.H. , Anal Chem, 2009, 81, 1715-1721.

[132] Rowlen, K. L., Duell, K. A., Avery, J. P., Birks, J. W., Anal Chem, 1989, 61, 2624-2630.

[133] Wang, T., Hartwick, R.A., Anal. Chem., 1992, 64, 1745-1747.

[134] Das., C., Fan, Z. H., Electrophoresis, 2006, 27, 3619-3626.

[135] Yao, B., Yang, H. H., Liang, Q. L., Luo, G., Wang, L. D., Ren, K. N., et. al., Anal Chem, 2006, 78, 5845-5850.

[136] Ren, K. N., Liang, Q. L., Yao, B., Luo, G., Wang, L. D., Gao, Y. D., et. al., Lab Chip, 2007, 7, 1574-1580.

[137] Jin, L. J., Giordano, B. C., Landers, J. P., Anal Chem, 2001, 73, 4994-4999.

[138] Ro, K. W., Lim, K., Shim, B. C., Hahn, J. H., Anal Chem, 2005, 77, 5160-5166.

[139] Liu, Z., Ou, J., Samy, R., Glawdel, T., Huang, T., Ren, C. L., Pawliszyn, J., Lab Chip, 2008, 8, 1738-1741.

[140] Ou, J., Glawdel, T., Samy, R., Wang, S., Liu, Z., Ren, C. L., Pawliszyn, J., Anal Chem, 2008, 80, 7401-7407.

[141] Ou, J., Glawdel, T., Ren, C. L., Pawliszyn, J., Lab Chip, 2009, 9, 1926-1932.

[142] Ou, J., Ren, C. L., Pawliszyn, J., Anal Chimic. Acta, 2010, 662, 200-205.

[143] Tolley, H. D., Wang, Q., LeFebre, D. A., Lee, M. L., Anal. Chem. 2002, 74, 4456–4463.

[144] Sun, X., Li, D., Woolley, A.T., Farnsworth, P.B., Tolley, H.D., Warnick, K.F., Lee, M.L., J. Chromatogr. A 2009, 1216, 6532–6538.

[145] Ross, D., Gaitan, M., Locascio, L. E., Anal. Chem. 2001, 73, 4117–4123.

[146] Funatani, S., Fujisawa, N., Ikeda, H., Measurement Science and Tech. 2004, 15, 983–990.

[147] Samy, R., Glawdel, T., Ren, C.L., Anal. Chem. 2008, 80, 369–375.

[148] Duhr, S., Arduini, S., Braun, D., Eur. Phys. J. E 2004, 15, 277–286.

[149] Munkholm, C., Parkinson, D.R., Walt, D.R., J. Am. Chem. Soc. 1990, 112, 2608–2612.

[150] Bischoff, R., Roecklin, D., Roitsch, C., Electrophoresis, 1992, 13, 214–219.

[151] Shimura, k., Electrophoresis, 2009, 30, 11–28.

[152] Dibbern-Brunelli, D., De Oliveira, M.G., Atvars, T.D.Z., Journal of Photochemistry and Photobiology A Chemistry 1995, 85, 285–289.

[153] Jeong, D.W., Lee, C.Y., Lee, S.Y., J. Heat Transfer 2009, 131, 1–8.

[154] Dolan, J. W. LC-GC North America 2002, 20, 430−436.

[155] Cheng, Y.F., Dovichi, N.J., Science 1988, 242, 562-564.

[156] Wu, S.L., Dovichi, N.J., J. Chromatogr. 1989, 480, 141-155.

[157] Edwards, S.H., Shamsi, S.A., J. Chrom.. A 2000, 903, 227–236.

[158] Wang, Q., Tolley, H.D., LeFebre, D.A., Lee, M.L., Anal. Bioanal. Chem. 2002, 373, 125–135.

[159] Van Milligen, B. P., Bons, P. D., Carreras, B. A., Snchez, R., Eur. J. Phys. 2005, 26, 913–925.

[160] Giddings, J.C., Unified Separation Science, Wiley 1991.

[161] Aris, R., Proc. Roy. Soc. London A 1956, 235, 67–77.

[162] Hou, C, Herr, A.E., Anal. Chem. 2010, 82, 3343–3351.

[163] He, M., Herr, A., Anal. Chem. 2009, 81, 8177-8184.

[164] He, M., Herr, A., Nat. Protoc. 2010, 5, 1844-1856.

[165] Cohen, A.S., Karger, B.L., Journal of Chromatography A, 1987, 397, 409-417.

[166] Kenyon, S.M., Meighan, M.M., Hayes, M.A., Electrophoresis, 2011, 32, 482-49.

[167] Du, Y., Wang, E., Journal of Separation Science, 2007, 30, 875-890.